South American Climate Dynamics and Evolution of the Andes

by

Nadja Insel

A dissertation submitted in partial fulfillment
of the requirements for the degree of
Doctor of Philosophy
(Geology)
in The University of Michigan
2011

Doctoral Committee:

Associate Professor Christopher J. Poulsen, Chair
Professor Todd A. Ehlers
Professor Donald R. Zak
Assistant Professor Nathan A. Niemi
Assistant Professor Allison L. Steiner

Change is the only constant.

- Heraclitus

ACKNOWLEDGEMENTS

First, I would like to thank my advisors Todd Ehlers and Chris Poulsen for constant mentoring, encouragement, and support. With their different but complementary characters, they provided me with invaluable scientific help. Thanks to Todd for his ideas and enthusiasm for this project, and for his guidance and insights into all aspects of scientific research, from conducting field- and lab work to writing and presenting results. Special thanks also for the lab parties with all the amazing Swiss food and good wine. Thanks to Chris for introducing me to the world of climate modeling, for his endurance during the paper writing process, and his patience throughout some of our heated scientific discussions.

I am grateful to my other committee members, Don Zak, Nathan Niemi, and Allison Steiner for their helpful constructive advices. Allison (and her graduate student Ahmed Tawfik) also helped me to improve my understanding of the RegCM regional climate model.

I also would like to thank Christophe Sturm from the University of Stockholm for his help with REMOiso, to this point the only existing state-of-the-art regional general circulation model with isotope tracking capabilities. Without Christophe's detailed knowledge of the isotope module and helpful advice in setting up the model experiments much of the presented work would not have been possible.

My thanks also goes to Mirjam Schaller who provided many insights into chemical separation procedures for cosmogenic radionuclide sampling processing and the analysis of denudation rates.

Special thanks to Jason Barnes for introducing me to the amazing world of the Andes and for being a good friend throughout hours of debates and discussions on Andean geology and the rest of life. Thanks for all the motivation and support.

Also I owe a large debt to our colleague Sohrab Tawackoli for logistic support during several months of field work in Bolivia and Peru.

I'd like to express my thanks to past and current members of the (now joined) Earth Surface Processes research group and the Paleoclimate modeling lab as well as the SCALE lab members. I am especially grateful to have shared general support, trouble shooting, scientific discussions, and friendship with Dave Whipp, Matt Densmore, Louise Jeffery, Stephanie Olen, Dan Horton, Jing Zhou, Shi Yu Lee, Alison Duvall, Boris Avdeev, Alex Lechler, and Brian and Alli Yanites.

Many other people have helped to ensure my sanity throughout all those years in Ann Arbor and there are too many to acknowledge them all. However, life would not have been the same without the theme parties at Jen's and Laura's house. Thanks for all those funny and sometimes ridiculous moments. Special thanks also to Vanessa for becoming a great friend and travel companion. Hawaii was amazing!

Finally, I wish to thank my family for being supportive throughout my whole education and for always being there for me.

TABLE OF CONTENTS

LIST OF FIGURES

Figure

LIST OF TABLES

Table

CHAPTER I

Introduction

Orogenic plateaus are some of the most dramatic topographic features on Earth. Next to the Tibetan-Himalayan system, the Andean Mountains are the second largest tectonically active orogen on Earth, extending over 7,000 km from north to south. The Andes are mainly the result of Nazca Plate subduction below South America throughout the Cenozoic (e.g., Isacks, 1988). The Andean Plateau is defined as the broad area of moderate relief and internal drainage with elevations >3 km. High extensive plateaus are thought to influence local-to-far-field lithospheric deformation as well as global sediment flux, ocean chemistry, and precipitation pattern (Richter et al., 1992; Molnar et al., 1993; Masek et al., 1994; Lenters and Cook, 1995; Royden, 1996; Ruddiman et al., 1997; Sobel and Strecker, 2003). It has been known for a long time that tectonics plays a critical role in the evolution of global climate, affecting atmospheric circulation and ocean currents (e.g., Ruddiman and Kutzbach, 1989; Prell and Kutzbach, 1992; Kutzbach et al., 1993; Lenters and Cook, 1995). On regional scales, tectonic deformation leads to rock uplift and generates topographic relief, thereby enhancing the possibilities for orographic precipitation, which in turn focuses erosion. Erosion on the other hand enhances denudation and mass transfer that guide advanced uplift. However, the task of correctly differentiating between tectonically and climatically driven processes and their influence on denudation and topographic evolution is complicated by variations in tectonic rates and long- and short- term climate variability. In the Andes, our limited understanding of the elevation history of the Andean Plateau and the regional climate change that takes place in response to surface uplift is the most uncertain constraint in quantifying the interaction between tectonic deformation, surface uplift, climate, and surface processes.

The timing and rates at which current Andean elevations were attained are strongly debated. Elevation reconstructions based on fossil-leaf morphologies, carbonate clumped-isotope thermometry, and carbonate oxygen isotopic compositions suggest a rapid and recent rise of the Andean Plateau whereby ~2.5 km of elevation (>1/2 the current plateau height) was obtained during the late Miocene (~10-6Ma) (Fig. 1.1; Gregory-Wodzicki 2000; Garzione et al. 2006; Ghosh et al. 2006). Oxygen isotope paleoaltimetry is assumed to provide the most robust estimation of Andean paleoelevations. This approach uses preserved δ^{18}O in sedimentary carbonates as a proxy for ancient meteoric δ^{18}O. The composition of δ^{18}O in these archives is controlled by the temperature and the composition of meteoric water at the time of mineral formation, both of which are related to elevation. Due to the correlation between δ^{18}O of meteoric water and elevation, mountain surface uplift can be reconstructed through stable isotope studies of in situ formed minerals, assuming that the climate did not change in the past and that isotopic lapse rates (the rate of changes in isotopic ratio with altitude) are linear and analogues to modern. Based on these assumptions, a 3-4‰ δ^{18}O shift in late Miocene carbonate nodules from the Andean Plateau has been interpreted to reflect 2.5 ± 1 km of surface uplift. However, the proposed scenario is inconsistent with significant geological evidence (sedimentologic,

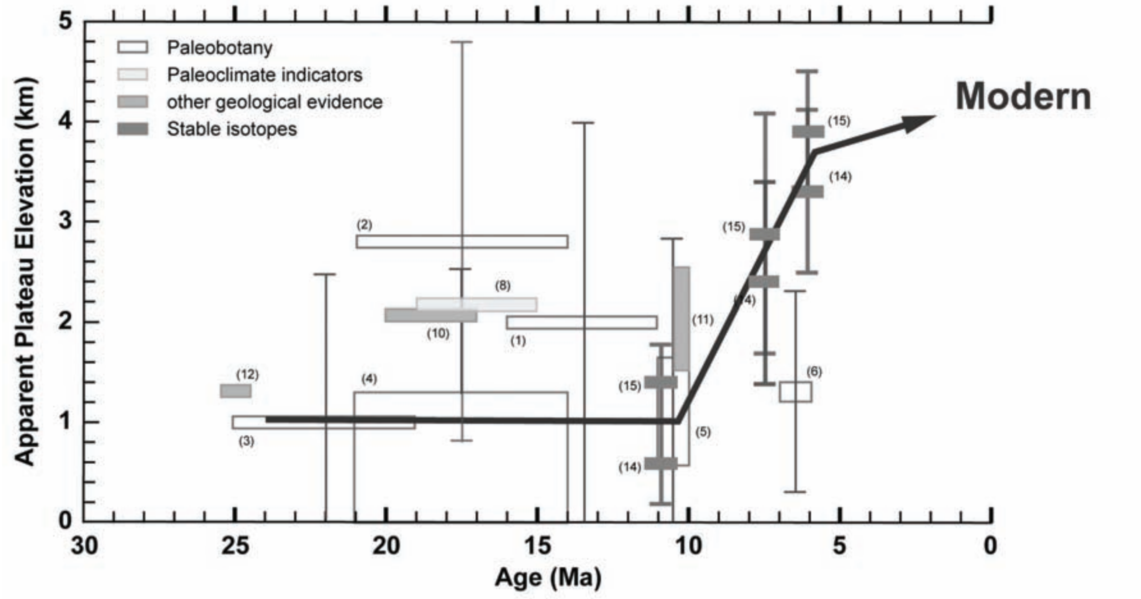

Figure 1.1: Recent paleoelevation reconstructions of the central Andes. Apparent Plateau elevation (km) is plotted as a function of age (Ma). Gray boxes represent paleoelevation estimations from previous studies; dark gray line highlights the interpretation of fast and recent AP uplift. Previous studies of AP uplift: Paleobotany: (1) Singewald and Berry (1922), (2) Berry (1939), (3) Muoz and Charrier (1996), (4) Gregory-Wodzicki et al. (1998), (5) Gregory-Wodzicki et al. (1998), (6) Graham et al. (2001); Paleoclimate indicators: (8) Alpers and Brimhall (1988); other geological evidence: (10) Sebrier et al. (1988), (11) Gubbels et al. (1993), (12) Lamb and Davis (2003); Stable Isotopes: (14) Ghosh et al. (2006); Quade et al. (2007), (15) Garzione et al. (2006)

structural, and volcanic observations) that suggest Andean Plateau growth was slow and steady since at least the Eocene (∼40Ma) (Fig. 1.1; Sebrier et al. e.g., 1988; Elger et al. e.g., 2005; Horton e.g., 2005; McQuarrie et al. e.g., 2005; Barnes and Ehlers e.g., 2009). Recent debates focus on the issue that the stable-isotope based paleoaltimetry samples may underestimate the true paleoelevation due to such effects as seasonality and evaporative enrichment (Hartley et al., 2007), burial diagenesis (Sempere et al., 2006), and/or past climate change as the plateau grew to its current height (Ehlers and Poulsen, 2009). The present dissertation tests the hypothesis that the depletion of Andean precipitation δ^{18}O in ancient carbonate nodules could be related to changes in South American Cenozoic climate associated with relatively minor surface uplift. To test this hypothesis the following questions need to be addressed: (a) What determines the modern isotopic composition of meteoric water along the Andes? (b) What is the effect of Andean surface uplift on regional climate and the processes that control the isotopic composition of precipitation? (c) How does climate change impact the interpretation of Andean paleoelevations?

However, it has been shown that the links between the rise of large mountain ranges and climate not only work in one direction with surface uplift provoking climate change, but that large-scale climate variations could also have a first-order control on mountain morphology. The topography of the Andes evolves through a balance between tectonic uplift and uplift- related orographic precipitation which causes an asymmetrical spatial distribution of surface processes (e.g., Masek et al., 1994; Horton, 1999; Montgomery et al., 2001). Because the Andes are perpendicular to principle wind directions and moisture is effectively intercepted, spatial variations in climate could strongly influence the erosional efficiency, thereby affecting the style and location of deformation and exhumation. For example, it has been suggested that the steep frontal slopes, high peaks, and the narrow shape of the northern central Andes are related to high orographic precipitation and high denudation rates, while the wider mountain belt with a more gentle topography and lower relief in the semiarid southern part of the central Andes may reflect a tectonic landform only slightly modified by denudation (Masek et al., 1994; Horton, 1999). The second hypothesis to be tested is that spatial and temporal variations in denudation could reflect climate variability over different time scales.

To understand the links between tectonics, climate and Earth surface processes on geological to annual time scales and to test the above hypotheses, this dissertation uses a multidisciplinary approach at the intersection between geology and atmospheric sciences. Methods I integrate include numerical modeling of climate, stable isotopes, topography and erosion as well as field and laboratory (cosmogenic radionuclide (CRN) analyses) work. Numerical modeling of climate for different topographies will help to answer long-standing questions concerning how the tectonic evolution of the Andes has influenced South American climate change (Strecker et al., 2007; Poulsen et al., 2010). Limited-domain general circulation models (RCMs) predict the three-dimensional climate based on the primitive equations for atmospheric circulation and on representations (parameterizations) of physical processes that occur on sub-grid scales. Climate models fitted with stable water isotope diagnostics provide additional information about the modern hydrological cycle and the water isotopic system in the past. Modeling results are applied to paleoaltimetry estimations to evaluate the predictions for the Cenozoic evolution of the Andes. Field observations and CRN dating techniques are used to investigate the coupling between climate and surface processes on decadal to millennial timescales. Quantifying basin-wide denudation rates from river sediments, in combination with numerical modeling of denudation for different climate scenarios, provides the tools to assess the role of climatic forcing in governing denudation processes (Masek et al., 1994; Montgomery et al., 2001).

This approach offers unique, direct insights into process rates and their determinants, ultimately providing information on the tectonic and climatic forcing mechanisms that shape the Earths surface.

1.1 Dissertation outline

This dissertation is composed of 4 main chapters (2-5) proceeded by this introductory chapter 1 and followed by the summary and conclusions chapter 6. Chapter

2-4 utilize regional general circulation models (RegCM, REMOiso) to analyze modern and past relationships between tectonics, climate, and stable isotopes and provide constrains for the interpretation of paleoclimate and paleoaltimetry from δ^{18}O archives. Chapter 2 elucidates the dominant regional processes that drive modern δ^{18}O variability. Chapter 3 evaluates dynamical and physical atmospheric changes associated with Andean surface uplift, while Chapter 4 quantifies changes in δ^{18}O and isotopic lapse rates in response to Andean surface uplift and regional climate change. An associated paper presents paleoclimate simulations of Andean surface uplift with a global atmospheric general circulation model (GENESIS) (Poulsen et al., 2010). Chapter 5 is an observational study that illustrates the link between climate variability and surface processes by evaluating the sensitivity of Holocene climate change on the denudation history across the central Andes.

1.2 Publications and abstracts resulting from this dissertation

Publications (peer-reviewed)

Insel, N., C. J. Poulsen, C. Sturm, and T.A. Ehlers (in review), Climate controls on temporal and spatial variability of Andean precipitation δ^{18}O, *Climate Dynamics.* **(Chapter 2)**

Insel, N., C. J. Poulsen, and T. A. Ehlers (2009), Spatial and temporal variability in denudation across the Bolivian Andes from multiple geochronometers, *Climate Dynamics*, doi:10.1007/s00382-009-0637-1 [highlighted in Nature Geoscience: Langenberg, H., 2009, Climate science: Andean rainfall, Nature Geoscience, 2, 607]. **(Chapter 3)**

Insel, N., C. J. Poulsen, T.A. Ehlers, and C. Sturm (in review with co-authors), Oxygen isotopic response to late Cenozoic Andean surface uplift, *EPSL.* **(Chapter 4)**

Poulsen, C. J., T. A. Ehlers, and **Insel, N.** (2010), Onset of convective rainfall during gradual late Miocene rise of the central Andes, *Science*, 328, 490-493

Insel, N., T. A. Ehlers, M. Schaller, J. B. Barnes, S. Tawackoli, and C. J. Poulsen (2010), Spatial and temporal variability in denudation across the Bolivian Andes from multiple geochronometers, *Geomorphology*, 122, 65-77. **(Chapter 5)**

Conference abstracts

Insel, N., C. J. Poulsen, T. A. Ehlers, and C. Sturm (2010), Climate controls on precipitation δ^{18}O along the Andes, *Eos Trans. AGU*, 91, Fall Meet. Suppl., Abstract A51E-0178.

Jeffery, L., C.J. Poulsen, T.A. Ehlers, and **N. Insel** (2010), Andean uplift in the context of global climate change. *EGU General Assembly*, 12, EGU2010-13542

Poulsen, C.J., **N. Insel**, T.A. Ehlers, C. Sturm, and R. Simon (2009), Andean surface uplift, climate change, and the evolution of precipitation δ^{18}O *Eos Trans. AGU*, 90(54), Fall Meet. Suppl., Abstract EP51D-06.

Insel, N., C.J. Poulsen, C. Sturm, and T.A. Ehlers (2009), Paleo and present δ^{18}O variability of central Andean precipitation: constraints from isotope-tracking climate models, *GSA*, Abstract with Programs, 41, 521

Insel, N., C.J. Poulsen, and T. A. Ehlers (2008), Influence of Andean plateau rise on South American climate dynamics, *Eos Trans. AGU*, 89(53), Fall Meet. Suppl., Abstract T42A-01.

Insel, N., T. A. Ehlers, and M. Schaller (2007), Sensitivity of denudation rates to latitudinal and orographic variations in climate, central Andes, Bolivia, *Eos Trans. AGU*, 88(52), Fall Meet. Suppl., Abstract T12D-08.

Insel, N., T. A. Ehlers, C.J. Poulsen, E. Bachynski, and M. Schaller (2006), Quantifying Quaternary climate variability and erosion of the central Andes with paleoclimate modeling and cosmogenic ^{10}Be, *Eos Trans. AGU*, 87(51), Fall Meet. Suppl., Abstract T11A-0413.

Bibliography

Alpers, C. N. and Brimhall, G. H. Middle Miocene climate change in the Atacama Desert, northern Chile: Evidence from supergene mineralization at La Escondida. *Geological Society of America Bulletin*, 100:1640 – 1656, 1988.

Barnes, J. B. and Ehlers, T. End member models for Andean Plateau uplift. *Earth Science Reviews*, 97(1-4):105–132, 2009.

Berry, E. W. The fossil flora of Potosi, Bolivia. *Johns Hopkins University Studies in Geology*, 13:1–67, 1939.

Ehlers, T. and Poulsen, C. J. Influence of Andean uplift on climate and paleoaltimetry estimates. *Earth and Planetary Science Letter*, 281:238–248, 2009.

Elger, K., Oncken, O. and Glodny, J. Plateau-style accumulation of deformation: Southern Altiplano. *Tectonics*, 24:TC4020, doi:10/1029/2004TC001675, 2005.

Garzione, C. N., Molnar, P., Libarkin, J. and MacFadden, B. Rapid late Miocene rise of the Bolivian Altiplano: Evidence for removal of mantle lithosphere. *Earth and Planetary Science Letters*, 241:543–556, 2006.

Ghosh, P., Garzione, C. and Eiler, J. Rapid uplift of the Altiplano revealed through 13C-18O bonds in paleosol carbonates. *Science*, 311:511 – 515, 2006.

Graham, A., Gregory-Wodzicki, K. M. and Wright, K. L. A Mio-Pliocene palynoflora from the Eastern Cordillera, Bolivia: implications for the uplift history of the central Andes. *American Journal of Botany*, 88(9):1545–1557, 2001.

Gregory-Wodzicki, K. M. Uplift history of the Central and Northern Andes; a review. *Geological Society of America Bulletin*, 112(7):1091–1105, 2000.

Gregory-Wodzicki, K. M., McIntosh, W. C. and Velasquez, K. Climatic and tectonic implications of the late Miocene Jakokkota Flora, Bolivian Altiplano. *Journal of South American Earth Sciences*, 11(6):533–560, 1998.

Gubbels, T. L., Isacks, B. L. and Farrar, E. High-level surfaces, plateau uplift, and foreland development, Bolivian central Andes. *Geology*, 21(8):695–698, 1993.

Hartley, A. J., Sempere, T. and Worner, G. A comment on "Rapid late Miocene rise of the Bolivian Altiplano: Evidence for removal of mantle lithosphere" by C.N. Garzione et al. [Earth Planet. Sci. Lett. 241 (2006) 543-556. *Earth and Planetary Science Letter*, 259:625–629, 2007.

Horton, B. K. Erosional control on the geometry and kinematics of thrust belt development in the central Andes. *Tectonics*, 18(6):1292–1304, 1999.

Horton, B. K. Revised deformation history of the central Andes: Inferences from Cenozoic foredeep and intermontane basins of the Eastern Cordillera, Bolivia. *Tectonics*, 24(TC3011):doi:10.1029/2003TC001619, 2005.

Isacks, B. L. Uplift of the Central Andean Plateau and bending of the Bolivian Orocline. *Journal of Geophysical Research*, 93(4):3211–3231, 1988.

Kutzbach, J. E., Prell, W. L., Ruddiman, W. F. and Anonymous. Sensitivity of Eurasian climate to surface uplift of the Tibetan Plateau. In *Journal of Geology*, volume 101, pages 177–190. 1993.

Lamb, S. and Davis, P. Cenozoic climate change as a possible cause for the rise of the Andes. *Nature*, 425:792–797, 2003.

Lenters, J. D. and Cook, K. H. Simulation and diagnosis of the regional summertime precipitation climatology of South America. *Journal of Climate*, 8(12):2988–3005, 1995.

Masek, J. G., Isacks, B. L., Gubbels, T. L. and Fielding, E. J. Erosion and tectonics at the margins of continental plateaus. *Journal of Geophysical Research*, 99(7):13,941–13,956, 1994.

McQuarrie, N., Horton, B. K., Zandt, G., Beck, S. and DeCelles, P. G. Lithospheric evolution of the Andean fold-thrust belt, Bolivia, and the origin of the central Andean plateau. *Tectonophysics*, 399(1-4):15–37, 2005.

Molnar, P., England, P. and Martinod, J. Mantle dynamics, uplift of the Tibetan Plateau, and the Indian monsoon. *Reviews of Geophysics*, 31(4):357–396, 1993.

Montgomery, D. R., Balco, G. and Willett, S. D. Climate, tectonics, and the morphology of the Andes. *Geology*, 29(7):579–582, 2001.

Muoz, N. and Charrier, R. Uplift of the western border of the Altiplano on a west-vergent thrust system, Northern Chile. *Journal of South American Earth Sciences*, 9(3-4):171–181, 1996.

Poulsen, C. J., Ehlers, T. and Insel, N. Onset of convective rainfall during gradual late Miocene rise of the central Andes. *Science*, page doi:10.1126/science.1185078, 2010.

Prell, W. and Kutzbach, J. Sensitivity of the Indian monsoon to forcing parameters and implications for its evolution. *Nature*, 360:647–652, 1992.

Quade, J., Garzione, C. and Eiler, J. Paleoelevation reconstructions using pedogenic carbonates. *Reviews in Mineralogy and Geochemistry*, 66:53–87, 2007.

Richter, F. M., Rowley, D. B. and DePaolo, D. J. Sr isotope evolution of seawater: The role of tectonics. *Earth and Planetary Science Letters*, 109(1-2):11–23, 1992.

Royden, L. Coupling and decoupling of crust and mantle in convergent orogens; implications for strain partitioning in the crust. *Journal of Geophysical Research, B, Solid Earth and Planets*, 101(8):17,679–17,705, 1996.

Ruddiman, W. F. and Kutzbach, J. E. Forcing of late Cenozoic Northern Hemisphere climate by plateau uplift in southern Asia and the American West. *Journal of Geophysical Research*, 94(D15):18,409–18,427, 1989.

Ruddiman, W. F., Raymo, M. E., Prell, W. L. and Kutzbach, J. E. The uplift-climate connection; a synthesis. In Ruddiman, W. F., editor, *Tectonic uplift and climate change*, pages 471–515. Plenum Press, New York, 1997.

Sebrier, M., Lavenu, A., Fornari, M., Soulas, J. P. and Anonymous. Tectonics and uplift in Central Andes (Peru, Bolivia and northern Chile) from Eocene to present. In *Seminaire; Geodynamique des Andes centrales. Seminar on Geodynamics of the Central Andes*, volume 3, pages 85–106. Office de la Recherche Scientifique et Technique Outre-Mer (ORSTOM), Bondy, 1988.

Sempere, T., Hartley, A. J. and Roperch, P. Comment on "Rapid uplift of the Altiplano revealed through 13C-18O bonds in paleosol carbonates". *Science*, 314:760, 2006.

Singewald, J. T. and Berry, E. W. The geology of the Corocoro copper district of Bolivia. *Johns Hopkins University Studies in Geology*, 1:1–117, 1922.

Sobel, E. R. and Strecker, M. R. Uplift, exhumation and precipitation: tectonic and climatic control of Late Cenozoic landscape evolution in the northern Sierras Pampeanas, Argentina. *Basin Research*, 15(4):431–451, 2003.

Strecker, M. R., Alonso, R. N., Bookhagen, B., Carrapa, B., Hilley, G. E., Sobel, E. R. and Trauth, M. H. Tectonics and climate of the southern Central Andes. *Annual Review of Earth and Planetary Sciences*, 35:747–787, 2007.

CHAPTER II

Climate control on temporal and spatial variability of Andean precipitation δ^{18}O

2.1 Abstract

The stable oxygen isotopic composition of precipitation ($\delta^{18}O_p$) is used as a proxy for modern and paleo atmospheric, biological, and surface processes. Although the physical processes that fractionate ^{18}O in vapor are known, regional controls and sources of $\delta^{18}O_p$ are not well understood. Here we present results from a limited-domain general circulation model (REMOiso) to quantify regional controls on modern (1976−1999) interannual and spatial variations of $\delta^{18}O_p$ across four Andean domains spanning 50° latitude. Results are compared to observed δ $^{18}O_p$ from meteorological stations. Simulated annual amount-weighted mean $\delta^{18}O_p$ ranges between -4 and -7‰ (0-5°S), -8 and -20‰ (14-26°S), -4 and -8.5‰ (30-35°S), and -7 to -10‰ (45-50°S). Annual isotopic lapse rates on the windward side of the mountain vary between -1.49 and -0.04‰ km^{-1} (0-5°S), -2.46 and -0.05‰ km^{-1} (14-26°S), -1.39 and -0.42‰ km^{-1} (30-35°S), and -3.16 and -2.46‰ km^{-1} (45-50°S). Relationships between climate and $\delta^{18}O_p$ vary along the Andes. In the northern Andes, interannual variations

---

Official citation:
Insel, N., C.J. Poulsen, C. Sturm, T.A. Ehlers (in review). Climate controls on temporal and spatial variability of Andean precipitation δ^{18}O. *Climate Dynamics*

in $\delta^{18}O_p$ are mainly associated with precipitation amounts driven by low-latitude sea-surface temperature. In the northern central Andes, $\delta^{18}O_p$ correlates with precipitation amount, which is related to the position of the Bolivian High and moisture source. In the southern central Andes, $\delta^{18}O_p$ variability is mainly influenced by rain-out linked to the strength of zonal winds and vertical ascent on the Andean flanks. In the southern Andes, temperature determines $\delta^{18}O_p$ variability. The regional climate - $\delta\ ^{18}O_p$ relationships are discussed in the context of interpretations of Quaternary ice core and pre-Quaternary sedimentary $\delta^{18}O_p$ proxy records.

2.2 Introduction

The stable isotopic composition of meteoric water ($\delta^{18}O_p$) is a function of hydrologic and atmospheric processes that act on vapor as it is transported from its source region to its destination. In many regions, the isotopic composition of meteoric water is tightly linked to climatic (i.e. temperature, amount of precipitation) or land-surface (i.e. elevation, vegetation) parameters. These modern relationships have been used to extract paleoclimatic and paleoenvironmental conditions from terrestrial isotopic records in geologic archives. For example, in tropical and subtropical South America, past climate conditions through Cenozoic and Quaternary times have been inferred from proxy records, such as ice cores (Thompson et al., 1985, 1995; Vimeux et al., 2008), fluid inclusions in chemical sediments (Godfrey et al., 2003), and speleothem records (Cruz et al., 2009). The variations in isotopic compositions of precipitation stored in mountain glaciers have been variously interpreted to represent Quaternary changes in local temperature (Thompson et al., 2000), atmospheric vapor content (Broecker, 1997), runoff efficiency (Pierrehumbert, 1999), tropical Pacific sea-surface temperatures (Bradley et al., 2003), or upwind rainout (Hoffmann et al., 2003; Ramirez et al., 2003). More recently, archives of precipitation δ ^{18}O preserved in ancient soil carbonates have been interpreted to indicate abrupt Andean surface uplift by ~2.5 km (Garzione et al., 2006) or climate change associated with uplift of the Andean Plateau (Ehlers and Poulsen, 2009; Insel et al., 2009) and the onset of convective rainfall over the central Andes during the late Miocene (Poulsen et al., 2010).

The controversy in the interpretation of $\delta^{18}O_p$ records arises because the processes that control the isotopic composition of meteoric water in South America are not completely understood. In high-latitude regions, $\delta^{18}O_p$ is strongly, inversely related to surface air temperature due to kinetic fractionation. In low latitudes, where temperature gradients and variations are smaller, other factors are more important. For example, previous studies have documented systematic variations in isotope ratios of precipitation with the source of moisture and precipitation rate (e.g., Dansgaard, 1964; Rozanski et al., 1993). Quantifying the influence of different processes on the isotopic composition of meteoric water is required for understanding both modern and past $\delta^{18}O_p$ and climate variability.

In South America, our understanding of meteoric $\delta^{18}O_p$ is hampered by the availability of modern $\delta^{18}O_p$ records (e.g. in the International Atomic Energy Agency Global Network of Isotopes in Precipitation (IAEA-GNIP) database), which are short, discontinuous, and limited in spatial coverage (e.g., Rozanski et al., 1993; Garcia et al., 1998; Aravena et al., 1999; Gonfiantini et al., 2001). To overcome these deficiencies, global general circulation models (GCMs) with the ability to track stable water isotopes have been used to understand the major climate controls on the isotopic composition in meteoric water (e.g., Jouzel et al., 1987; Cole et al., 1999; Hoffmann et al., 2000; Vuille et al., 2003a; Sturm et al., 2007). Climate modeling studies emphasize that there is no single control on South American $\delta\ ^{18}O_p$. Precipitation amount, moisture source, moisture transport history and the degree of rainout upstream, temperature, atmospheric circulation, and re-evaporation from vegetation-covered continental surfaces all of these processes can be important in influencing $\delta^{18}O_p$ in certain areas (Vuille et al., 2003a; Vuille and Werner, 2005; Sturm et al., 2007). In addition, interannual variations in $\delta^{18}O_p$ have been related to El Niño / Southern Oscillation (ENSO) (e.g., Vuille and Werner, 2005). These studies have focused mainly on the large-scale distribution and seasonality of meteorological processes influencing $\delta\ ^{18}O_p$. Moreover, over regions with steep topographic gradients, such as the Andes, coarse resolution global GCMs tend to underestimate peak elevations and smooth topographic gradients. To address these issues, water isotope modules have been incorporated into higher resolution, limited-domain climate models. Using the REMOiso model, Sturm et al. (2005, 2007) demonstrate improved simulation of climatic and isotopic feature across South America in regions where higher resolution improved the simulation of local processes.

The goal of this study is to investigate the processes that control variability in the isotopic composition of precipitation in the Andean region, the area from which most geological archives have been extracted. To do so, we conduct climate simulations over South America using REMOiso, a high-resolution, limited-domain, general circulation model (GCM) fitted with water isotope diagnostics. To address paleoclimate and paleoaltimetry issues, we focus on both interannual variability in $\delta^{18}O_p$ and isotopic lapse rates. More specifically, we (1) describe interannual variations of $\delta^{18}O_p$ and precipitation along the Andes, (2) analyze spatial and temporal variations in isotopic lapse rates, and (3) investigate the processes that control regional and interannual variability in $\delta^{18}O_p$. Finally we discuss the implications of $\delta\ ^{18}O_p$ variability on paleoclimate and paleoaltimetry reconstructions. Our analysis is focused on the northern, central, and southern Andes to quantify the dominant processes influencing $\delta^{18}O_p$ in mountainous regions for different climatic zones (tropical, subtropical, mid-latitudes) (Fig. 2.1).

2.3 Methods

We use the limited-domain, regional climate model REMOiso to quantify modern interannual and spatial variations of $\delta^{18}O_p$ along and across the Andes. REMOiso is a numerical, three-dimensional regional circulation model (RCM), with a dynamical core that is adopted from the former numerical weather prediction model of the German Weather Service (EUROPA-MODELL, EM) (Majewski, 1991). It is a primitive-equation, hydrostatic, compressible model with hybrid-vertical coordinates. The physical parameterization scheme was implemented from the global climate model ECHAM-4 (Roeckner et al., 1996). Critical hydrological processes are parameterized as sub-grid-scale processes. The cumulus convection, subdivided in shallow, middle and deep convection, follows the bulk mass concept of Tiedtke (1989), and was adapted according to Nordeng (1994). Organized detrainment, computed for a spectrum of clouds detraining at different heights, is related to buoyancy instead of moisture convergence. Cloud water detrained at the top of cumulus clouds enters as a source term in the stratiform cloud equation. Stratiform cloud water is computed as a function of phase changes and precipitation formation (Sturm et al., 2005). Soil temperatures are computed from diffusion equations at 5 levels between 10 m depth and the surface, with an additional diffusion through the snow layer

(Sturm et al., 2005). Only bulk soil moisture is computed (bucket-type). Apart from soil moisture, two other prognostic reservoirs are considered: interception of precipitation by the canopy (skin layer) and snow layer depth.

Isotope fractionation and transport processes are embedded at all stages of the hydrological cycle by defining isotopic counterparts to all water-related variables. Therefore, the species H_2O^{18} and HDO are treated independently from the predominant H_2O^{16}, but undergo the same processes including equilibrium and kinetic fractionations (Sturm et al., 2005). Condensation into droplets or ice crystals is treated as an equilibrium fractionation under temperate conditions. Partial re-evaporation of rain drops below the cloud base and the resulting kinetic fractionation is treated differently for stratiform and convective clouds, identically to the ECHAM parameterization (Hoffmann et al., 1998; Sturm et al., 2005). Stable water isotopes are treated as passive tracers in soil moisture and snow layer. Isotopic compositions are assimilated at the lateral boundaries in a similar way as other prognostic variables. For a more detailed description of the current version of REMOiso (5.0-EC4) and its water isotope module see Sturm et al. (2005, 2007).

REMOiso experiments are forced using boundary conditions, including stable water isotopes, from the ECHAM-4 global climate model with specified sea-surface temperatures (SSTs) derived from monthly satellite data (i.e. HadSST; Hoffmann et al. 1998). Lateral and surface boundary conditions for the prognostic variables (surface pressure, air temperature, SSTs, horizontal wind speed, water vapor and liquid water content, stable isotopes) are specified every 6 hours to account for the diurnal cycle. The prognostic variables are linearly interpolated between time steps.

A 24-year simulation (1976-1999) was performed for South America using a continental scale domain with 0.5° (~55 km) horizontal resolution with 160x120 grid points and 31 vertical levels (Fig. 2.1). Due to long simulation times, REMOiso was not run continuously through 24 years. Instead, each simulation year was conducted as an individual experiment representing 15 months (October of the previous year to December of the simulation year) and analyzed for the actual year (January-December). Each simulation was initialized from a spinup simulation of 21 month (January to October) with boundary conditions for year 1993 to assure the same initial conditions for each simulation in the experiment series. Year 1993 was chosen for the spinup, because it deviated least from the 30yr precipitation mean over the study area.

2.4 Large-scale South American climate and isotopes

REMOiso captures the general climatology of South America. The model simulates well the distribution of precipitation across South America, including the regions of maximum precipitation (Amazon Basin, northern, central, and southern Andes, South Atlantic Convergence Zone), and arid conditions over northeast Brazil, Venezuela, northern Chile and southern Argentina (Fig. 2.1b) The main discrepancy (~20% difference) between predicted and observed precipitation occurs over the southwestern part of the Amazon Basin. We attribute this discrepancy to the convective mass flux parameterization scheme in REMOiso (Nordeng, 1994; Aldrian et al., 2004) that results in intense evapotranspiration and overestimation of the atmospheric moisture component that is recycled over the Amazon Basin. A similar bias has been found in other general circulation model simulations of South American climate (e.g., Lenters and Cook, 1995; Rojas and Seth, 2003; Insel et al., 2009). REMOiso also overestimates precipitation (~30%) along the upstream flank of the

Andes. This discrepancy is not unique to REMO (Insel et al., 2009), and results from an overestimation of convective precipitation in orographic regions characterized by large moisture convergence (Sturm et al., 2007).

The low-level circulation and moisture transport is well represented in the simulations (Fig. 2.1b). Northeasterly trade winds flow from the Atlantic Ocean across the Amazon Basin. From there, northeasterly winds transport water vapor into the central part of South America and to the eastern slopes of the Andes. Westerly flow from the South Pacific Ocean is the primary source for South American precipitation south of 40°S (Fig. 2.1b).

Simulated annual surface temperatures agree well in structure and magnitude with observed values with maximum temperatures in northern Argentina, northeast Brazil and Venezuela (Fig. 2.1c). The Chaco Low, a low-pressure system observed in central South America and usually characterized by high temperatures, is well developed. However, surface temperatures over the eastern part of the Amazon Basin are too high (approximately 2-4°C). A seasonally constant LAI (leaf area index) and surface albedo, as currently implemented in REMO5.0 (and later improved in newer versions) underestimates transpiration and latent heat transfer, resulting in temperatures that are too high.

REMOiso realistically captures the large-scale patterns in $\delta^{18}O_p$ compared to observations (Fig. 2.1d). Simulated $\delta^{18}O_p$ is relatively high over the Amazon Basin due to evapotranspiration and slightly decreases to the west and south due to isotopic fractionation through the preferential removal of the heavier isotope with further condensation (the continental effect). In agreement with previous studies (e.g., Salati et al., 1979) the continental gradient over the Amazon Basin is small due to strong evapotranspiration by plants which replenishes the atmosphere with isotopi-

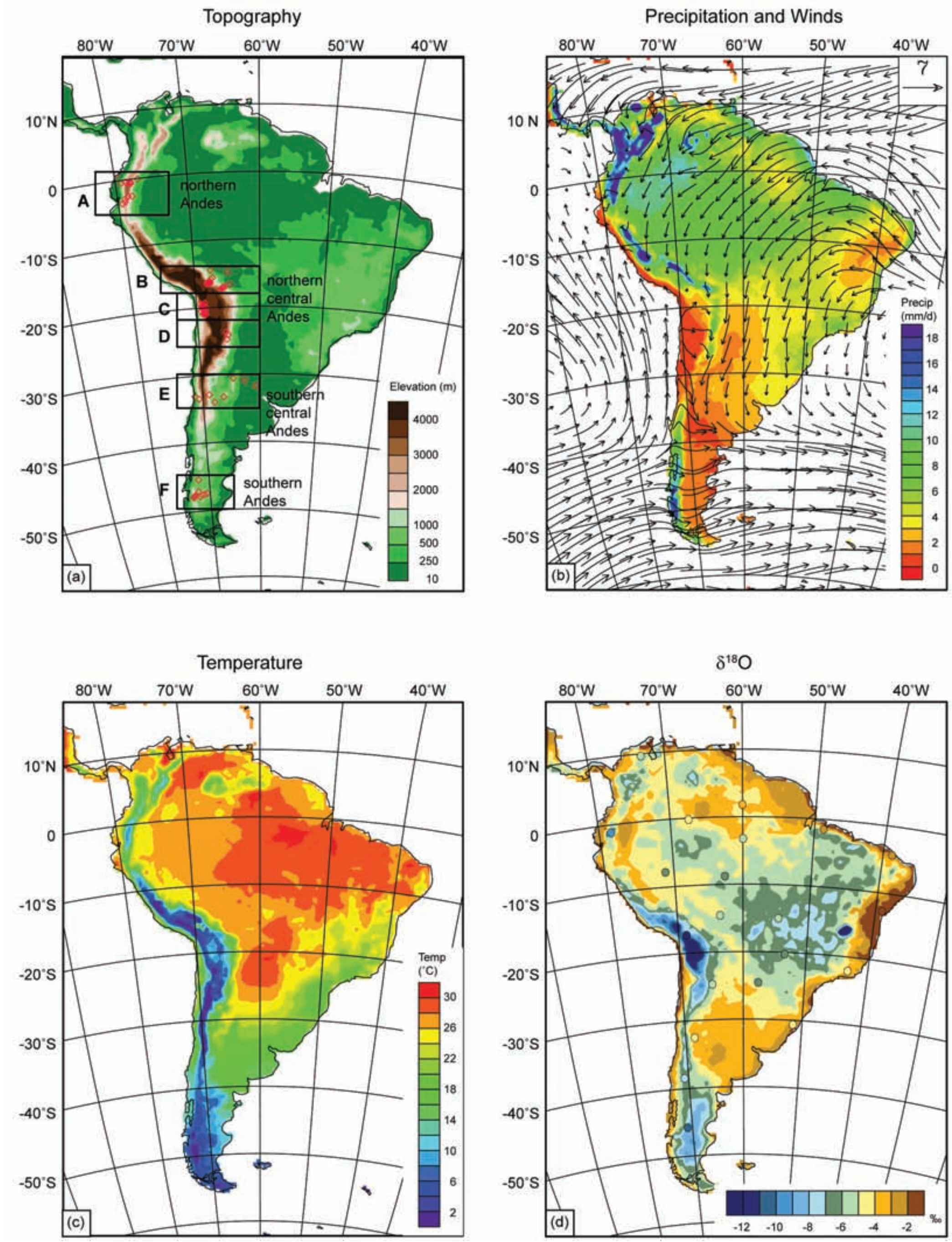

Figure 2.1: Map of the South American domain and REMOiso climatology for the time period 1976 to 1999. (a) Map of South American topography used in REMOiso is from the United States Geological Survey (USGS). Solid boxes indicate the regions on which our analysis focuses. Red diamonds show available observational meteoric $\delta^{18}O_p$ data. (b) Simulated mean annual precipitation (mm day^{-1}) and wind vectors (m s^{-1}) over South America. (c) Simulated mean annual surface temperature (°C). (d) Simulated annual amount-weighted mean $\delta^{18}O_p$ (‰) values. Colored dots represent $\delta^{18}O_p$ at certain GNIP stations.

cally enriched water vapor. Once air masses reach the Andes, adiabatic cooling and precipitation associated with the rising masses contribute to the isotope depletion of vapor (altitude effect) and results in the lowest $\delta^{18}O_p$ values in South America. Low $\delta^{18}O_p$ is also observed in southern South America due to the temperature effect that accounts for progressive depletion of precipitation $\delta^{18}O_p$ at higher latitudes.

2.5 Results

2.5.1 Interannual $\delta^{18}O_p$ variability

In this section, we describe the distribution and variability in $\delta^{18}O_p$ along and across the Andes. Annual amount-weighted mean $\delta^{18}O_p$ for the 24 individual years between 1976 and 1999 as well as the annual amount-weighted climatological mean are shown in Fig. 2.3. Results are compared to observations from the northern, northern central, southern central, and southern Andes (Fig. 2.1). Unless specifically stated otherwise climatological means (24-yr averages) are presented. Although our comparisons are based on annual amount-weighted mean $\delta^{18}O_p$, we also report the climatological amount-weighted monthly minimum and maximum $\delta^{18}O_p$ to indicate the full range of $\delta^{18}O_p$ variability and to facilitate comparison with monthly observations and proxy records.

Northern Andes

The northern Andes between 0 and 5°S are ~50-100 km wide with elevations up to 3500 m (Fig. 2.1a, profile A). The area is characterized by a bimodal distribution of precipitation related to seasonal displacement of the Intertropical Convergence Zone (ITCZ). The northward passage of the ITCZ over the domain causes a precipi-

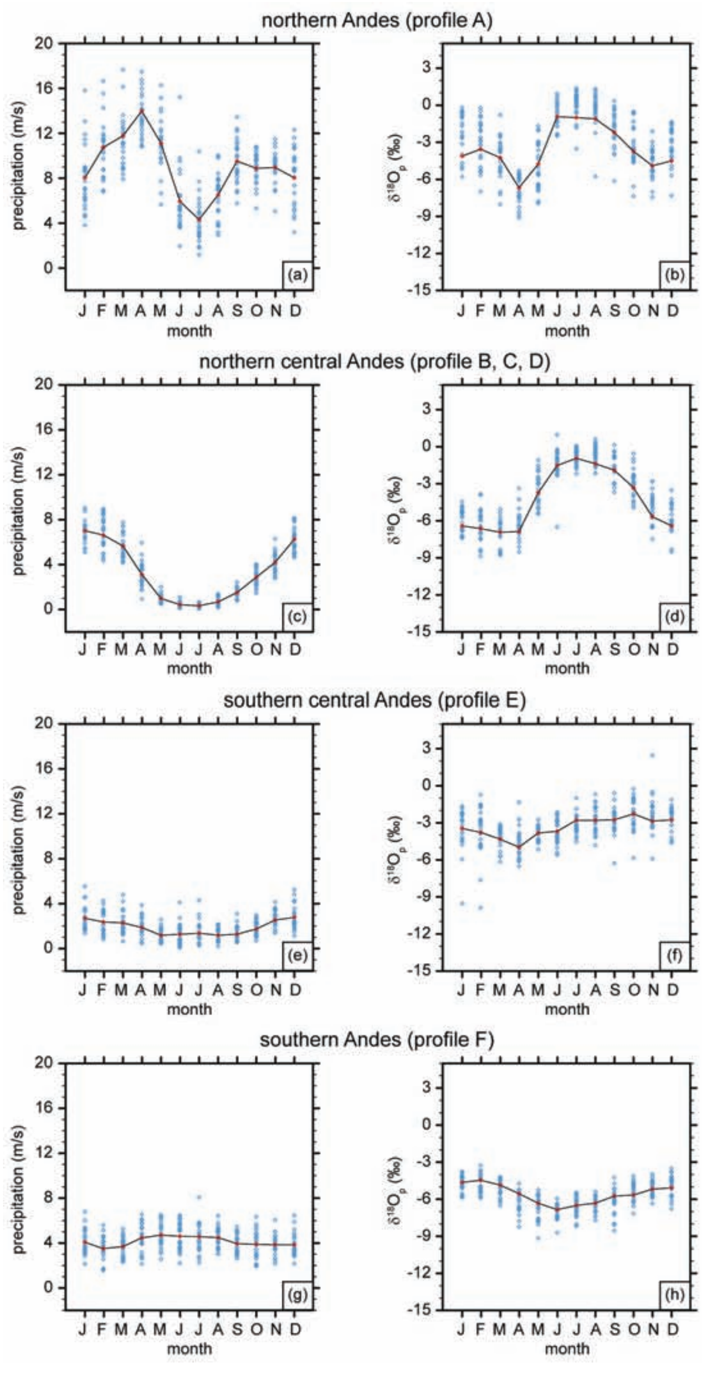

Figure 2.2: Simulated monthly precipitation (mm day^{-1}; left panel) and $\delta^{18}O_p$ (‰; right panel) averaged over each transect. Blue diamonds represent monthly values for individual years; red filled circles and black line indicate the climatological mean precipitation.

tation maximum between March and May, while the southward passage of the ITCZ produces a second maximum in the amount of precipitation between September and November (Fig. 2.2a). The most depleted stable water isotope compositions are associated with months of highest precipitation amount (Fig. 2.2b). Simulated annual amount-weighted mean $\delta^{18}O_p$ values are -3 to -4‰ east of the Andes, then drop to approximately -5‰ over the Andes, and increase to values of ~-2‰ in coastal regions (Fig. 2.3a). Interannual $\delta^{18}O_p$ variability is relatively small, varying by approximately ±1.5‰ over the Andes (Fig. 2.3a). The climatological monthly maximum and minimum $\delta^{18}O_p$ over the Andes (above 2000 m) is -1 and -9‰, respectively (Fig. 2.3a). Modeled $\delta^{18}O_p$ is slightly higher than observed $\delta^{18}O_p$ from meteorological stations situated along two transects in the northern Andes region (Fig. 2.1a). Observed annual amount-weighted mean precipitation $\delta^{18}O_p$ values range from about -2‰ in coastal stations to -10‰ in stations located above 3000 m (Fig. 2.3a) (Garcia et al., 1998).

Northern central Andes

The northern central Andes (14-26°S) form the widest and highest portion of the Andean Cordillera with model elevations exceeding 4500 m (Fig. 2.1, profiles B-D). A significant seasonal precipitation cycle exists in the Andean plateau region with precipitation maxima between December and March (Fig. 2.2c), accompanied by the most depleted $\delta^{18}O_p$ (Fig. 2.2d). Because the northern central Andes are characterized by a significant climate gradient with much higher precipitation in the north and drier conditions in the south (Fig. 2.1b), we distinguish three northern central Andean transects, northern (B), central (C), and southern (D).

In the northern transect (14-18°S; Fig. 2.1a, profile B) the South American low-

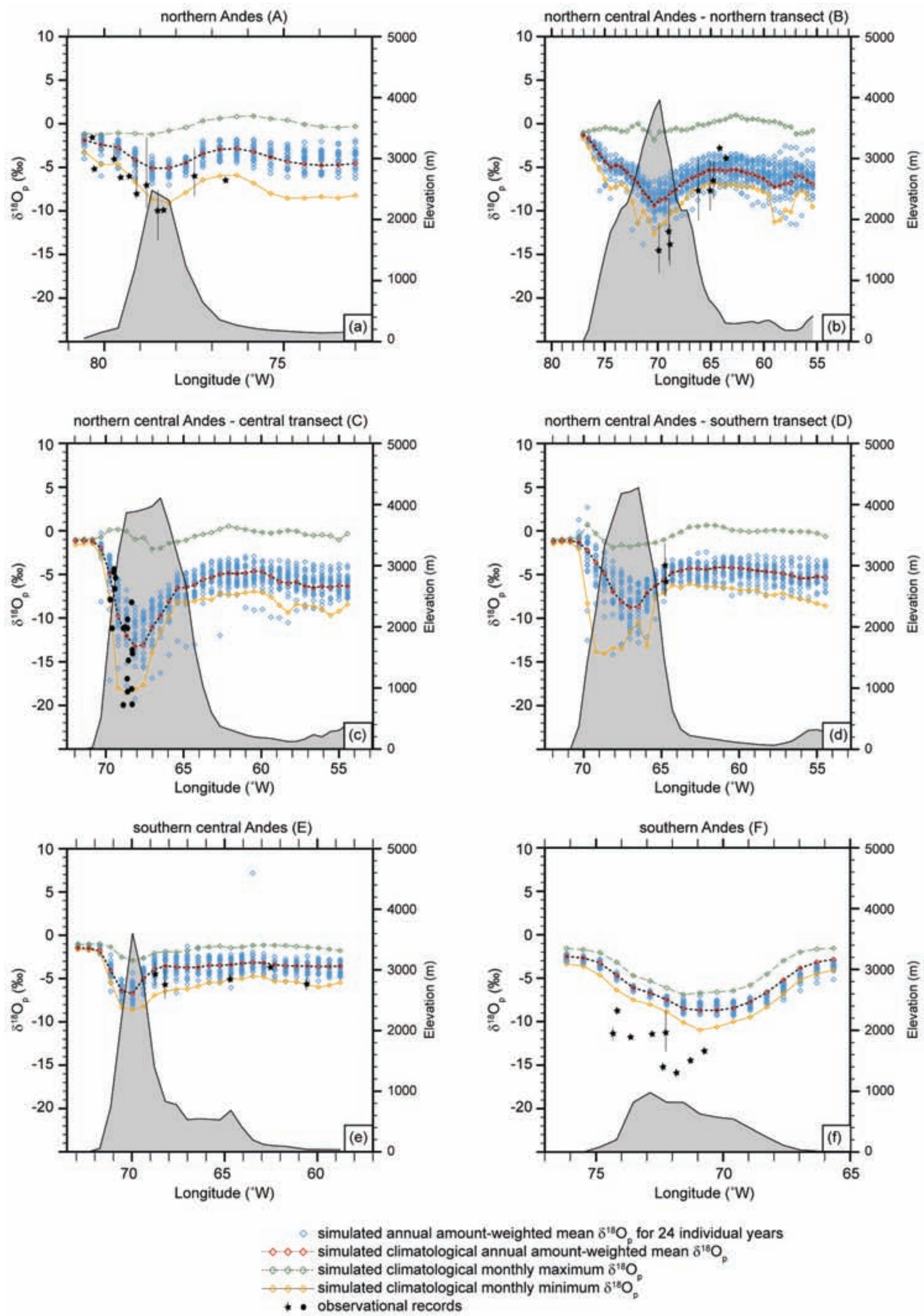

Figure 2.3: East-west transects showing $\delta^{18}O_p$ distribution across the Andes for each domain. The gray shading indicates topography (m). Blue diamonds represent annual amount-weighted mean δ $^{18}O_p$ (‰) for individual years between 1976 and 1999; red diamonds indicate the climatological annual amount-weighted mean δ $^{18}O_p$ (‰). Green and yellow diamonds show the monthly maximum and minimum $\delta^{18}O_p$ (‰), respectively. Black stars show observed annual amount-weighted $\delta^{18}O_p$ (‰); black polygons show observed $\delta^{18}O_p$ (‰) from individual storm events or amount-weighted mean monthly data (a) Northern Andes; (b-d) northern central Andes; (e) southern central Andes; (f) southern Andes

level jet is the dominant climatic feature, transporting moisture from the Amazon Basin along the eastern flank of the Andes (Fig. 2.1b, see also Insel et al. 2009). Simulated annual amount-weighted mean $\delta^{18}O_p$ decreases from -6‰ across the eastern Andean flank to -9.5‰ over the plateau area and then increases to -1‰ along the Pacific coast. The isotopic composition of rainfall for individual years ranges between -4 and -14‰ across the mountain range (Fig. 2.3). The climatological monthly maximum and minimum $\delta^{18}O_p$ over the plateau area is -1 and -13‰ (Fig. 2.3b). Observed monthly data on the isotopic composition of precipitation for this region are available for 2 years (Fig. 2.1a and Fig. 2.3b; Gonfiantini et al. (2001)). The annual amount-weighted isotope data for 1983, which was an anomalously dry year due to El Niño conditions, vary between -3.4‰ in the lowlands (300 m) to -11.7‰ in the high altitude areas (>5000 m; Gonfiantini et al. (2001)). In 1984, a relatively wet year, annual amount-weighted $\delta^{18}O_p$ are more negative with values between -9.5 to -20.4‰ (Gonfiantini et al. 2001). $\delta^{18}O_p$ observations for the relatively dry year fall within the modeled range, while $\delta^{18}O_p$ in the wet year is more depleted than simulated $\delta^{18}O_p$.

The central transect (18-22°S; Fig. 2.1a, profile C) includes the widest part of the Andean plateau and shows the most depleted $\delta\ ^{18}O_p$ values in South America. Moisture is mainly supplied by transport of vapor from the Amazon Basin to the eastern slopes of the Andes (Fig. 2.1b). Simulated annual amount-weighted mean $\delta\ ^{18}O_p$ is -5 to -6‰ in the eastern foreland. It decreases to approximately -13‰ in the central Andes, with annual values ranging between -7 and -19‰ for individual years at elevations above 3800 m (Fig. 2.3c). The annual amount-weighted mean $\delta^{18}O_p$ increases to -2 to -5‰ on the Pacific coast. Interannual variability in $\delta^{18}O_p$ is large varying by over 10‰ (Fig. 2.3c). The climatological monthly maximum and minimum $\delta^{18}O_p$ over the plateau is -1 and -19‰, respectively. There are currently no mean-annual $\delta^{18}O_p$ observations for the central transect, because $\delta^{18}O_p$ is only available for individual days or a few months. $\delta^{18}O_p$ from individual storm events along the western flank of the Andes in northern Chile (Fig. 2.1a) range between -15 and -20‰ at high altitude (>3000 m) stations and $\delta^{18}O_p$ between -5 and -10‰ at lower elevations (<3000 m) (Fritz et al., 1981; Aravena et al., 1999) and are in good agreement with model results (Fig. 2.2c).

In the southern transect (22-26°S; Fig. 2.1a, profile D) the annual amount-weighted mean $\delta^{18}O_p$ decreases from -5‰ in the eastern foreland to -9‰ in the mountain region and increases across the western flank up to -2‰ (Fig. 2.3d). Interannual variability is large with ±4‰ over the plateau area. The climatological monthly maximum and minimum $\delta^{18}O_p$ is -2 and -15‰ along both flanks (Fig. 2.3d). Annual amount-weighted mean $\delta^{18}O_p$ are available from two low-elevation (below 1500 m) meteorological stations situated along the eastern flank of the Argentinean Andes (Fig. 2.1a), and range between -1.3 and -7.6‰ (Rozanski et al., 1993). Observations are in good agreement with model predicted $\delta^{18}O_p$ (Fig. 2.3d).

Southern central Andes

The southern central Andes (30-35°S) have elevations up to 4000 m and are ~150 km wide (Fig. 2.1a, profile E). The atmospheric circulation and precipitation in this area are characterized by two regimes depending on the season. In austral winter, westerly flow across the Andes produces a precipitation maximum along the western flank, while austral summer is dominated by low-level northeasterly moisture transport from the South Atlantic producing a precipitation maximum along the eastern flank (Fig. 2.1b). REMOiso simulates a seasonal precipitation maximum between November and February, while the most depleted isotope values occur between March and May (Fig. 2.2e, f). Annual amount-weighted mean $\delta^{18}O_p$ decreases from ~-4‰ on the eastern side to approximately -6‰ over the Andes to -1‰ along the Pacific coast (Fig. 2.3e). Interannual variability is less pronounced than in the northern central Andean regions; amount-weighted mean $\delta^{18}O_p$ values differ by ~2‰. The climatological monthly maximum $\delta^{18}O_p$ is -3‰, while the monthly minimum $\delta^{18}O_p$ is as low as -9‰ over high altitude regions (<3500 m).

Data for this transect exist from 5 low-elevation meteorological stations in Chile and Argentina (Fig. 2.1a; Rozanski et al. (1993)). The annual amount-weighted mean $\delta^{18}O_p$ for stations on the eastern side of the Andes is between -4 and -6‰ (Rozanski et al., 1993). No $\delta^{18}O_p$ data exist for the high elevation Andes. Overall, model results are consistent with the observational records (Fig. 2.3e).

Southern Andes

The southern Andes (~45-50°S) are ~100 km wide and have model elevations of 1500 to 2000 m (Fig. 2.1a, profile F). In contrast to the northern regions, the dominant moisture source is the South Pacific. Strong Westerlies result in orographic precipitation on the western side of the mountain range and a rain shadow on the eastern side (Fig. 2.1b). The seasonal precipitation maximum occurs between May and July, and is accompanied by the most depleted $\delta^{18}O_p$ values for that region (Fig. 2.2g, h). Annual amount-weighted mean $\delta^{18}O_p$ decreases from -2.5‰ along the Pacific coast to ~-6.5‰ at the highest elevations and to -8.5‰ downwind of peak elevations (Fig. 2.3f). Precipitation $\delta^{18}O_p$ increases to -3‰ at low elevation areas further east of the mountain range. This pattern reflects the decrease in $\delta^{18}O_p$ with increasing distance from the moisture source. Interannual variability in the south is small with annual amount-weighted mean $\delta^{18}O_p$ values for individual years within 1‰ of the average (Fig. 2.3f). The climatological monthly maximum and minimum $\delta^{18}O_p$ is -6.5 and -11‰, respectively, and is located downwind of peak elevations (Fig. 2.3f).

Simulated $\delta^{18}O_p$ values are more enriched than observed values from a transect across the southern Patagonian Andes (47° to 48°S) (Stern and Blisniuk, 2002). Observed $\delta^{18}O_p$ of the westernmost samples at ~73°W range between -9 and -12‰, while precipitation on the leeward side of the Andes (east of 72°15'W) has a mean δ^{18} O_p of -14.4‰ and ranges from -12 to -16‰ (Fig. 2.3f). In agreement with our model results, Stern and Blisniuk (2002) report a decrease in $\delta^{18}O_p$ on the leeward side of the Andes.

Comparison between transects

All transects have similar cross-Andean $\delta^{18}O_p$ distributions with relatively enriched values along the Pacific coast, strongly depleted isotopic composition over the Andes and intermediate values along the eastern side (Fig. 2.3a-f). However, the absolute magnitudes of precipitation $\delta^{18}O_p$ and the interannual variability differ. The interannual variability is most significant in the northern central Andes with variations from the amount-weighted mean $\delta^{18}O_p$ of up to ±6‰ (Fig. 2.3b-d). Interannual variability is much less pronounced in the northern, southern central, and southern Andes. Annual amount-weighted mean $\delta^{18}O_p$ values in these regions generally differ by less than 2‰ (Fig. 2.3a, e, f). Overall, observations and model result are in good agreement. Model results are slightly more enriched in comparison to observed $\delta^{18}O_p$ in the northern and southern Andes.

2.5.2 Isotopic lapse rates

In this section, we report and compare modeled and observed isotopic lapse rates. Modeled isotopic lapse rates, shown in Fig. 2.4, are calculated by linear regression of $\delta^{18}O_p$ for all modeled data points from 24 individual years and are reported with their 2σ error (Table 2.1). Lapse rates were also calculated from meteorological data (Table 2.2). Observed lapse rates for individual years fall within the period simulated by REMOiso (1976-1999) with the exception of one year in the southern Andes where observations are available for year 2000. As discussed in more detail below (section 2.6.5), the lengths of the observed records are much shorter than the model period. Rather than compare individual years, we compare model and observed data to determine if the variability in the model captures the observed values.

We note that by definition the lapse rate is defined as the rate of decrease of an atmospheric variable (e.g. temperature) with height. However, to be consistent with previous studies, we report isotopic lapse rates as the change in $\delta\ ^{18}O_p$ with altitude. Thus, a $\delta^{18}O_p$ decrease of -1‰ km^{-1} elevation gain is reported as a lapse rate of -1‰ km^{-1}, rather than 1‰ km^{-1}.

Northern Andes

Simulated annual amount-weighted $\delta^{18}O_p$ lapse rates in the northern Andes are -0.88 $\pm$ 0.69‰ km^{-1} ($r = 0.58$) along the eastern flank and -1.13 $\pm$ 0.46‰ km^{-1}($r = 0.66$) along the western flank (Fig. 2.4a, b; Table 2.1). The modeled isotopic lapse rate is smaller than observed. Isotopic lapse rates calculated from annual amount-weighted $\delta^{18}O_p$ from multi-year (1- to 18-year) meteorological records are -1.75‰ km^{-1} ($r = 0.70$) along the eastern flank and -2.03‰ km^{-1} ($r = 0.74$) along the

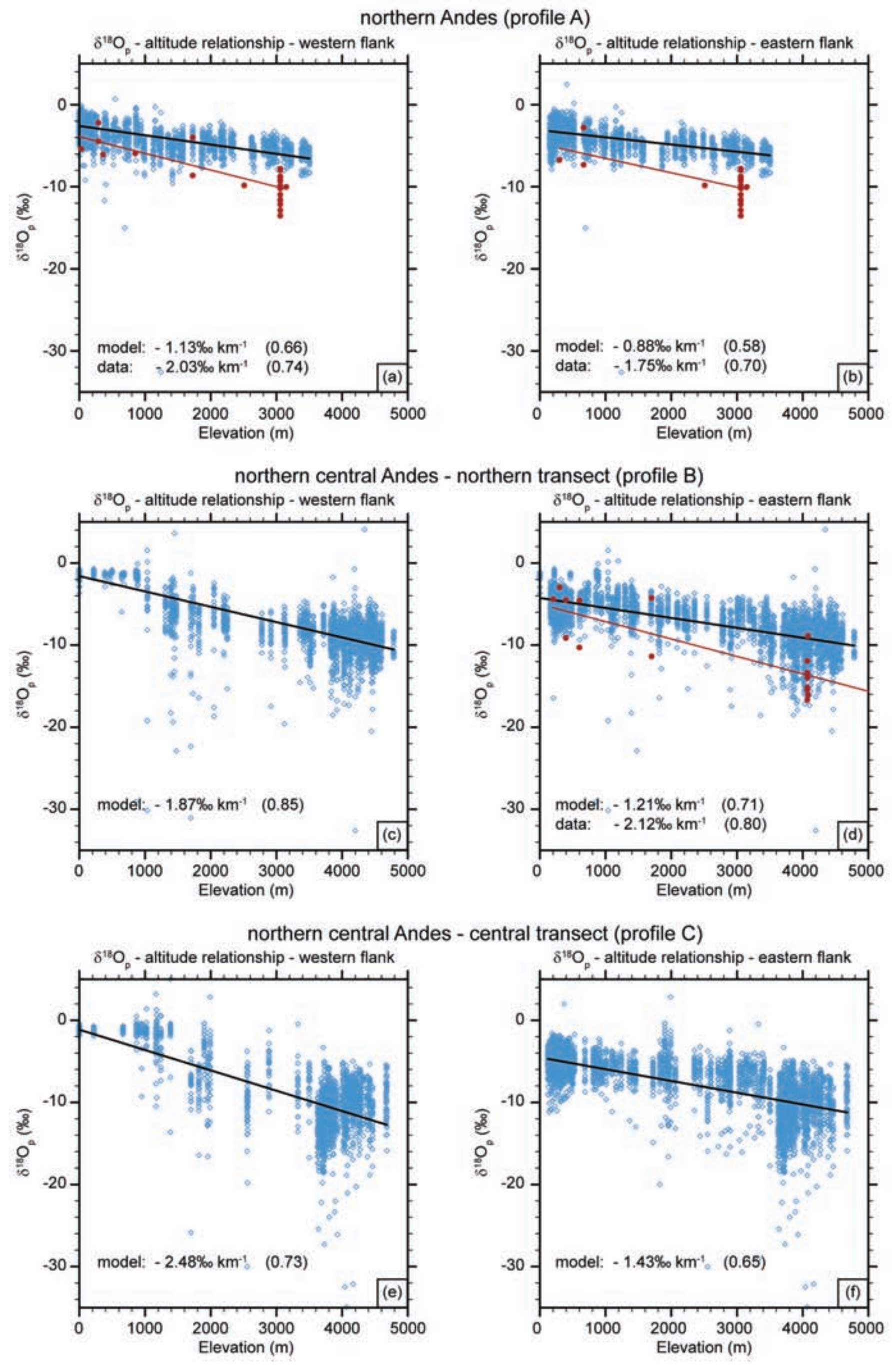

Figure 2.4: Simulated annual precipitation amount-weighted mean $\delta^{18}O_p$ versus altitude for the western (left panel) and eastern (right panel) flank of the Andean domains. Blue diamonds represent simulated $\delta^{18}O_p$ (‰) for individual years between 1976 and 1999. The black line shows the modeled annual isotopic lapse rate (‰ km^{-1}) estimated by linear regression. Red filled circles show annual amount-weighted mean $\delta\ ^{18}O_p$ (‰) from meteorological stations; the red line is the calculated observed annual isotopic lapse rate (‰ km^{-1}) also estimated by linear regression. Panels correspond to the following regions: (a-b) northern Andes (profile A); (c-h) central Andes with (c-d) northern transect (profile B), (e-f) central transect (profile C), and (g-h) southern transect (profile D); (i-j) southern central Andes (profile E); and (k-l) Southern Andes (profile F).

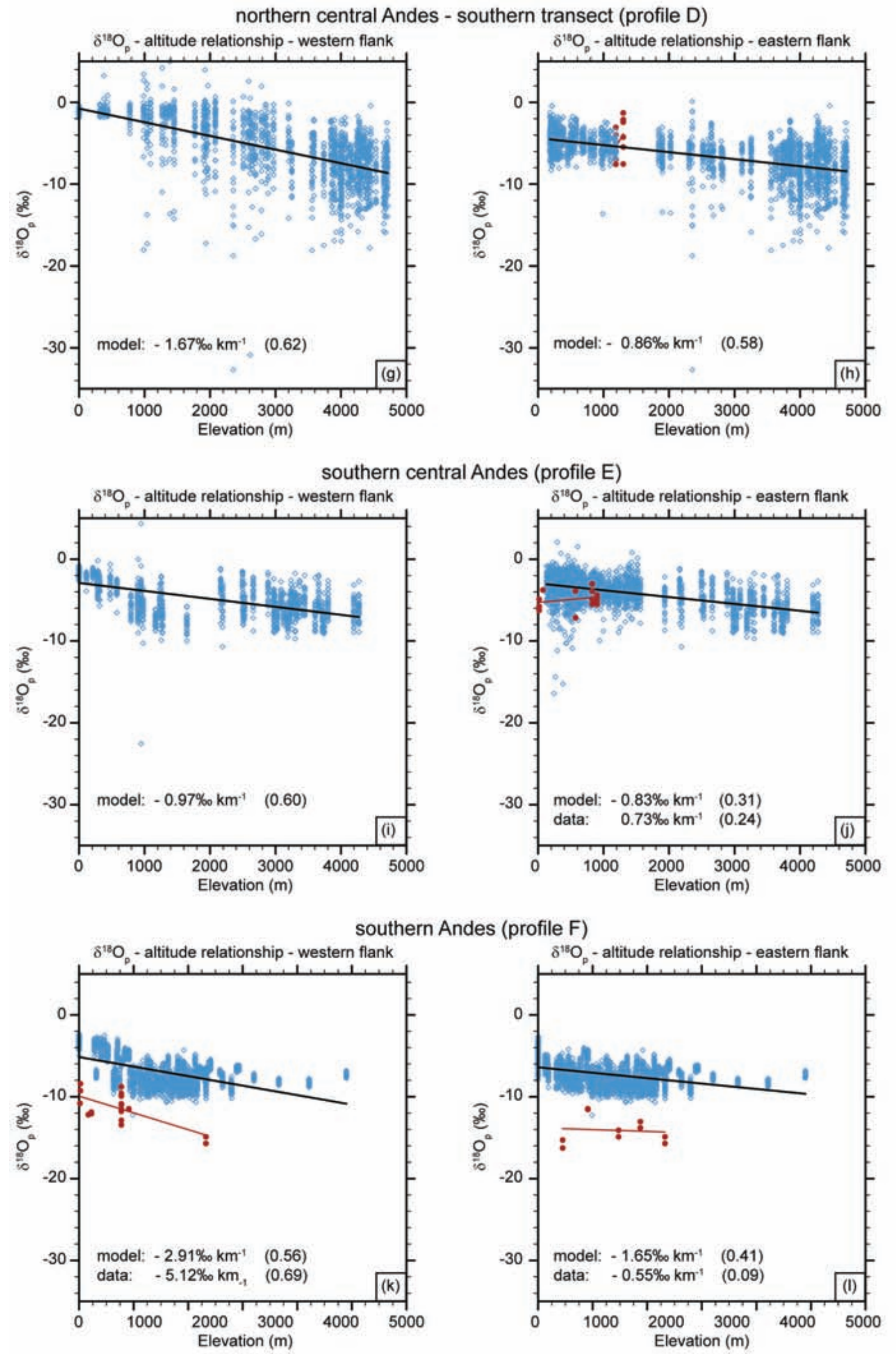

.
Figure 2.4: continued

western flank (Fig. 2.4a,b). Simulated isotopic lapse rates for individual years range between -1.49 and -0.04‰ km^{-1} on the east side of the Andes and between -1.51 and -0.74‰ km^{-1} in the west. Station data from high and low elevation points only overlap for two years. Observed lapse rates along the eastern flank for 1992 and 1993 are -1.39‰ km^{-1}, and -1.52‰ km^{-1}, respectively. The observed values are larger than simulated lapse rates for the same years (-0.79 and -1.07‰ km^{-1}, respectively), but within the 2σ error of the average model lapse rate.

Northern central Andes

Oxygen isotopic lapse rates in the northern central Andes vary across the Andean Plateau. In the northern transect (profile B), the simulated mean isotopic lapse rate is -1.21 $\pm$ 0.50‰ km^{-1} (r = 0.71) along the eastern flank and -1.87 $\pm$ 0.46‰ km^{-1} (r =0.85) along the western flank (Fig. 2.4c, d). In comparison, lapse rates from meteorological stations along the eastern flank are almost twice as large (-2.12‰ km^{-1}; r = 0.80). The simulated isotopic lapse rate for individual years varies between -1.67 and -0.74‰ km^{-1} in the east and between -2.26 and -1.49‰ km^{-1} in the west (Table 2.1). The observed lapse rates along the eastern topographic flank range from -2.31 ‰ km^{-1} in a wet year (1984) to -1.46‰ km^{-1} in a dry year (1983). The observed values are significantly larger than simulated lapse rates for the same years (-1.22‰ km^{-1} in 1984 and -1.18 ‰ km^{-1} in 1983, respectively), and fall outside the 2σ error (Table 2.1).

The simulated isotopic lapse rate in the central part of the northern central Andes (profile C) is -1.43 $\pm$ 0.84‰ km^{-1} (r = 0.65) along the eastern flank of the mountains and -2.47 $\pm$ 0.96‰ km^{-1} (r = 0.73) along the western flank (Fig. 2.4e, f). Isotopic lapse rates for individual years vary between -2.46 and -0.69‰ km^{-1} in the east, and

Table 2.1: $\delta^{18}O_p$ and isotopic lapse rates for different Andean domains

	Annual weighted mean $\delta^{18}O_p$		**Isotopic lapse rates - west**			**Isotopic lapse rates - west**		
	24yr mean (‰)	Interannual variability (‰)	24yr mean (‰ km^{-1})		individual yrs (‰ km^{-1})	24yr mean (‰ km^{-1})		individual yrs (‰ km^{-1})
Northern Andes	-5	-3 to -7	-1.13 ± 0.46	r = 0.66	-1.51 to -0.74	-0.88 ± 0.69	r = 0.58	-1.49 to -0.04
Northern central Andes								
. Northern transect	-9	-4 to -14	-1.87 ± 0.46	r = 0.85	-2.26 to -1.49	-1.21 ± 0.50	r = 0.71	-1.67 to -0.74
. Central transect	-13	-7 to -19	-2.48 ± 0.96	r = 0.73	-3.53 to -1.38	-1.43 ± 0.84	r = 0.65	-2.46 to -0.69
. Southern transect	-9	-5 to -14	-1.67 ± 0.89	r = 0.62	-2.65 to -0.94	-0.86 ± 0.77	r = 0.58	-1.61 to -0.05
Southern central Andes	-6	-4 to -8	-0.97 ± 0.49	r = 0.60	-1.39 to -0.42	-0.83 ± 0.61	r = 0.31	-1.37 to -0.30
Southern Andes	-9	-7 to -10	-2.91 ± 0.37	r = 0.56	-3.16 to -2.46	-1.65 ± 0.68	r = 0.41	-2.30 to -0.90

between -3.53 and -1.38‰ km^{-1} in the west (Table 2.1). Isotopic lapse rates are not available for the central transect; the only reported $\delta^{18}O_p$ measurements for the central transect come from individual storm events (Fritz et al., 1981; Aravena et al., 1999).

Annual amount-weighted $\delta^{18}O_p$ lapse rates along the southern transect are smaller than those in the northern and central transects with values of -0.86 ± 0.77‰ km^{-1} (r = 0.58) and -1.67 ± 0.89‰ km^{-1} (r = 0.62) along the eastern and western flank, respectively (Fig. 2.4g, h). Isotopic lapse rates for individual years vary between -1.61 and -0.05‰ km^{-1} in the east and -2.65 and -0.94‰ km^{-1} in the west (Table 2.1). Relatively long (6-7 yrs) records of annual amount-weighted $\delta^{18}O_p$ values exist for two meteorological stations at the lowlands of the eastern Andean foreland at elevations of 1187 and 1300 m, respectively (Fig. 2.1j, Table 2.2). The elevation difference between the two stations is too small to calculate accurate lapse rates. The more depleted isotopic composition at the lower station is caused by stronger rainout in comparison to the slightly higher station that is located approximately 75 km to the southwest.

Southern central Andes

The simulated isotopic lapse rate in the southern central Andes (profile E) is -0.83 $\pm$ 0.61‰ km^{-1} (r =0.31) along the eastern flank and -0.97 $\pm$ 0.49‰ km^{-1} (r = 0.60) along the western flank (Fig. 2.4i, j). The observed isotopic lapse rate along the eastern flank based on station data records with durations varying from 1 to 5 years is 0.73‰ km^{-1} (Fig. 2.4j, r = 0.24). Simulated isotopic lapse rates for individual years vary between -1.37 and -0.30‰ km^{-1} in the east, and between -1.39 and -0.42‰ km^{-1} in the west (Table 2.1). Individual meteorological station data only overlap for two years. Isotopic lapse rates from the eastern slope for the years 1983 and 1984 are -3.09‰ km^{-1} and 7.07‰ km^{-1}, respectively. We caution that the observed lapse rates are based on low-elevation data collected over a very small elevation range (<900 m, Table 2.2), and thus are unlikely to accurately represent the lapse rate over the full elevation range. In addition, because the interannual variability (e.g. 1983 versus 1984) is high, the few annual observations are unlikely to provide a robust climatology. More data are needed from this region to accurately estimate the lapse rate.

Southern Andes

Simulated isotopic lapse rates are greatest in the southern Andes and have values of -1.65 $\pm$ 0.68‰ km^{-1} (r = 0.41) in the east and -2.91 $\pm$ 0.37‰ km^{-1} (r = 0.56) in the west (Fig. 2.4k, l). An isotopic lapse rate of -5.12‰ km^{-1} (r = 0.69) is calculated based on data from Stern and Blisniuk (2002) and records from the meteorological station in Coyhaique (Fig. 2.4k, l, Table 2.2). Simulated isotopic lapse rates for individual years range between -2.30 and -0.90‰ km^{-1} in the east and between -3.16

Table 2.2: Meteorological station locations and recorded annual amount-weighted $\delta^{18}O$

sample site	country[1]	lat	lon	altitude	year	annual	month	number of years total[3]	reference
northern Andes									
Esmeralda	EC	0.97	-79.63	30	1993	-5.38	9		
Esmeralda	**EC**	**0.97**	**-79.63**	**30**	**avg-wgt**	**-5.38**	**12**	**3**	GNIP; Garcia et al. 1998
Lago Agrio	EC	-0.08	-76.87	297	1993	-6.74	12		
Lago Agrio	**EC**	**-0.08**	**-76.87**	**297**	**avg-wgt**	**-6.74**	**12**	**5**	GNIP; Garcia et al. 1998
Alluriquin	EC	-0.33	-78.60	850	1993	-5.94	11		
Alluriquin	**EC**	**-0.33**	**-78.60**	**850**	**avg-wgt**	**-5.94**	**12**	**5**	GNIP; Garcia et al. 1998
La Concordia	EC	- 0.42	-79.17	360	1993	-6.07	12		
La Concordia	**EC**	**-0.42**	**-79.17**	**360**	**avg-wgt**	**-6.07**	**12**	**5**	GNIP; Garcia et al. 1998
Papallacta	EC	-0.50	-78.10	3150	1993	-10.01	12		
Palpallacta	**EC**	**-0.50**	**-78.10**	**3150**	**avg-wgt**	**-10.01**	**12**	**3**	GNIP; Garcia et al. 1998
Izobamba	EC	-0.37	-78.55	3058	1974	-8.74	11		
Izobamba	EC	-0.37	-78.55	3058	1975	-7.80	9		
Izobamba	EC	-0.37	-78.55	3058	1976	-11.59	11		
Izobamba	EC	-0.37	-78.55	3058	1977	-10.20	11		
Izobamba	EC	-0.37	-78.55	3058	1978	-11.67	11		
Izobamba	EC	-0.37	-78.55	3058	1979	-9.85	10		
Izobamba	EC	-0.37	-78.55	3058	1980	-9.29	11		
Izobamba	EC	-0.37	-78.55	3058	1981	-8.80	11		
Izobamba	EC	-0.37	-78.55	3058	1982	-9.14	10		
Izobamba	EC	-0.37	-78.55	3058	1991	-10.13	12		
Izobamba	EC	-0.37	-78.55	3058	1992	-7.83	11		
Izobamba	EC	-0.37	-78.55	3058	1993	-12.14	12		
Izobamba	EC	-0.37	-78.55	3058	1994	-7.99	8		
Izobamba	EC	-0.37	-78.55	3058	1996	-10.95	9		
Izobamba	EC	-0.37	-78.55	3058	1998	-13.52	11		
Izobamba	EC	-0.37	-78.55	3058	2000	-12.85	9		
Izobamba	**EC**	**-0.37**	**-78.55**	**3058**	**avg-wgt**	**-10.1**	**12**	**25**	GNIP; Garcia et al. 1998
Amaluza	EC	-2.47	-78.47	1726	1992	-4.00	8		
Amaluza	EC	-2.47	-78.47	1726	1993	-8.62	12		
Amaluza	**EC**	**-2.47**	**-78.47**	**1726**	**avg-wgt**	**-7.97**	**12**	**3**	GNIP; Garcia et al. 1998
Mendez	EC	-2.53	-77.92	665	1992	-2.79	8		
Mendez	EC	-2.53	-77.92	665	1993	-7.23	12		
Mendez	**EC**	**-2.53**	**-77.92**	**665**	**avg-wgt**	**-5.93**	**12**	**3**	GNIP; Garcia et al. 1998
Cuenca	EC	-2.88	-78.98	2510	1992	-1.48	8		
Cuenca	EC	-2.88	-78.98	2510	1993	-9.83	10		
Cuenca	**EC**	**-2.88**	**-78.98**	**2510**	**avg-wgt**	**-7.03**	**12**	**5**	GNIP; Garcia et al. 1998
Machala	**EC**	**-3.25**	**-78.98**	**6**	**avg-wgt**	**-1.34**	**12**	**5**	GNIP; Garcia et al. 1998
Uzhcurrumi	EC	-3.25	-79.23	290	1992	-2.20	8		
Uzhcurrumi	EC	-3.25	-79.23	290	1993	-4.46	12		
Uzhcurrumi	**EC**	**-3.25**	**-79.23**	**290**	**avg-wgt**	**-4.01**	**12**	**5**	GNIP; Garcia et al. 1998
northern central Andes									
Trinidad	BO	-14.83	-64.90	200	1983	-4.08	10		
Trinidad	**BO**	**-14.83**	**-64.90**	**200**	**avg-wgt**	**-4.08**	**10**	**3**	GNIP; Gonfiantini et al. 2001
Rurrenabaque	BO	-14.44	-67.53	300	1983	-2.63	10		
Rurrenabaque	**BO**	**-14.44**	**-67.53**	**300**	**avg-wgt**	**-2.63**	**12**	**3**	GNIP; Gonfiantini et al. 2001
Sapecho	BO	-15.58	-67.26	395	1983	-4.18	10		
Sapecho	BO	-15.58	-67.26	395	1984	-8.79	11		
Sapecho	**BO**	**-15.58**	**-67.26**	**395**	**avg-wgt**	**-6.58**	**12**	**3**	GNIP; Gonfiantini et al. 2001
Caranavi	BO	-15.83	-67.57	600	1983	-4.23	11		
Caranavi	BO	-15.83	-67.57	600	1984	-9.95	11		
Caranavi	**BO**	**-15.83**	**-67.57**	**600**	**avg-wgt**	**-7.68**	**12**	**4**	GNIP; Gonfiantini et al. 2001

Table 2.2 (continue): Meteorological station locations and recorded annual amount-weighted δ^{18}O

sample site	country[1]	lat	lon	altitude	year	annual	month	number of years total[3]	reference
Coroico	BO	-16.19	-67.73	1700	1983	-3.93	12		
Coroico	BO	-16.19	-67.73	1700	1984	-11.04	11		
Coroico	**BO**	**-16.19**	**-67.73**	**1700**	**avg-wgt**	**-7.79**	**12**	**4**	GNIP; Gonfiantini et al. 2001
Chacaltaya	BO	-16.33	-68.13	5200	1983	-11.72	11		
Chacaltaya	BO	-16.33	-68.13	5200	1984	-17.11	10		
Chacaltaya	**BO**	**-16.33**	**-68.13**	**5200**	**avg-wgt**	**-14.82**	**12**	**4**	GNIP; Gonfiantini et al. 2001
El Alto	BO	-16.50	-68.17	4080	1983	-8.55	11		
El Alto	BO	-16.50	-68.17	4080	1984	-15.75	10		
El Alto	**BO**	**-16.50**	**-68.17**	**4080**	**avg-wgt**	**-12.41**	**12**	**5**	GNIP; Gonfiantini et al. 2001
La Paz	BO	-16.29	-68.08	4071	1996	-14.81	12		
La Paz	BO	-16.29	-68.08	4071	1997	-13.35	11		
La Paz	BO	-16.29	-68.08	4071	1998	-13.03	10		
La Paz	BO	-16.29	-68.08	4071	1999	-13.04	12		
La Paz	BO	-16.29	-68.08	4071	2000	-15.13	11		
La Paz	BO	-16.29	-68.08	4071	2001	-16.35	12		
La Paz	BO	-16.29	-68.08	4071	2002	-13.65	12		
La Paz	BO	-16.29	-68.08	4071	2003	-14.95	12		
La Paz	BO	-16.29	-68.08	4071	2004	-11.59	12		
La Paz	**BO**	**-16.29**	**-68.08**	**4071**	**avg-wgt**	**-13.96**	**12**	**10**	GNIP; Gonfiantini et al. 2001
Los Molinos	AR	-24.11	-65.19	1300	1982	-5.46	10		
Los Molinos	AR	-24.11	-65.19	1300	1983	-4.25	12		
Los Molinos	AR	-24.11	-65.19	1300	1984	-7.54	10		
Los Molinos	AR	-24.11	-65.19	1300	1986	-1.29	9		
Los Molinos	AR	-24.11	-65.19	1300	1987	-2.42	9		
Los Molinos	AR	-24.11	-65.19	1300	1988	-2.11	10		
Los Molinos	**AR**	**-24.11**	**-65.19**	**1300**	**avg-wgt**	**-4.09**	**12**	**9**	GNIP; Rozanski et al. 1993
Salta	AR	-24.78	-65.40	1187	1982	-3.07	10		
Salta	AR	-24.78	-65.40	1187	1983	-4.01	11		
Salta	AR	-24.78	-65.40	1187	1999	-5.98	11		
Salta	AR	-24.78	-65.40	1187	2000	-6.94	8		
Salta	AR	-24.78	-65.40	1187	2001	-7.57	10		
Salta	AR	-24.78	-65.40	1187	2002	-4.97	9		
Salta	**AR**	**-24.78**	**-65.40**	**1187**	**avg-wgt**	**-5.84**	**12**	**12**	GNIP; Rozanski et al. 1993
southern central Andes									
La Suela	AR	-30.58	-64.58	900	1983	-5.33	11		
La Suela	AR	-30.58	-64.58	900	1984	-4.86	8		
La Suela	AR	-30.58	-64.58	900	1986	-5.60	10		
La Suela	AR	-30.58	-64.58	900	1987	-4.48	9		
La Suela	**AR**	**-30.58**	**-64.58**	**900**	**avg-wgt**	**-4.99**	**11**	**8**	GNIP; Rozanski et al. 1993
Mar Chiquita	AR	-30.92	-62.67	72	1996	-3.86	10		
Mar Chiquita	**AR**	**-30.92**	**-62.67**	**72**	**avg-wgt**	**-3.86**	**11**	**8**	GNIP
Santa Fe	AR	-31.75	-60.73	16	1999	-5.87	11		
Santa Fe	AR	-31.75	-60.73	16	2000	-4.99	12		
Santa Fe	AR	-31.75	-60.73	16	2001	-6.34	12		
Santa Fe	**AR**	**-31.75**	**-60.73**	**16**	**avg-wgt**	**-5.59**	**12**	**5**	GNIP
Mendoza	AR	-32.88	-68.85	827	1983	-3.99	10		
Mendoza	AR	-32.88	-68.85	827	1984	-5.57	9		
Mendoza	AR	-32.88	-68.85	827	1986	-3.97	8		
Mendoza	AR	-32.88	-68.85	827	1987	-4.98	9		
Mendoza	AR	-32.88	-68.85	827	1999	-3.11	9		
Mendoza	**AR**	**-32.88**	**-68.85**	**827**	**avg-wgt**	**-4.52**	**12**	**10**	GNIP; Rozanski et al. 1993
Nuncuan	AR	-34.03	-67.97	572	1983	-3.97	11		
Nuncuan	AR	-34.03	-67.97	572	1984	-7.24	9		
Nuncuan	**AR**	**-34.03**	**-67.97**	**572**	**avg-wgt**	**-5.84**	**12**	**4**	GNIP; Rozanski et al. 1993

Table 2.2 (continue): Meteorological station locations and recorded annual amount-weighted $\delta^{18}O$

sample site	country[1]	lat	lon	altitude	year	annual	month	number of years total[3]	reference
southern Andes									
Coyhaique	CL	-43.35	-72.07	310	1989	-9.61	11		
Coyhaique	CL	-43.35	-72.07	310	1990	-12.89	12		
Coyhaique	CL	-43.35	-72.07	310	1991	-11.78	12		
Coyhaique	CL	-43.35	-72.07	310	1992	-8.78	11		
Coyhaique	CL	-43.35	-72.07	310	1993	-10.87	12		
Coyhaique	CL	-43.35	-72.07	310	1994	-11.00	12		
Coyhaique	CL	-43.35	-72.07	310	1995	-10.99	11		
Coyhaique	CL	-43.35	-72.07	310	1996	-11.51	12		
Coyhaique	CL	-43.35	-72.07	310	1997	-13.44	12		
Coyhaique	CL	-43.35	-72.07	310	1998	-9.92	10		
Coyhaique	**CL**	**-43.35**	**-72.07**	**310**	**avg-wgt**	**-11.22**	**12**	**11**	GNIP

[1] country code: EC = Ecuador, BO = Bolivia, AR = Argentina, CL = Chile
[2] avg-wgt = annual amount-weighted mean
[3] number of years from which at least one month of $\delta^{18}O_p$ record is included in the amount-weighted mean $\delta^{18}O_p$

and -2.46‰ km^{-1} in the west (Table 2.1). Stern and Blisniuk (2002) calculated an isotopic lapse rate of -3.8‰ km^{-1} (r^2=0.3) and found a systematic but weak trend in $\delta^{18}O$ with elevation in the west, but no trend east of the Andes. They relate the low correlation coefficient to the small altitudinal range covered by their samples (~900 m elevation difference). Individual lapse rates calculated from Stern and Blisniuk's data and the additional station data are -6.23‰ km^{-1} in 1999 and -4.46‰ km^{-1} in 2000.

Comparison between transects

Simulated isotopic lapse rates differ along the Andean mountain range. The northern Andes, the southern transect of the central Andes, and the southern central Andes (profiles A, D, and E), have annual amount-weighted mean isotopic lapse rates ranging between -0.8 and -0.9‰ km^{-1} to the east and -1.0 to -1.7‰ km^{-1} to the west. In comparison to these transects, the eastern flank of the northern and central transect (profiles B and C) have an isotopic lapse rate of -1.2 to -1.4‰ km^{-1}, an increase of $\sim$40%. The isotopic lapse rate on the windward side of the southern Andes (profile F) is approximately 3 times higher than the lapse rates from northern regions. Observed isotopic lapse rates are generally more negative than simulated lapse rates.

2.5.3 Processes controlling precipitation δ^{18}O and isotopic lapse rates

In this section, we analyze the processes that control the isotopic composition and lapse rates along the Andes. Back-trajectories are estimated using a Lagrangian method with a 20-minute timestep. The back-trajectory calculation is driven by REMOiso 500-mb 6-hour wind fields. The 500-mb level was chosen because these upper-level winds steer the low-level pressure systems that produce rainfall. To estimate the wind field at every time step, velocities are linearly interpolated between 6-hour increments. For the central Andes, trajectories are initiated from points on the eastern flank ($\sim$20°S, 62°W) and the plateau area ($\sim$16°S, 69°W; $\sim$20°S, 68°W, $\sim$24°S, 67°W) and are back calculated for 7 days. In total, thirty-two trajectories are estimated for each simulation year and each domain, corresponding to individual days during the period Jan 15^{th} to Feb 16^{th} to estimate changes in vapor origin during the rainy season in the central Andes. On daily timescales, isotopic values are not calculated under very low humidity conditions. In these cases, back-trajectories were not estimated. To compare individual years, the moisture source is normalized for the days of precipitation per month.

Northern Andes

The interannual variability in $\delta^{18}O_p$ in the northern Andes is relatively small ($\sim \pm2$‰, Fig. 2.5a), and is correlated with precipitation amount. Mean annual precipitation over the northern Andes varies between 13 and 26 mm day^{-1} along the eastern flank and 7 to 16 mm day^{-1} along the western flank (Fig. 2.5b). Our model results indicate that the most enriched $\delta^{18}O_p$ over the Andes correlate well with minimum precipitation, while the most depleted $\delta^{18}O_p$ values are associated with strong convective rainout (r = 0.68, Fig. 2.5c).

High precipitation in the northern Andes is mainly related to El Niño/Southern Oscillation (ENSO) with El Niño years generally exhibiting above average precipitation (Fig. 2.5b). In general, $\delta^{18}O_p$ during El Niño years is below average to average over the western Andes, and slightly above average along the eastern flank (Fig. 2.5a, c).

Isotopic lapse rates are correlated to the isotopic composition of the highest elevation sites across the northern Andes (r_{east} = 0.66, r_{west}=0.6, Fig. 2.6a). This correlation suggests that the processes controlling the interannual variability in isotopic lapse rate are the same as those controlling variations in high elevation $\delta^{18}O_p$, namely Rayleigh distillation through rainout as air masses converge on and ascend the Andes.

Northern central Andes

The northern central Andes are characterized by substantial (± 6‰) interannual variability in $\delta^{18}O_p$ along the flank and the plateau region. Overall, there is good agreement between high precipitation along the eastern flank and the most depleted

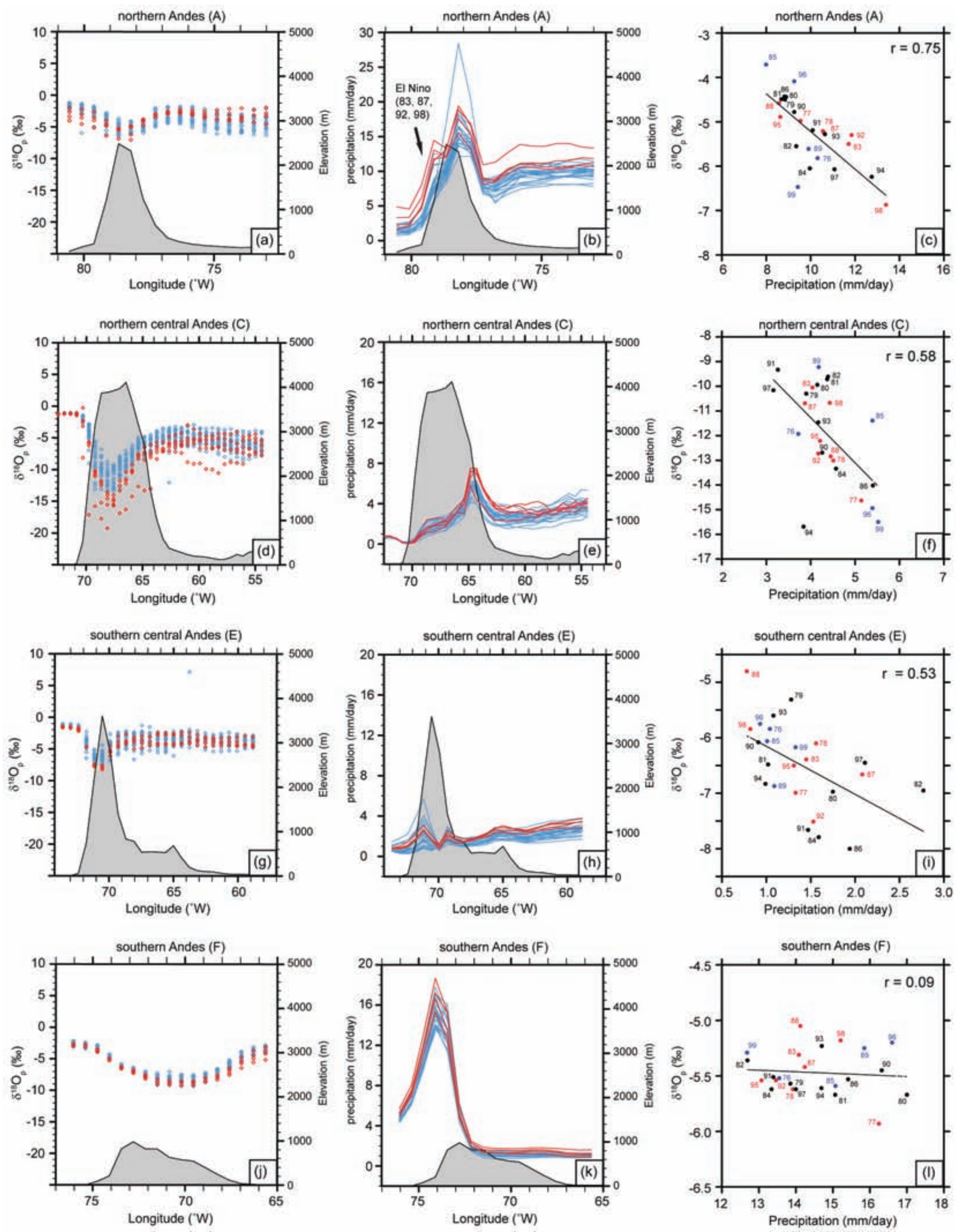

Figure 2.5: Relationship between $\delta^{18}O_p$ and precipitation (amount effect) over the Andes. East-west profiles showing the annual amount-weighted mean $\delta^{18}O_p$ (‰; left panel) and annual precipitation rate (mm day^{-1}; center panel) for individual years between 1976 and 1999 across the Andes for each domain. Red circles represent annual $\delta^{18}O_p$ compositions for strong El Niño events (a) or the most depleted annual $\delta^{18}O_p$ over the highest altitudes (d, g, j). Red lines (b, e, h ,k) represent the corresponding precipitation rates. The gray shading indicates topography (m). The right panel shows the correlation between annual $\delta^{18}O_p$ averaged over the highest elevation regions in each transect and annual precipitation rate averaged over the area with the most abundant rainfall across the profile. The black line indicates the linear regression line. Red filled circles indicate El Niño years; blue filled circles represent La Niña years; black filled circles signify normal years. Panels correspond to the following regions: (a-c) northern Andes (profile A); (d-f) northern central Andes (profile C); (g-i) southern central Andes (profile E); (j-l) southern Andes (profile F).

$\delta^{18}O_p$ over the plateau area (r = 0.58; Fig. 2.5d-f). However, the $\delta^{18}O_p$ variations are much larger than those in both the northern and southern Andes (Sections 2.5.1 even though the precipitation variability between the regions is lower, suggesting that both source and amount effects are at play.

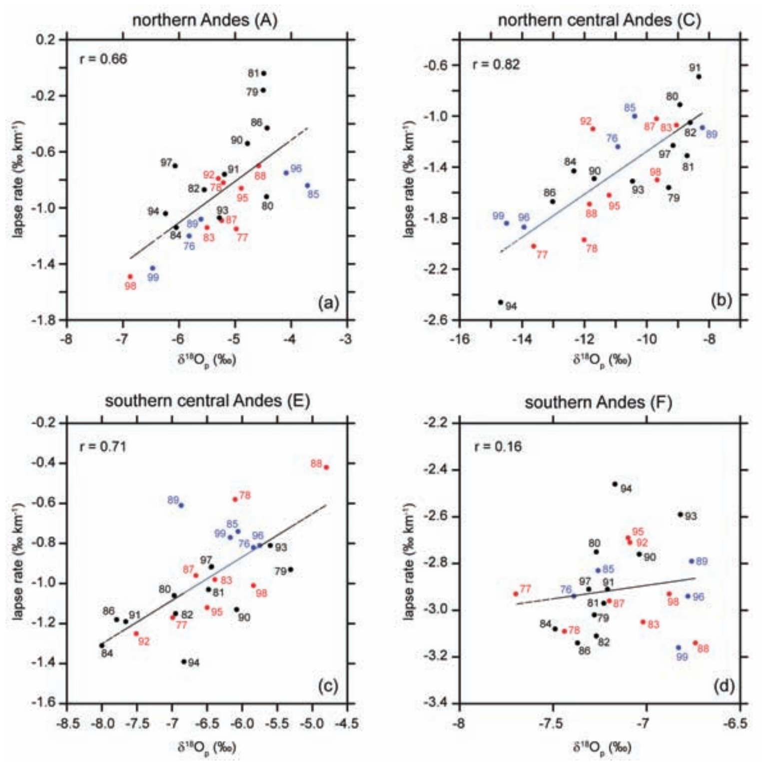

Figure 2.6: Relationship between annual $\delta^{18}O_p$ (‰) at high elevation sites and annual isotopic lapse rates (‰ km^{-1}) at the windward site in the (a) northern Andes (profile A), (b) northern central Andes (profile C), (c) southern central Andes (profile E) and, (d) southern Andes (profile F). Red filled circles indicate El Niño years; blue filled circles represent La Niña years; black filled circles signify normal years. Note the correlation ($r > 0.65$) between $\delta^{18}O_p$ and isotopic lapse rate for all but the southern domain.

To more closely examine the interannual variability in precipitation and $\delta^{18}O_p$, we quantify the influence of source effects on the interannual variability by calculating back-trajectories at the 500-mb level and comparing the vapor source to prevailing winds, precipitation amounts, and $\delta^{18}O_p$ over the central Andes. Our back-trajectory calculations indicate that the summertime moisture source varies considerably on both monthly and interannual timescales. Over a single month, the moisture source

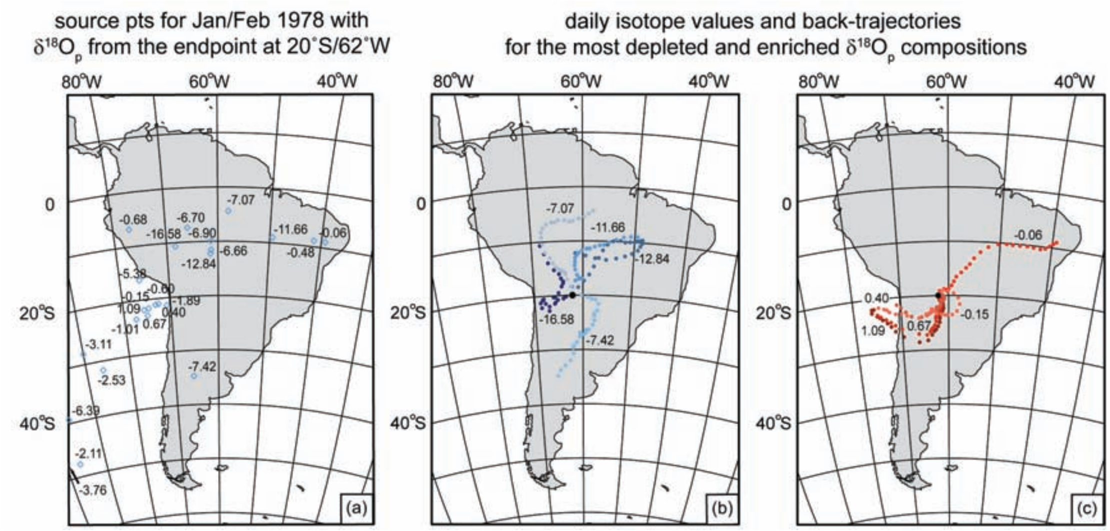

Figure 2.7: Back-trajectories (for 1 week) of air parcels at the 500-mb level for points along the eastern flank of the central Andes (20°S, 62°W) for the time period between Jan 15th and Feb 16th of 1978. (a) Plot showing all starting points of wind trajectories that end at 20°S, 62°W after 1 week. Isotopic values are not calculated under very low humidity conditions. In these cases, the wind path has not been calculated and the number of back-trajectory points can be less than 32. (b) Plot showing the back-trajectories for the five days with the most depleted $\delta\ ^{18}O_p$. (c) Plot showing the back-trajectories for the five days with the most enriched $\delta^{18}O_p$.

can come from the South Pacific, the North Atlantic, the South Atlantic, or the continent. On interannual timescales, the balance of moisture from these sources varies depending on the prevailing wind field. In general, the most depleted values are associated with an easterly path from the South Atlantic across the continent, while the most enriched values are sourced from the South Pacific as exemplified by year 1978 (Fig. 2.7a-c). The absolute $\delta^{18}O_p$ along the eastern flank of the central Andes and the plateau area increases as a higher proportion of air masses originate from the South Pacific (Fig. 2.8a-c). This relationship holds over the entire northern central Andes but strengthens from north to the south, because the abundance of air masses sourcing from the South Pacific increases (Fig. 2.8a-c). When air masses originate from the South Atlantic, the $\delta^{18}O_p$ is highly variable, most likely due to the mixing of tropical (more enriched) and subtropical (more depleted) air masses.

Precipitation variability, like $\delta^{18}O_p$ variability, is related to air parcel trajectory.

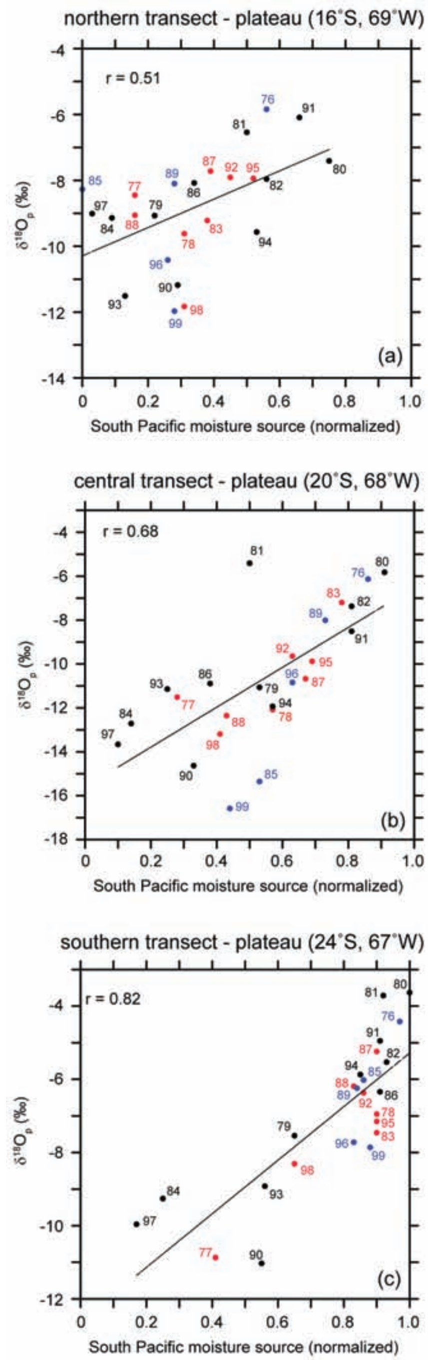

Figure 2.8: Relationship between $\delta^{18}O_p$ (‰) and moisture source (South Pacific) over the Andean Plateau in the northern central Andes for the time period between Jan 15^{th} and Feb 16^{th}. The moisture source has been normalized for the number of days in which non-negligible precipitation occurred. Red filled circles indicate El Niño years; blue filled circles represent La Niña years; black filled circles signify normal years. The panels correspond to the following regions: (a) northern transect (16°S, 69°W); (b) central transect (20°S, 68°W); (c) southern transect (24°S, 67°W). Note the correlation (r > 0.5) between $\delta^{18}O_p$ and a South Pacific moisture source for all parts of the Andean plateau. The correlation and the abundance of air masses from the South Pacific increase from north to south.

Precipitation in the central Andes is generally low when a large proportion of storms originate over the Pacific, due to the relatively low water vapor content of the air masses. Precipitation variability increases as the contribution from the South Pacific decreases. In these cases, high orographic precipitation (i.e. years 1977, 1985, Fig. 2.9c) is related to air masses that transport vapor long distances across the South American continent. Lower orographic precipitation (i.e. years 1993, 1997, Fig. 2.9c) occurs when air masses travel a more direct and faster route from the South Atlantic. In support of our trajectory analysis, and to generalize our results beyond the summer months, we show the relationship between mean-annual winds and precipitation and $\delta^{18}O_p$, respectively. A strong negative correlation (r = 0.6-0.8) exists between meridional winds and precipitation (Fig. 2.9a), reflecting the fact that southerly winds from the South Pacific are low in humidity, while northerly winds from the continent are characterized by high humidity. Mean-annual meridional winds are also positively correlated with mean-annual $\delta^{18}O_p$ (r = 0.6-0.8, Fig. 2.9b).

The number of storms tracking from the South Pacific is determined by the position of the Bolivian High, a prominent anticyclone at 200 mb over the central Andes. The summer (mid-January to mid-February in our analysis) position of the upper-level high-pressure system varies on interannual timescales with latitudinal positions between ~15°S and 23°S and longitudinal positions between ~61°W and 72°W. During El Niño, the Bolivian High migrates to a northerly position and enhances westerly storm tracks that originate over the Pacific (Fig. 2.10).

A strong correlation exists between isotopic lapse rates and high altitude isotopic composition across the northern central Andes (Fig. r_{east} = 0.83, r_{west}=0.77; Fig. 2.6b). As noted before, Rayleigh distillation during ascent is likely the reason.

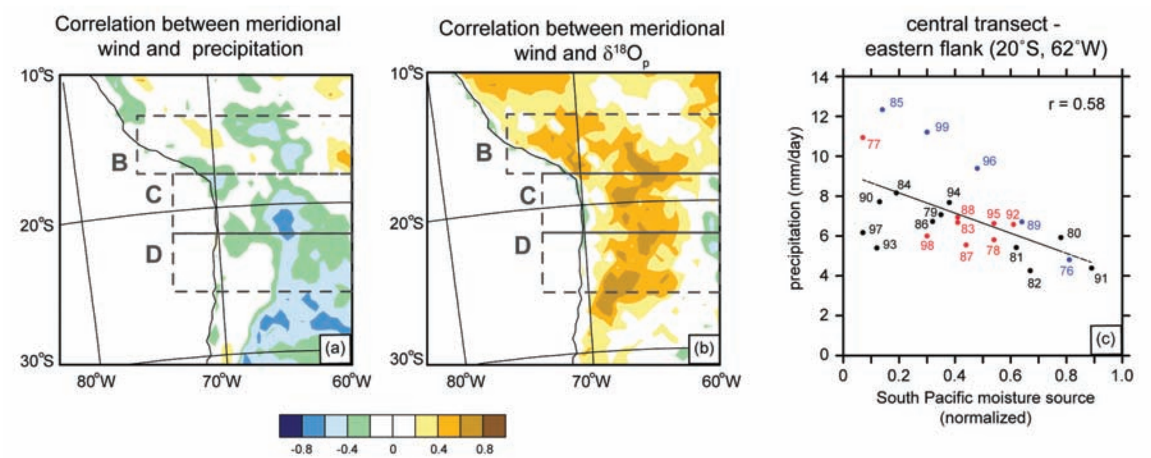

Figure 2.9: Relationship between meridional winds, moisture source, precipitation, and $\delta^{18}O_p$ across the northern central Andes. Meridional winds are calculated for the eastern side of the Andes (averaged over the central transect for longitudes between 60.5° and 68 °W). (a) Correlation between annual meridional winds (m s^{-1}) and annual precipitation rates (mm day^{-1}). A negative correlation indicates that southerlies transport less vapor and cause low precipitation. (b) Correlation between annual meridional winds (m s^{-1}) and annual $\delta^{18}O_p$ (‰). The positive correlation shows that southerly winds are characterized by more enriched $\delta^{18}O_p$. (c) Relationship between summer (Jan 15^{th} and Feb $15th$) vapor source and summer precipitation rate (mm day^{-1}). The vapor source represents the fraction of air parcels on the eastern Andean flank (20°S, 62°W) that originated from the South Pacific as estimated through our back trajectory calculations (see description in section 2, see Fig. 8 for the explanation of the normalization). Precipitation is calculated for the eastern side of the Andes (averaged over the central transect for longitudes between 60.5 and 68°W).

Southern central Andes

The southern central Andes are characterized by interannual $\delta^{18}O_p$ variability of ± 2‰ along the flanks and the highest elevations that is generally associated with precipitation amount (r = 0.53, Fig. 2.5g-i). Interannual variations in precipitation are relatively small and precipitation maxima occur along the western flank (Fig. 2.5h).

Annual precipitation in the southern central Andes is related to 850-mb winds. A positive correlation between zonal winds and precipitation (r = 0.6-0.8) and a negative correlation between meridional winds and precipitation (r = 0.4-0.6) indicate that precipitation is highest when winds transport moisture from the northwest to the southern central Andes (Fig. 2.11a, b). The relationship between winds and $\delta^{18}O_p$ is tied to wind speed. Fast-flowing northwesterlies induce strong convergence and

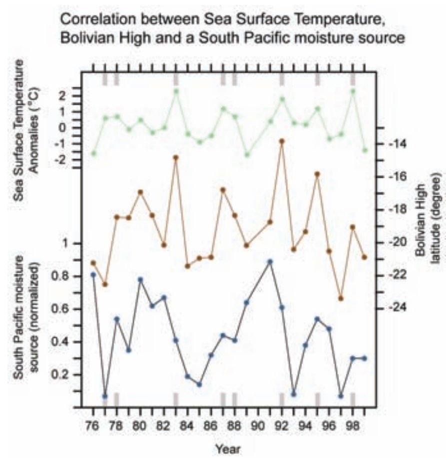

Figure 2.10: Interannual variability in SSTs, the center of the Bolivian High and a South Pacific moisture source for a location at 20°S, 62°W. See Fig. 8 for the explanation of the normalization. Positive SST anomalies greater than 0.5C (green line) indicate El Niño years (highlighted by gray hatches). Positive SST anomalies correlate with a northern position of the Bolivian High (red line). The number of air masses sourcing over the South Pacific (blue line) changes in response to the Bolivian High. A northerly position of the Bolivian High causes the Westerlies over the Andean Plateau to become stronger, steering storm tracks from the South Pacific.

vertical ascent of air masses along the Andean flank, resulting in stronger rainout and more depleted $\delta^{18}O_p$ (Fig. 2.11c, d). Because the winds in the region are dominantly westerlies with a nearly invariable Pacific Ocean vapor source, source effects are unlikely to account for the variability in precipitation and $\delta^{18}O_p$.

Isotopic lapse rates are correlated to the isotopic composition of the highest elevation sites across the southern central Andes (r_{east} = 0.59, r_{west}=0.71, Fig. 2.6c). The correlation between lapse rate and $\delta^{18}O_p$ at high elevations and the relationship between zonal winds and $\delta^{18}O_p$ suggest that strong convergence along the flanks leads to more rainout and Rayleigh distillation. These findings are supported by a good correlation between isotopic lapse rate and zonal winds with stronger Westerlies resulting in larger lapse rates (r = 0.6 - 0.8; not shown).

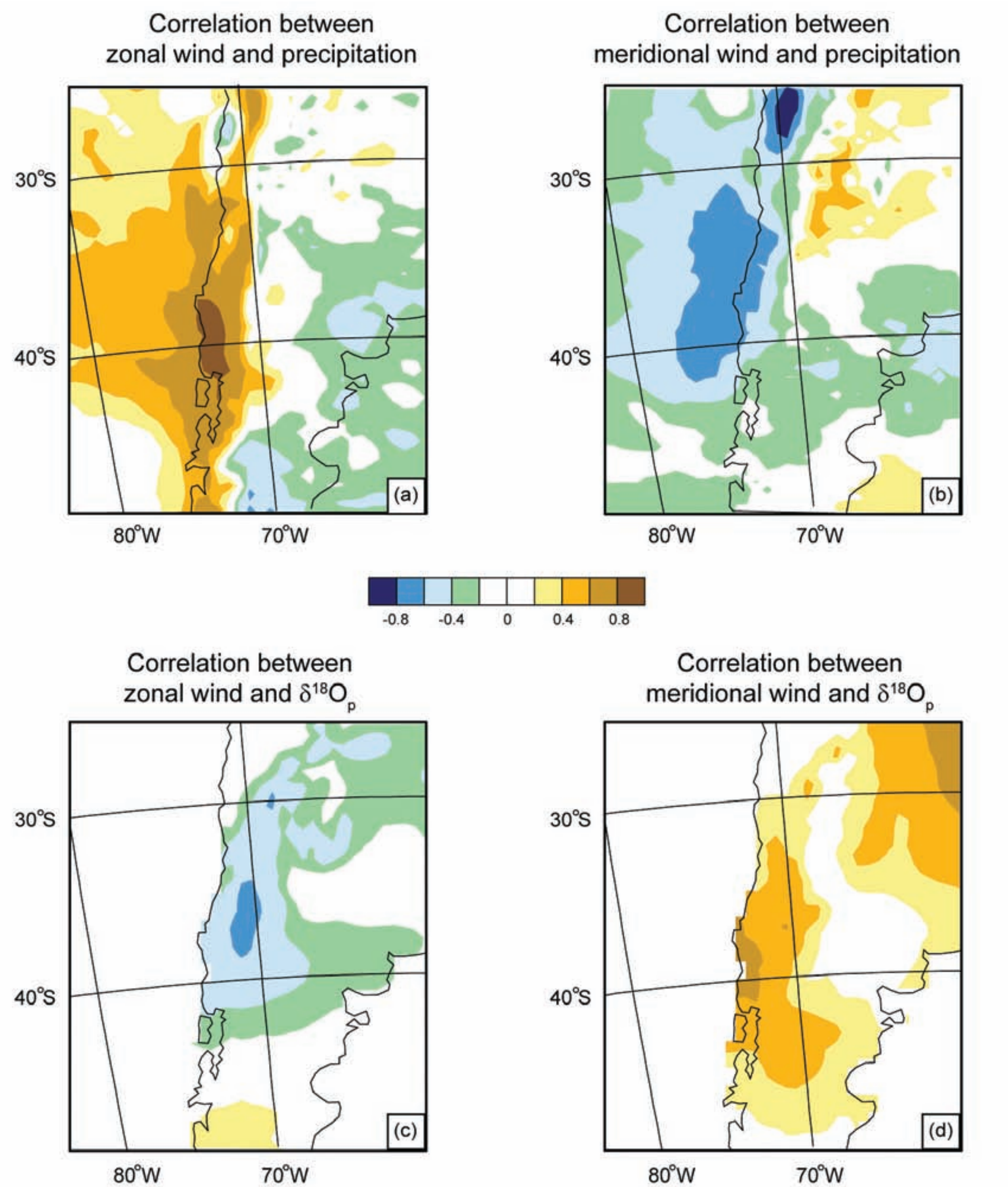

Figure 2.11: Relationship between annual zonal/ meridional winds and annual precipitation and $\delta^{18}O_p$ across the southern central Andes. (a) Point-by-point correlation between zonal winds (m s^{-1}) and precipitation rate (mm day^{-1}). A positive correlation indicates more rain with stronger Westerlies. (b) Point-by-point correlation between meridional winds (m s^{-1}) and precipitation rate (mm day^{-1}). A negative correlation shows that the amount of rain increases when winds are transporting moisture from the north. (c-d) Correlation between annual $\delta^{18}O_p$ (‰) averaged over the highest topography (approximately 70°-71°W) in the southern central Andes and annual zonal and meridional winds (m s^{-1}), respectively. The relationship shows that stronger winds from the northwest result in more depleted isotopic composition due to stronger vertical ascent and rainout.

Southern Andes

The southern Andes are characterized by interannual $\delta^{18}O_p$ variations of approximately 1 and high fluctuations in annual precipitation (13-18 mm day^{-1}; Fig. 2.5j, k). Nonetheless, there is not a direct relationship between orographic precipitation and $\delta^{18}O_p$ along the western flank (Fig. 2.5l). In contrast to low-latitude regions, interannual precipitation variability at high latitudes does not mainly reflect the intensity of seasonal rainfall but rather the number of rain events in a given year (see discussion in Section 2.6.2). Instead, $\delta^{18}O_p$ along the western southern Andean flank ($\delta^{18}O_{pwest}$) positively correlates with 850-mb air temperatures (r = 0.6, Fig. 2.12a). We interpret the $\delta^{18}O_p$-temperature relationship to indicate that $\delta^{18}O_p$ variability is primarily controlled by kinetic fractionation with greater ^{18}O depletion during cold precipitation events.

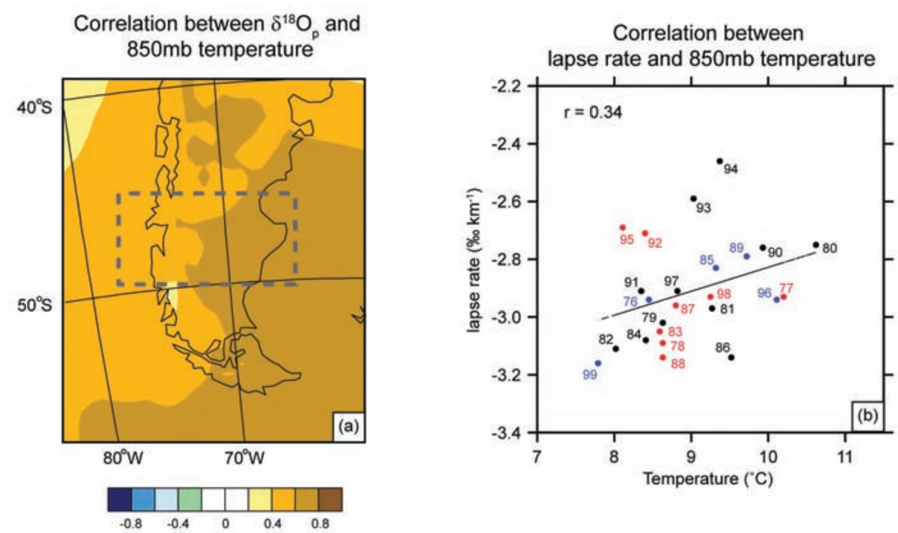

Figure 2.12: Relationship between air temperature and δ^{18} O_p and isotopic lapse rate for the southern Andes. (a) Correlation between annual $\delta^{18}O_p$ (‰) averaged over the western flank (approximately 73°-74°W) of the southern Andes and annual temperature (°C) at 850-mb level. A positive correlation indicates more depleted $\delta^{18}O_p$ with decreasing temperature. (b) Correlation between the isotopic lapse rate (‰ km^{-1}) along the western flank of the southern Andes and temperature at 850 mb (°C) averaged along the windward side (approximately 72.5°-74°W) of the mountain range. Red filled circles indicate El Niño years; blue filled circles represent La Niña years; black filled circles signify normal years. A weak trend exists with colder temperatures causing larger lapse rates.

The annual isotopic lapse rates along the western flank do not correlate with the isotopic composition of precipitation at the highest elevations ($r_{west} = 0.16$; Fig. 2.6d). This is consistent with our conclusion that Rayleigh distillation through rainout is not the main process determining the isotopic composition in the southern Andes. Small variations in isotopic lapse rates on the windward western flank show a general, but weak, trend with temperature variations at the 850-mb level, with larger lapse rates associated with cooler temperatures (Fig. 2.12b).

2.6 Discussion

Our model results and analysis indicate that the isotopic composition in the Andes is influenced by multiple factors that vary across regions. Among these factors are precipitation amount, moisture source and vapor trajectory, wind pattern, Pacific SSTs, and temperature. In this section we discuss the main processes controlling precipitation and $\delta^{18}O_p$ in the different parts of the Andes.

2.6.1 ENSO related variations in $\delta^{18}O_p$

In REMOiso, ENSO is the main driving mechanisms for $\delta^{18}O_p$ variability in the northern Andes. El Niño events are associated with higher precipitation amount on both flanks of the northern Andes and more depleted $\delta^{18}O_p$ along the western flank (Fig. 2.4a). The stronger amount effect during El Niño years is related to circulation changes. During El Niño westerly winds transport moisture from the Pacific to the Andean coast south of the equator and cause high-intensity precipitation (Mettier et al., 2009). In addition, surface waters in the equatorial Pacific have lower δ^{18} O_p than air masses sourced from the Atlantic (Brown et al., 2006). These two factors contribute to more depleted $\delta^{18}O_p$ along the western flank of the northern Andes during El Niño years (Fig. 2.13a). A strong negative relationship between warm ENSO events and $\delta^{18}O\ _p$ over the equatorial Pacific has been found in previous modeling studies, but in these simulations the correlation did not extend into the continent to the western Andean flank (Vuille et al., 2003a; Vuille and Werner, 2005), most likely as a result of the coarser resolution of the global climate models.

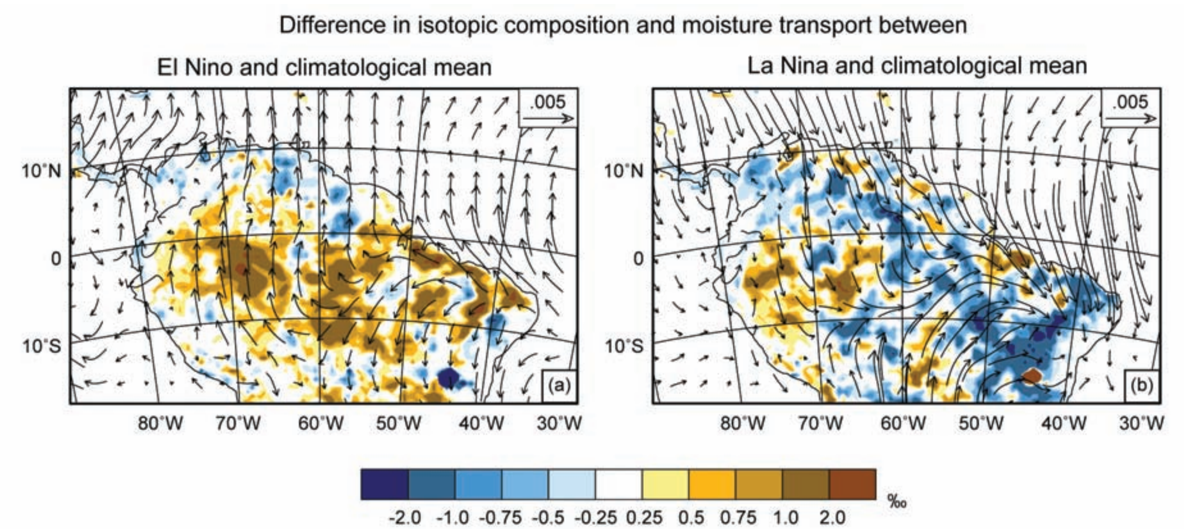

Figure 2.13: Simulated difference in $\delta^{18}O_p$ (‰, represent in colors) and moisture transport (g kg^{-1} m s^{-1}, represent as arrows) between years under ENSO conditions and the 24-year climatological mean over northern South America. (a) Difference between El Niño years and climatological mean. Blue colors along the western flank of the northern Andes (between 0 and 5°S) indicate more depleted $\delta^{18}O_p$ during El Niño years, while brown colors along the eastern flank indicate more enriched $\delta^{18}O_p$ due stronger moisture transport from the Amazon Basin. (b) Difference between La Niña years and climatological mean. More depleted $\delta^{18}O_p$ along both flanks during La Niña years due to stronger moisture transport form the equatorial Pacific and the North Atlantic.

In comparison to years with similar precipitation amounts, the simulated $\delta^{18}O_p$ over the eastern northern Andes is relatively enriched during El Niño years (Fig. 2.5b, c). The slightly above average $\delta^{18}O_p$ along the eastern flank is likely related to feedbacks between the northern Andes and the Amazon Basin. (South-) easterly surface winds transport vapor from the Atlantic and the Amazon Basin to the eastern flank of the Andes (Fig. 2.13a). The eastward migration of temperature and pressure anomalies leads to dry conditions in the Amazon Basin (Hoffmann et al., 2003; Poveda et al., 2006). Lower precipitation over the Amazon Basin results in more enriched $\delta^{18}O_p$ along the eastern flank of the northern Andes during warm ENSO phases (Fig. 2.13a). Precipitation in La Niña years is low, but the $\delta^{18}O_p$ is highly variable (Fig. 2.5c). Intense La Niña years are associated with more depleted $\delta^{18}O_p$ along the eastern Andean flank. Greater moisture transport from the North Atlantic Ocean southward to the northern Andean flank, bypassing the more enriched $\delta^{18}O_p$ from the Amazon Basin, causes $\delta^{18}O_p$ to be more depleted (Fig. 2.13b).

Previous studies have demonstrated a complicated relationship between ENSO and climate in central South America. The influence of individual El Niño/La Niña events on South American climate depends on the persistence and timing of the events in relation to the rainy season (Montecinos et al., 2000; Hoffmann et al., 2003). Although El Niño (La Niña) years are often associated with drier (wetter) conditions over the central Andes, wet (dry) years are not uncommon (Garreaud et al., 2003). We come to a similar conclusion and find that the precipitation and $\delta\ ^{18}O_p$ response to ENSO is inconsistent. Our results indicate that strong La Niña events (e.g. 1976, 1989) are characterized by relatively low precipitation amounts in the northern central Andes, while weaker La Niña events are associated with above average precipitation (e.g. 1985, 1996; Fig. 2.5f). $\delta\ ^{18}O_p$ during La Niña events is variable, and demonstrates no consistent response to weak and strong La Niñas. The stronger and more persistent El Niños (e.g. 1983, 1998) are associated with more enriched values (Fig. 2.5f), most likely as a result of enhanced vapor transport from the Amazon Basin with more enriched $\delta^{18}O_p$, while shorter and weaker El Niños (e.g. 1977, 1978) are characterized by slightly higher precipitation and more depleted $\delta^{18}O_p$ in the central Andes (Fig. 2.5f). From our back-trajectory analysis, we speculate that ENSO probably has the greatest influence on $\delta^{18}O_p$ in the central Andes when it modulates the position of the Bolivian High.

As expected, there is no relationship between interannual $\delta^{18}O\ _p$variability and ENSO in the southern central Andes (Fig. 2.5i) or the southern Andes (Fig. 2.5l).

2.6.2 Effect of moisture source and trajectory path on δ^{18}O variations

As discussed in section 2.5.3, moisture source is the dominant factor influencing precipitation and $\delta^{18}O_p$ in the northern central Andes. The moisture source is variable with air masses originating over the South Pacific, North and South Atlantic and trajectory paths that vary significantly. A strong positive correlation exists between a South Pacific trajectory and $\delta^{18}O_p$ (Fig. 2.7, Fig. 2.8). Two factors contribute to the enriched $\delta^{18}O_p$ composition of South Pacific air masses for the northern central Andes. (1) The vapor source from the South Pacific is associated with low precipitation amounts over the northern central Andes. South Pacific air masses are characterized by low water vapor content and low relative humidity due to subtropical subsidence and low surface temperatures associated with the Humboldt Current along the west coast of South America. With low moisture content and latent heat, convergence along the central Andes is less likely to trigger convective updrafts and intense convective precipitation. (2) Air masses originating from the Pacific travel less distance and undergo less condensation and rainout, and therefore less Rayleigh distillation.

In other Andean regions, the moisture source does not play a dominant role in controlling $\delta^{18}O_p$ interannual variability. The reason for that is that the variability in dominant moisture source is less pronounced than in the northern central Andes. In the northern Andes, 85% of the vapor that condenses over the mountains sources from the north Atlantic and/or the Amazon Basin. In the southern central Andes, the South Pacific is the principle moisture source for storm tracks with little influence from the continent (not shown). In the southern Andes, the vapor source is almost invariability the Pacific Ocean mainly due to the stability of the mid-latitude Westerlies.

2.6.3 Influence of wind speed and vertical ascent on $\delta^{18}O_p$ variations

The main control on interannual $\delta^{18}O_p$ variability in the southern central Andes is the zonal wind speed and associated vertical ascent. The region is very dry with precipitation and $\delta^{18}O_p$ showing relatively small interannual variability. Although the South Pacific air masses are characterized by relatively low water vapor content and more enriched $\delta^{18}O_p$, stronger eastward winds from the Pacific Ocean result in lower $\delta^{18}O_p$. Stronger zonal winds enhance vertical ascent which causes more adiabatic cooling that leads to more condensation, stronger Rayleigh distillation and ultimately to more depleted $\delta^{18}O_p$.

In the southern Andes, variations in the zonal winds cause variations in orographic precipitation along the western flank. Stronger Westerlies cause more precipitation (not shown), but the isotopic composition in the southern Andes is little affected for two reasons. First, mid-latitude storms are frequent but relatively low in precipitation, therefore, individual storms have little effect on the seasonal and annual $\delta^{18}O_p$. Second, the vapor source is proximal and convective updrafts are unusual, and consequently air masses undergo little Rayleigh distillation. Vapor from the South Atlantic is probably occasionally mixed in with Pacific air masses. However, because the vapor $\delta^{18}O_p$ to the west and east of the southern Andes are similar these incursions are unlikely to substantially affect $\delta^{18}O_p$ over the southern Andes.

As described above, in the northern and northern central Andes, other factors than wind speed and vertical ascent dominate the composition of precipitation and $\delta^{18}O_p$.

2.6.4 Effect of temperature on $\delta^{18}O_p$ variations

Temperature variations at 850 mb are the dominant factors influencing $\delta^{18}O_p$ in the southern Andes. The fractionation factor for oxygen isotopes increases for decreasing temperature resulting in a more pronounced depletion of cloud vapor at lower temperatures.

Temperature does not affect the interannual variability in the isotopic composition of precipitation in other Andean regions. A negative correlation (r = 0.3-0.5) exists between temperature and $\delta^{18}O_p$ along the eastern flank of the northern central Andes, indicating that higher temperatures along the mountain range are associated with air masses that have a higher vapor content causing more rain during ascent and therefore more depleted $\delta^{18}O_p$. This relationship is more pronounced on a monthly timescale, where a negative correlation between temperature and $\delta\ ^{18}O_p$ indicates the contemporaneous appearance of the warm and wet season in subtropical South America.

2.6.5 Data - model comparison

In general, simulated annual amount-weighted $\delta^{18}O_p$ and observed $\delta^{18}O_p$ agree in minimum, maximum and mean values for different transects along the Andes. The observed $\delta^{18}O_p$ variability falls within our simulated $\delta^{18}O_p$ variability in most regions (Fig. 2.3), except for the southern Andes where observed $\delta^{18}O_p$ are significantly lower.

However, the lapse rate estimates do not compare as well (Fig. 2.4). Several issues complicate the comparison between model $\delta^{18}O_p$ and observed $\delta^{18}O_p$:

First, the model and observations differ in spatial scales. Meteorological observations record precipitation $\delta^{18}O_p$ from station sites, which may not be representative of larger domains. In South America, inadequate data coverage makes it impossible to interpolate local observations to regional scales. Likewise, relatively high-resolution limited-domain climate models are too coarse to make direct comparisons with station observations. For example, we report a simulated isotopic lapse rate for the western flank of the southern Andes of 2.91‰ km^{-1} that is calculated for the entire domain between 45 and 50°S. If we calculate the lapse rate only for latitudes at around 48°S, similar to sample sites from Stern and Blisniuk (2002), our isotopic lapse rate is -4.92‰ km^{-1} in comparison to an observed lapse rate of -5.12‰ km^{-1}.

Second, observational data typically span only a few years. Often, observed $\delta^{18}O_p$ have missing monthly $\delta^{18}O_p$ values or only record individual storm events. Short observation periods may bias a record towards anomalous events (e.g. ENSO). For example, our modeled isotopic lapse rates in the northern transect vary significantly when calculated over a three year period. The averaged lapse rate is -1.51‰ km^{-1} for 1976 to 1978 and -1.34‰ km^{-1} for 1986 to 1988. Both periods include two El Niño events. In comparison, the isotopic lapse rate during three year periods with mostly normal tropical Pacific conditions is -0.98‰ km^{-1} (1980-1982) and -0.95‰ km^{-1} (1989-1991), respectively. That indicates a discrepancy in lapse rate of 50% depending on the years the lapse rates are calculated for.

Third, although the higher resolution in REMOiso results in a better representation of topography than in global models, the steep topographic gradient and absolute height of the southern Andes is still underestimated. For example, Stern and Blisniuk (2002) report windward elevations of up to 3000 m, while REMOiso simulates peak elevations of <1700 m. The discrepancy in elevation is the most likely reason for the large differences between simulated and observed $\delta^{18}O_p$ in the southern Andes.

Fourth, observational data do not sample the complete elevation range, and as a result are likely to overestimate lapse rates. In the central Andes observed $\delta^{18}O_p$ is sampled at elevations below 1500 m and above 4000 m (Fig. 2.3h, l). $\delta^{18}O_p$ observations at elevations between 1500 and 4000 m do not have corresponding precipitation amount data and cannot be amount-weighted. In the northern and central part of the central Andes the relationship between $\delta^{18}O_p$ and elevation is not linear; the lapse rate increases at higher altitudes (>3500 m) due to the advanced stage of condensation fractionation. As a result, isotopic lapse rates derived by linear extrapolation likely overestimate the true lapse rate at low elevations and underestimate the lapse rate at high elevations. For example, in the northern transect an observed isotopic lapse rate of -1.46‰ km^{-1} has been reported for year 1983, based on data from elevations below 600 m, at 1700 m, and at 4080 m (Gonfiantini et al., 2001). Our modeled lapse rate for 1983 based on a complete elevation range is -1.18‰ km^{-1}. However, if we model $\delta^{18}O_p$ for the northern transects at elevations lower than 600 m, between 1600 and 1800 m, and between 4000 and 4100 m, the modeled isotopic lapse rate is -1.44‰ km^{-1}.

Fifth, REMOiso (and other regional climate models) have precipitation biases. As discussed in section 2.3, REMOiso tend to predict too much orographic precipitation along the Andean front. Therefore, we would expect an overestimation of lapse rates. However, REMOiso overestimates the recycling of vapor by evapotranspiration (Sturm et al., 2007) due to the bucket-type soil hydrology scheme that does not account for surface and sub-surface drainage and groundwater formation. Vapor fluxes from the surface are assumed to be dominantly transpiration, and thus soil moisture is released into the atmosphere without fractionation (Bariac et al., 1994). Therefore, the vapor transported from the lowlands to the flank of the Andes could be more enriched in $\delta^{18}O_p$. Because Rayleigh distillation along the flanks causes $\delta^{18}O_p$ to decrease exponentially with the cumulative precipitation, the isotopic content of the precipitation is a function of the initial isotope mass and water vapor mass within the air parcel and of the water vapor mass remaining when precipitation forms. Thus, more enriched $\delta^{18}O_p$ in low-elevation air masses can lead to lower-than-expected lapse rates.

In summary, spatial and temporal limitations in observed data may lead to biases in the analysis and interpretation of isotopic variability in the Andes. More data are needed to robustly determine local isotopic lapse rates and records reported in the literature need to be interpreted with caution.

2.7 Implications

The difficulty in interpreting isotopic records from the geological record stems in part from our limited understanding of the physical processes that control the isotope behavior. Our results and previous investigations indicate that a large number of factors can affect $\delta^{18}O_p$ in South America. In order to make use of isotopic records, it is necessary to understand the factors that are operating in a specific region. In general, our experiments suggest that the dominant processes influencing $\delta\ ^{18}O_p$ variability are (1) in the northern Andes, precipitation amounts controlled by low-latitude SST variability (e.g. ENSO), (2) in the northern central Andes, precipitation amounts and moisture source variability associated with the position of the Bolivian High, (3) in the southern central Andes, zonal wind speed and forced ascent, and (4) in the southern Andes, temperature variations. Although our study focuses on interannual variations on short (decadal) timescales, it is likely that the same physical relationships hold for longer (millennial, geological) timescales, and thus that we can extend the same processes to understand paleoclimate.

Our results can shed light on the ongoing debate of what influences the isotopic records in Andean ice cores. Tropical glaciers in Peru (Huascaran, Quelccaya) and Bolivia (Sajama) indicate mean annual $\delta^{18}O_p$ values at high altitudes vary by more than ∼10‰ over the last 40 years (e.g., Thompson et al., 1992, 1995, 1998). Earlier studies used the isotope-temperature relationship for high latitudes to interpret changes in tropical isotopic records as reflection of significant temperature fluctuations (Thompson et al., 2000). Our results are more consistent with recent studies that interpret Andean isotopic records in terms of ENSO variations, precipitation amount, or variable wind patterns. A link between Andean isotope records in glaciers and ENSO has been mainly suggested for the Huascaran and Quelccaya ice caps (Vuille et al., 2003b), located between our northern and northern central Andes domain, with cold (warm) conditions in the tropical Pacific during the Andean rainy season leading to more depleted (enriched) $\delta^{18}O_p$ values. However, the relationship mainly holds on longer timescales (several decades), but only appears weakly on interannual time scales (Henderson et al., 1999; Hoffmann et al., 2003). Our results suggest that glacier $\delta^{18}O_p$ in South America might also record variations in the Bolivian High. The position and strength of the Bolivian High is related to low- and mid-tropospheric heating, and thus, shows an overall correlation with ENSO conditions, but the upper-level circulation feature acts as an independent factor in influencing $\delta\ ^{18}O_p$ through changing wind pattern and vapor transport across the central Andes. In the Sajama record (northern central Andes domain), a statistically significant relationship between annual precipitation- weighted mean $\delta^{18}O_p$ and precipitation amount has been found over the past 50 years (Bradley et al., 2003).

This study emphasizes the importance of water vapor source on $\delta\ ^{18}O_p$. In contrast to previous studies that argue that the moisture influx from the Pacific is negligible for $\delta^{18}O_p$ in most regions in the Andes (Garreaud et al., 2003; Vuille et al., 2003a), our simulations demonstrate a strong tendency to more enriched $\delta^{18}O_p$ compositions in the central Andes when vapor is sourced over the subtropical South Pacific. A correlation between the origin of wind trajectories at 500 mb and annual amount-weighted $\delta^{18}O_p$ over the central Andes is consistent with previous findings by Henderson et al. (1999), which shows a relationship between interannual variations in Huascaran $\delta^{18}O_p$ and zonal wind variations over tropical South America at the 500-mb level over a 25-year period (1968 -1992). Our results suggest that the variability in $\delta^{18}O_p$ stored in Andean glaciers can be at least partly ascribed to changes in moisture source with more enriched $\delta^{18}O_p$ compositions related to a larger Pacific influence.

On millennial or geological time scales ENSO variations are likely less relevant, unless there is a significant increase or decrease in the frequency (Stott et al., 2002). Large-scale changes in the mean state of the Pacific on the other hand, as has been suggested at least in Pliocene times (e.g., Ravelo et al., 2004; Wara et al., 2005; Lee and Poulsen, 2006; Martinez-Garcia et al., 2010), might be important in influencing the isotopic composition of precipitation in the past. Tropical conditions during the Pliocene have been suggested to resemble a permanent El Niño with a weak or absent Walker circulation (Barreiro et al., 2006). Our results suggest that in the northern Andes, where variable Pacific sea surface temperatures play a crucial role in determining $\delta\ ^{18}O_p$, the absence of an east-west SST gradient in the tropical Pacific with stronger easterlies transporting drier air masses from the Amazon Basin could result in reduced precipitation and enriched $\delta^{18}O_p$ compositions in comparison to modern conditions. In the northern central Andes a permanent El Niño could cause a northward position of the Bolivian High, which enhances westerly winds and results in more enriched $\delta^{18}O_p$ compositions in the past.

Our results also have implications for paleoaltimetry interpretations on geological timescales. Significant changes in the isotopic composition of precipitation, recorded in paleosol carbonates from the central Andes, have been interpreted to reflect changes in surface elevations (e.g., Garzione et al., 2006) or in rainfall amounts (Poulsen et al., 2010). The interpretation of significant surface uplift in the central Andes since the late Miocene is based on the assumption that the depletion of 3-4‰ of $\delta^{18}O$ in ancient carbonate nodules is related to altitude, assuming modern climate conditions and isotopic lapse rates through time. Our results indicate that climate change, in particular changes in precipitation amount and moisture source, can have a significant effect on the central Andean $\delta^{18}O_p$ and $\delta^{18}O_p$ lapse rates. This conclusion supports previous work suggesting that the late Miocene $\delta^{18}O$ depletion reflects climate change (Ehlers and Poulsen, 2009) and most likely an initiation and intensification of convective rainfall along the eastern Andean flank (Poulsen et al., 2010). In addition, our results emphasize the difficulty in using observed modern lapse rates to interpret past changes in $\delta\ ^{18}O_p$ with altitude. Paleoaltimetry studies often use modern $\delta^{18}O$ - altitude relationships that were observed at a single location over a period of one or two years. Our model results indicate that annual lapse rates in the central Andes can vary by up to 300% over 24 years. Therefore, short-term observations may not represent mean conditions.

2.8 Conclusions

A high-resolution (~55 km) limited-domain climate model was used to investigate the causes of spatial and temporal variations in precipitation $\delta^{18}O$ and isotopic lapse rates along and across the Andes. Simulated annual amount-weighted $\delta^{18}O_p$ at the highest elevation sites in the Andes vary significantly with isotopic composition of approximately -5‰ in the northern Andes, -13‰ in the northern central Andes, -6‰ in the southern central Andes, and -9‰ in the south. Predicted isotopic lapse rates along the windward side of the mountain range between -0.88 $\pm$ 0.69 ‰ km^{-1} in the northern Andes, -1.43 $\pm$ 0.84‰ km $^{-1}$ in the northern central Andes, -0.97 $\pm$ 0.49‰ km^{-1} in the southern central Andes, and -2.91 $\pm$ 0.37‰ km^{-1} in the southern Andes. Interannual variability in precipitation $\delta^{18}O_p$ is relatively small in the northern, south central, and southern Andes ($\pm$2‰), and greater in the northern central Andes ($\pm$6‰). Isotopic lapse rates are characterized by high interannual variability in all regions.

Results indicate that climate controls on $\delta^{18}O_p$ vary from region to region along the Andes. In the northern Andes, the main factor influencing interannual variability in $\delta^{18}O_p$ is the amount effect with Pacific SSTs mainly controlling variations in precipitation. In the northern central Andes, the dominant controls on $\delta^{18}O_p$ are the amount of precipitation and moisture source with vapor originating over the South Pacific, North or South Atlantic, or the South American continent. In the southern central Andes $\delta^{18}O_p$ variations are related to zonal and meridional wind pattern influencing the amount of rainout along the Andean flanks. In the southern Andes

$\delta^{18}O_p$ is mainly influenced by temperature, while the amount effect is negligible due to the location of the southern Andes in the mid-latitude Westerlies and the lack of large convective storms.

Our model results are in good agreement with observation for $\delta^{18}O_p$, but annual amount-weighted mean isotopic lapse rates are smaller than observed data. The discrepancies between model and observation are caused by spatial and temporal limitations in observations and/or model limitations in dealing with orographic convergence. Our results elucidate the dominant regional process that drive $\delta^{18}O_p$ variability and, in this way, provide constraints for the interpretation of $\delta^{18}O_p$ archives.

2.9 Acknowledgments

This work was supported by grants to C.J.P. and T.A.E. from NSF (EAR Awards 0738822 and 0907817) and the University of Michigans Graham Environmental Sustainability Institute. C.J.P. also received support from the Alexander von Humboldt Foundation.

Bibliography

Aldrian, E., Duemenil-Gates, L., Jacob, D., Podzun, R. and Gunawan, D. Long-term simulation of Indonesian rainfall with the MPI regional model. *Climate Dynamics*, 22:795–814, 2004.

Aravena, R., Suzuki, O., Pena, H., Pollastri, A., Fuenzalida, H. and Grilli, A. Isotopic composition and origin of the precipitation in Northern Chile. *Applied Geochemistry*, 14:411–422, 1999.

Bariac, T., Gonzalez-Dunia, J., Katerji, N., Bethenod, O., Bertolini, J. and Mariotti, A. Spatial variation of the isotopic composition of water (18O, 2H) in the soil-plant-atmosphere system, 2. Assessment under field conditions. *Chemical Geology*, 115:317 – 333, 1994.

Barreiro, M., Philander, G., Pacanowski, R. and Fedorov, A. Simulations of warm tropical conditions with application to middle Pliocene atmospheres. *Climate Dynamics*, 26:349 – 365, 2006.

Bradley, R. S., Vuille, M., Hardy, D. and Thompson, L. Low latitude ice cores record Pacific sea surface temperatures. *Geophysical Research Letters*, 30(4):doi:10.1029/2002GL016546, 2003.

Broecker, W. Mountain glaciers: Recorders of atmospheric water vapor content? *Global Biogeochemical Cycles*, 11(4):589–597, 1997.

Brown, J., Simmonds, I. and Noone, D. Modeling d18O in tropical precipitation and the surface ocean for present-day climate. *Journal of Geophysical Research*, 111(D05105):doi:10.1029/2004JD005611, 2006.

Cole, J. E., Rind, D., Webb, R. S., Jouzel, J. and Healy, R. Climatic controls on interannual variability of precipitation d18O: Simulated influence of temperature, precipitation amount, and vapor source region. *Journal of Geophysical Research*, 104(D12):14,223 – 14,235, 1999.

Cruz, F. W., Wang, X., Auler, A., Vuille, M., Burns, S. J., Edwards, L. R., Karmann, I. and Cheng, H. Orbital and millennial-scale precipitation changes in Brazil from speleothem records. *Developments in Paleoenvironmental Research*, 14:29 – 60, 2009.

Dansgaard, W. Stable isotopes in precipitation. *Tellus*, XVI:436 – 468, 1964.

Ehlers, T. and Poulsen, C. J. Influence of Andean uplift on climate and paleoaltimetry estimates. *Earth and Planetary Science Letter*, 281:238–248, 2009.

Fritz, P., Suzuki, O., Silva, C. and Salati, E. Isotope hydrology of groundwaters in the Pampa del Tamarugal, Chile. *Journal of Hydrology*, 53:161–184, 1981.

Garcia, M., Villalba, F., Araguas Araguas, L. and Rozanski, K. The role of atmospheric circulation patterns in controlling the regional distribution of stable isotope contents in precipitation. *Isotope techniques in the study of environmental change*, IAEA-SM-349/7: Vienna, International Atomic Energy agency:127–140, 1998.

Garreaud, R., Vuille, M. and Clement, A. C. The climate of the Altiplano; observed current conditions and mechanisms of past changes. *Palaeogeography, Palaeoclimatology, Palaeoecology*, 194:5–22, 2003.

Garzione, C. N., Molnar, P., Libarkin, J. and MacFadden, B. Rapid late Miocene rise of the Bolivian Altiplano: Evidence for removal of mantle lithosphere. *Earth and Planetary Science Letters*, 241:543–556, 2006.

Godfrey, L., Jordan, T., Lowenstein, T. K. and Alonso, R. Stable isotope constraints on the transport of water to the Andes between 22? and 26?S during the last glacial cycle. *Palaeogeography, Palaeoclimatology, Palaeoecology*, 194:299 – 317, 2003.

Gonfiantini, R., Roche, M.-A., Olivry, J.-C., Fontes, J.-C. and Zuppi, G. M. The altitude effect on the isotopic composition of tropical rains. *Chemical Geology*, 181:147 – 167, 2001.

Henderson, K., Thompson, L. and Lin, P.-N. Recording of El Nio in ice core d18O records from Nevado Huascarn, Peru. *Journal of Geophysical Research*, 104(D24):31053 – 31065, 1999.

Hoffmann, G., Jouzel, J. and Masson, V. Stable water isotopes in atmospheric general circulation models. *Hydrological Processes*, 14:1385 – 1406, 2000.

Hoffmann, G., Ramirez, E., Taupin, J., Francou, B., Ribstein, P., Delmas, R., Duerr, H., Gallaire, R., Simoes, J., Schotterer, U., Stievenard, M. and Werner, M. Coherent isotope history of Andean ice cores over the last century. *Geophysical Research Letters*, 30(4):doi:10.1029/2002GL014870, 2003.

Hoffmann, G., Werner, M. and Heimann, M. Water isotope module of the ECHAM atmospheric general circulation model: A study on timescales from days to several years. *Journal of Geophysical Research*, 103(D14):16871 – 16896, 1998.

Insel, N., Poulsen, C. J. and Ehlers, T. A. Influence of the Andes mountains on South American moisture transport, convection, and precipitation. *Climate Dynamics*, pages doi:10.1007/s00382–009–0637–1, 2009.

Jouzel, J., Russell, G., Suozzo, R., Koster, R., White, J. and Broecker, W. Simulations of the HDO and H218O atmospheric cycles using the NASA GISS general circulation model: The seasonal cycle for present-day conditions. *Journal of Geophysical Research*, 92(D12):14739 – 14760, 1987.

Lee, S. and Poulsen, C. J. Sea ice control of Plio-Pleistocene tropical Pacific climate evolution. *Earth and Planetary Science Letter*, 248:253 – 262, 2006.

Lenters, J. D. and Cook, K. H. Simulation and diagnosis of the regional summertime precipitation climatology of South America. *Journal of Climate*, 8(12):2988–3005, 1995.

Majewski, D. The Europa-Modell of the Deutscher Wetterdienst. *ECMWF Seminar on numerical methods in atmospheric models*, 2:147–191, 1991.

Martinez-Garcia, A., Rosell-Mele, A., McClymont, E., Gersonde, R. and Haug, G. Subpolar link to the emergence of the modern equatorial Pacific cold tongue. *Science*, 328:1550 – 1553, 2010.

Mettier, R., Schlunegger, F., Schneider, H., Rieke-Zapp, D. and Schwab, M. Relationships between landscape morphology, climate and surface erosion in northern Peru at 5?S latitude. *International Journal of Earth Sciences*, 98:doi:10.1007/s00531–008–0355–7, 2009.

Montecinos, A., Diaz, A. and Aceituno, P. Seasonal diagnostic and predictability of rainfall in subtropical South America based on tropical Pacific SST. *Journal of Climate*, 13:746 –758, 2000.

Nordeng, T. Extended version of the convective parameterization scheme at ECMWF and the impact on the mean and transient activity of the model in the tropics. *ECMWF Tech. Memo*, 206:7 pp., 1994.

Pierrehumbert, R. T. Huascarn d18O as an indicator of tropical climate during the Last Glacial Maximum. *Geophysical Research Letters*, 26(9):1345 – 1348, 1999.

Poulsen, C. J., Ehlers, T. and Insel, N. Onset of convective rainfall during gradual late Miocene rise of the central Andes. *Science*, page doi:10.1126/science.1185078, 2010.

Poveda, G., Waylen, P. R. and Pulwarty, R. S. Annual and inter-annual variability of the present climate in northern South America and southern Mesoamerica. *Palaeogeography, Palaeoclimatology, Palaeoecology*, 234:3–27, 2006.

Ramirez, E., Hoffmann, G., Taupin, J., Francou, B., Ribstein, P., Caillon, N., Ferron, F., Landais, A., Petit, J., Pouyaud, B., Schotterer, U., Simoes, J. and Stievenard, M. A new Andean deep ice core from Nevado Illimani (6350 m), Bolivia. *Earth and Planetary Science Letter*, 212:337 – 350, 2003.

Ravelo, A., Andreasen, D., Lyle, M., Olivarez Lyle, A. and Wara, M. Regional climate shifts caused by gradual global cooling in the Pliocene epoch. *Nature*, 429:263 – 267, 2004.

Roeckner, E., Arpe, K., Bengtsson, L., Christoph, M., Claussen, M., Duemenil, L., Esch, M., Giorgetta, M., Schlese, U. and Schulzweida, U. The atmospheric general circulation model ECHAM-4: Model description and simulation of the present day climate. *Max-Planck-Institut fuer Meteorologie Report*, No. 218, 1996.

Rojas, M. and Seth, A. Simulation and sensitivity in a nested modeling system for South America. Part II: GCM boundary forcing. *Journal of Climate*, 16:2454–2471, 2003.

Rozanski, K., Araguas Araguas, L. and Gonfiantini, R. Isotopic patterns in modern global precipitation. *in: Swart, P.K., Lohmann, K.C, McKenzie, J., Savin, S. (Eds), Climate Changes in Continental Isotopic Records. Am. Geophys. Union, Geophys. Monograph*, 78:1–36, 1993.

Salati, E., A, D., Matsui, E. and Gat, J. Recycling of water in the Amazon Basin: An isotopic study. *Water Resources Research*, 15(5):1250 – 1258, 1979.

Stern, L. A. and Blisniuk, P. M. Stable isotope composition of precipitation across the southern Patagonian Andes. *Journal of Geophysical Research*, 107(D23)(4667):doi:10.1029/2002JD002509, 2002.

Stott, L., Poulsen, C. J., Lund, S. and Thunell, R. Super ENSO and global climate oscillations at millenial time scales. *Science*, 297:222 – 226, 2002.

Sturm, C., Hoffmann, G. and Langmann, B. Simulation of the stable water isotopes in precipitation over South America: Comparing regional to global circulation models. *Journal of Climate*, 20:3730 – 3750, 2007.

Sturm, K., Hoffmann, G., Langmann, B. and Stichler, W. Simulation of d18O in precipitation by the regional circulation model REMOiso. *Hydrological Processes*, 19:3425 – 3444, 2005.

Thompson, L., Davis, M., Mosley Thompson, E., Sowers, T., Henderson, K., Zagorodnov, V., Lin, P.-N., Mikhalenko, B., Campen, R., Bolzan, J., Cole-Dai,

J. and Francou, B. A 25,000 year tropical climate history from Bolivian ice cores. *Science*, 282(5295):1858 – 1864, 1998.

Thompson, L., Mosley Thompson, E., Bolzan, J. and Koci, B. A 1500-year record of tropical precipitation in ice cores from the Quelccaya ice cap, Peru. *Science*, 229(4717):971–973, 1985.

Thompson, L., Mosley Thompson, E., Davis, M., Lin, P.-N., Henderson, K., Cole-Dai, J., Bolzan, J. and Liu, K.-b. Late glacial stage and Holocene tropical ice core records from Huascarn, Peru. *Science*, 269:46 – 50, 1995.

Thompson, L., Mosley Thompson, E. and Henderson, K. Ice-core palaeoclimate records in tropical South America since the Last Glacial Maximum. *Journal of Quaternary Science*, 15(4):377 – 394, 2000.

Thompson, L., Mosley Thompson, E. and Thompson, P. *Reconstructing interannual climate variability from subtropical and tropical ice-core records*. El Nio: Historical and paleoclimate aspects of the Southern Oscillation. Cambridge Univ. Press, New York, 1992.

Tiedtke, M. A comprehensive mass flux scheme for cumulus parameterization in large-scale models. *Monthly Weather Review*, 117:1779 – 1800, 1989.

Vimeux, F., Ginot, P., Schwikowski, M., Vuille, M., Hoffman, G., Thompson, L. and Schotterer, U. Climate variability during the last 1000 years inferred from Andean ice cores: A review of methodology and recent results. *Palaeogeography, Palaeoclimatology, Palaeoecology*, 281(3-4):229–241, 2008.

Vuille, M., Bradley, R. S., Healy, R., Werner, M., Hardy, D., Thompson, L. and Keimig, F. Modeling d18O in precipitation over the tropical Americas: 2. Simulation of the stable isotope signal in Andean ice cores. *Journal of Geophysical Research*, 108(D6):doi:10.1029/2001JD002039, 2003a.

Vuille, M., Bradley, R. S., Werner, M., Healy, R. and Keimig, F. Modeling d18O in precipitation over the tropical Americas: 1. Interannual variability and climate controls. *Journal of Geophysical Research*, 108(D6):doi:10.1029/2001JD002038, 2003b.

Vuille, M. and Werner, M. Stable isotopes in precipitation recording South American summer monsoon and ENSO variability: observations and model results. *Climate Dynamics*, 25:401 – 413, 2005.

Wara, M., Ravelo, A. and Delaney, M. Permanent El Nio-like conditions during the Pliocene warm period. *Science*, 309:758 – 761, 2005.

CHAPTER III

Influence of the Andes Mountains on South American moisture transport, convection, and precipitation

3.1 Abstract

Mountain ranges are known to have a first-order control on mid-latitude climate, but previous studies have shown that the Andes have little effect on the large-scale circulation over South America. We use a limited-domain general circulation model (RegCM3) to evaluate the effect of the Andes on regional-scale atmospheric dynamics and precipitation. We present experiments in which Andean heights are specified at 250 m, and 25, 50, 75, and 100% of their modern values. Our experiments indicate that the Andes have a significant influence on moisture transport between the Amazon Basin and the central Andes, deep convective processes, and precipitation over much of South America through mechanical forcing of the South American low-level jet(LLJ) and topographic blocking of westerly flow from the Pacific Ocean. When the Andes are absent, the LLJ is absent and moisture transport over the central Andes is mainly northeastward. As a result, deep convection is suppressed and precipitation is low along the Andes. Above 50% of the modern elevation, a southward

Official citation:
Insel, N., C.J. Poulsen, T.A. Ehlers (2009). Influence of the Andes Mountains on South American moisture transport, convection, and precipitation. *Climate Dynamics*, doi:10.1007/s00382-009-0637-1

flowing LLJ develops along the eastern Andean flank and transports moisture from the tropics to the subtropics. Moisture drawn from the Amazon Basin provides the latent energy required to drive convection and precipitation along the Andean front. Large northerly moisture flux and reduced low-level convergence over the Amazon Basin leads to a reduction in precipitation over much of the basin. Our model results are largely consistent with proxy evidence of Andean climate change, and have implications for the timing and rate of Andean surface uplift.

3.2 Introduction

Large, mid-latitude mountain ranges have a first-order control on large-scale atmospheric circulation by modifying stationary wave patterns. For example, the Rocky Mountains and the Tibetan plateau modify the mid-latitude storm tracks and regions of subsidence and drying by influencing upper-tropospheric flow (e.g., Broccoli and Manabe, 1992; Kutzbach et al., 1989). The Andes Mountains are the dominant topographic feature in South America, extending over 7,000 km from $\sim$7° to 45°S, with Andean plateau elevations as high as $\sim$4,000 m over a large portion of the central Andes. Despite its enormity, previous studies have suggested the Andes Mountains have only a minor influence on large-scale atmospheric patterns over South America. The major stationary features, including the Bolivian High and the Nordeste Low, the low-level northerly flow over northern and central South America, and the large-scale precipitation are mainly products of diabatic heating over the Amazon Basin and are only marginally affected by the Andes (e.g., Figueroa et al., 1995; Kleeman, 1989; Lenters and Cook, 1995, 1997).

However, it has been shown that the Andes affect regional-scale climate by blocking zonal flow and influencing regional wind pattern and precipitation. Mechanical forcing by the Andes is critical to the formation of the South American low-level jet (LLJ) (Campetella and Vera, 2002; Gandu and Geisler, 1991). The Andes block and deflect low-level trade winds from the equatorial Atlantic to form a northerly/northwesterly barrier jet that flows along the eastern flanks of the mountains (Virji, 1981) and transports moisture from the Amazon Basin to the subtropical regions of the continent (Vera et al., 2006). On a more local scale, the Andes focus precipitation along the eastern flanks of the northern and central Andes due to orographic lifting and the inducement of small-scale convergence and convection (Lenters and Cook, 1995). Though linkages between the Andes and regional dynamics and precipitation have been established, the details and significance of these interactions on modern climate are less certain. For example, it is unclear to what extent the Andes, through their impact on the LLJ, affect the heat and moisture transport from the tropics to higher latitudes and how important this moisture transport is to convective processes that drive precipitation. It is also not known whether the Andes significantly influence low-level flow away from the Andean flanks or whether it affects precipitation in remote regions, including the Amazon Basin and the South Atlantic Convergence Zone (SACZ).

Knowledge of these interactions is important for understanding paleoclimate as well as modern climate processes. The modern Andes are a geologically young feature that was uplifted during the Neogene ($\sim$25 Ma to present) due to the subduction of the Nazca Plate below South America (Isacks, 1988). Paleoclimate proxies for this time indicate that climate conditions along the eastern margin of the Andean plateau changed from arid to humid (e.g., Kleinert and Strecker, 2001; Starck and Anzotegui, 2001), while the western flanks of the plateau became hyperarid (e.g., Alpers and

Brimhall, 1988; Rech et al., 2006). To determine whether Neogene paleoclimate was responding mainly to surface uplift or some other forcing requires an understanding of the evolution of interactions between the Andes and regional climate.

The objective of this study is to investigate the influence of the Andes on regional climate over South America. In particular, we focus on the effect of the Andes on the LLJ, moisture transport, and precipitation processes. The influence of the Andes on South American climate has been previously studied through the use of global and regional climate models (Campetella and Vera, 2002; Figueroa et al., 1995; Gandu and Geisler, 1991; Lenters and Cook, 1995). However, these models are limited in their utility due to their coarse resolution, lack of diurnal and/or seasonal heating, or absence of hydrological processes. As a result of these limitations, moisture transport and seasonal precipitation could not be simulated, or was biased by the unrealistic representation of the Andes as a low, broad topographic feature. This study represents an advance on previous studies by using a regional general circulation model (RegCM3) capable of representing the narrow, steep topography of the Andes (Fig. 3.1a), and a convection scheme that has been shown to provide a realistic simulation of present-day climatology. To evaluate dynamical and physical atmospheric changes associated with variations in Andean plateau height during the Cenozoic, we present a series of experiments in which Andean heights are specified at 250 m, and 25, 50, 75, and 100% of their modern values. Our results indicate that even though the Andes have little effect on large-scale stationary features they have a fundamental impact on moisture transport and precipitation across South America.

3.3 Methods

3.3.1 Model

The RegCM3 (Pal et al., 2007) is a third generation, three-dimensional regional climate model, based on the original model developed by Giorgi et al. (1993a,b), with a dynamical core that is adopted from the hydrostatic version of the Pennsylvania State University-National Center for Atmospheric Research Mesoscale Model (MM5) (Grell et al., 1994). It is a primitive-equation, hydrostatic, compressible model with sigma-vertical coordinates (Giorgi et al., 1993a). Improvements in the representation of precipitation physics, surface physics, atmospheric chemistry and aerosols in the RegCM allows an enhanced model performance in tropical and subtropical regions (Pal et al., 2007).

RegCM3 experiments were performed for South America using a continental scale domain with 60 km horizontal resolution and 18 levels in the vertical (Fig. 3.1). The land surface is represented by the Biosphere-Atmosphere Transfer Scheme (BATS, Dickinson et al. (1993)) that is designed to describe the role of vegetation and interactive soil moisture in modifying the surface-atmosphere exchanges in momentum, energy, and water vapor (Fig. 3.1b)(Giorgi and Marinucci, 1996). Sea-surface temperatures (SST) were obtained from the NOAA optimum interpolation (OI) SST analysis (Reynolds et al., 2002). Atmospheric lateral boundary conditions from 40 yr reanalysis (ERA-40) data are derived from the European Centre for Medium-Range Weather Forecast (ECMWF). Simulations are 10 years in length (January 1991 - December 2000) and results are based on the last 5 years of simulation.

Convective precipitation was computed by two different schemes, the Grell scheme (Grell, 1993) and the MIT Emanuel scheme (Emanuel, 1991). In this study, we present results from experiments using the MIT-Emanuel convection scheme, because it provides the best fit to modern precipitation over the tropics and subtropics of South America. This convective scheme assumes that the mixing in clouds is highly episodic and inhomogeneous and considers convective fluxes based on idealized model of subcloud-scale updrafts and downdrafts (Pal et al., 2007). In comparison to other convective schemes, the Emanuel scheme includes a formulation for auto conversion of cloud water into precipitation in cumulus clouds (Pal et al., 2007). Our experiments are in good agreement with previous studies that have shown that the use of the RegCM3 version together with the Emanuel convection scheme leads to improved simulations of precipitation, temperature and low-level wind pattern compared to the RegCM3/Grell configuration and other RCMs (Pal et al., 2007; Seth et al., 2006). In particular, previous results have shown a strong dry bias in austral summer over the Amazon region mostly related to deficient parameterization of convection and poor presentation of surface processes over tropical areas (e.g., Berbery and Collini, 2000; Chou et al., 2002; DeSales and Xue, 2006; Rojas and Seth, 2003) that is absent in analogous simulations with the Emanuel scheme (Seth et al., 2006).

3.3.2 Model setup and free parameters

The goal of this study is to quantify the impact of Andean uplift on South American climate dynamics. Our model domain ranges from 100°W to 15°W and 12°N to 45°S. Previous studies have shown that large domains are necessary to accurately simulate sensitivity to forcings within the domain (Seth and Giorgi, 1998; Seth and Rojas, 2003). For this reason, a large domain, extending over parts of the Atlantic and Pacific Ocean, was chosen (Fig. 3.1). To this end, we designed experiments to account for different Andean elevations without changing other parameters. In total, five experiments were completed with discrete Andean elevations (AE). The 100%

AE simulation assumes a present-day Andean elevation that is based on a global digital elevation model from the USGS with elevations regularly spaced at 30-arc seconds (USGS, 1996). Unlike previous GCM studies of the region, our simulations resolve the high elevations (exceeding 4,000 m) and narrow extent of the Andes (Fig. 3.1). The 75, 50, and 25% experiments simulate the climate when the Andes were reduced to three quarters, one half, and one quarter of the modern Andean elevation, respectively. For the no Andes case (0% AE), Andean elevations were specified as 250 m. In other regions of South America, the topography was maintained at modern elevations. In this study, we do not account for global climate change during the Cenozoic. Trace gases (i.e. 355 ppmv CO_2, 1714 ppbv CH_4, 311 ppbv NO_2), SST, vegetation cover, solar luminosity, and orbital parameters were specified to represent modern conditions and remain constant in all experiments. The influence of these factors on the Cenozoic evolution of South American climate will be addressed in a future study.

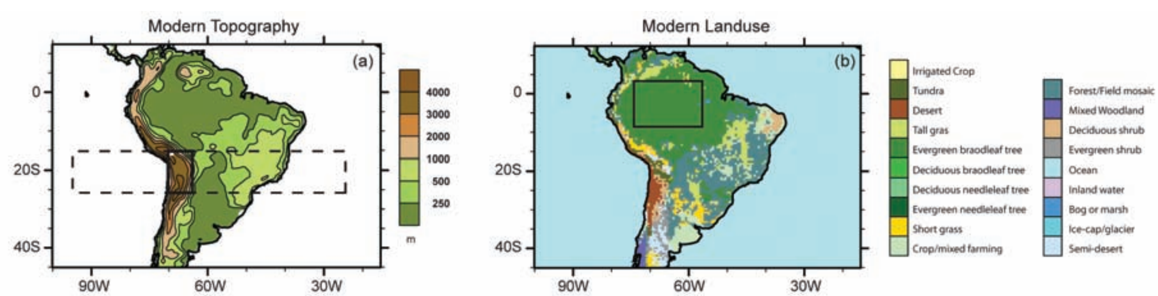

Figure 3.1: Model domain with topography and land cover in South America. (a) Present day elevations used in RegCM3 are from the United States Geological Survey (USGS). Solid box indicates the domain for the Andean plateau region; dashed box shows the profile location for height/pressure-longitude plots. (b) Land surface description used in RegCM3 is based on the Global Land Cover Characterization dataset and defined by BATS (Biosphere Atmosphere Transfer Scheme). Box indicates the domain for the Amazon Basin.

3.4 Modern climatology

A comparison between simulated and observed data indicates that RegCM3 performs very well in capturing the general climatology in South America. The model performance for modern precipitation is assessed by using independent precipitation observations from the Global Historical Climatology Network (GHCN) data base (Figures 3.2a, b) (NOAA/NESDIS/NCDC, 2003). We interpolated the mean seasonal precipitation from climate stations in South America with records of monthly precipitation exceeding 10 years. The model captures the distribution of summer (DJF, December; January; February) precipitation across South America, including regions of maximum precipitation in the central part of the Amazon Basin and along the eastern flanks of the central Andes, as well as arid conditions over northeast Brazil, Venezuela, northern Chile and southern Argentina (compare Figures 3.2a, b). The modeled summer precipitation over the Amazon Basin is approximately 30% higher than the observed precipitation in this area. We attribute the overestimate of precipitation to the land surface model that likely overestimates the moisture component that is recycled over the Amazon Basin, resulting in high precipitation rates. Preliminary experiments with RegCM coupled to the Community Land Model (CLM), with an improved canopy integration scheme and a better simulation of the hydrological cycle, yield lower precipitation rates in line with observations. In addition to overestimating Amazon precipitation, the modeled summer precipitation along the eastern flank of the Andes and on the Andean plateau is more pronounced than in the observed pattern with the Andean plateau region receiving several mm/day rainfall that is not observed in the station data. However, seasonal variations in precipitation including the high rainfall associated with seasonal migration of the SACZ (e.g., Horel et al., 1989; Wang and Fu, 2002) are well simulated by RegCM3. Therefore, despite small discrepancies in the absolute amounts of precipitation over the Andean plateau region, the relative precipitation amounts between different scenarios are most likely realistic.

In addition to the precipitation distribution, RegCM3 also captures other important climatological features over South America. For example, simulated summer surface temperatures agree well in structure and magnitude with the Climatic Research Unit (CRU) derived temperatures, with maximum values in Northern Argentina, northeast Brazil, and Venezuela (Fig. 3.2c,d). The Chaco Low, a low pressure system observed in central South America during the summer, is well developed. The modeled low-level (800-mbar) circulation over South America, with strong easterlies in the northern part of South America and an anticlockwise rotation of winds over the central part of the continent, resembles NCEP reanalysis winds at the same level (compare Figures 3.2e and 3.2f). Moreover, the upper-level (200 mbar) circulation, including the Bolivian High (see Section 3.5.3), an intense quasi- stationary anticyclone (e.g., Horel et al., 1989; Lenters and Cook, 1997; Virji, 1981) that forms in a region of high precipitation in response to condensational heating (e.g., DeMaria, 1985; Lenters and Cook, 1997; Silva-Dias et al., 1983), is simulated. Our simulation places the center of the anticyclone at around 20°S and 65°W (Fig. 2g), in good agreement with data obtained from geostationary satellite images that locate the Bolivian High at 17°S and 65°W (Virji, 1981) and NCEP reanalysis data (Fig. 3.4).

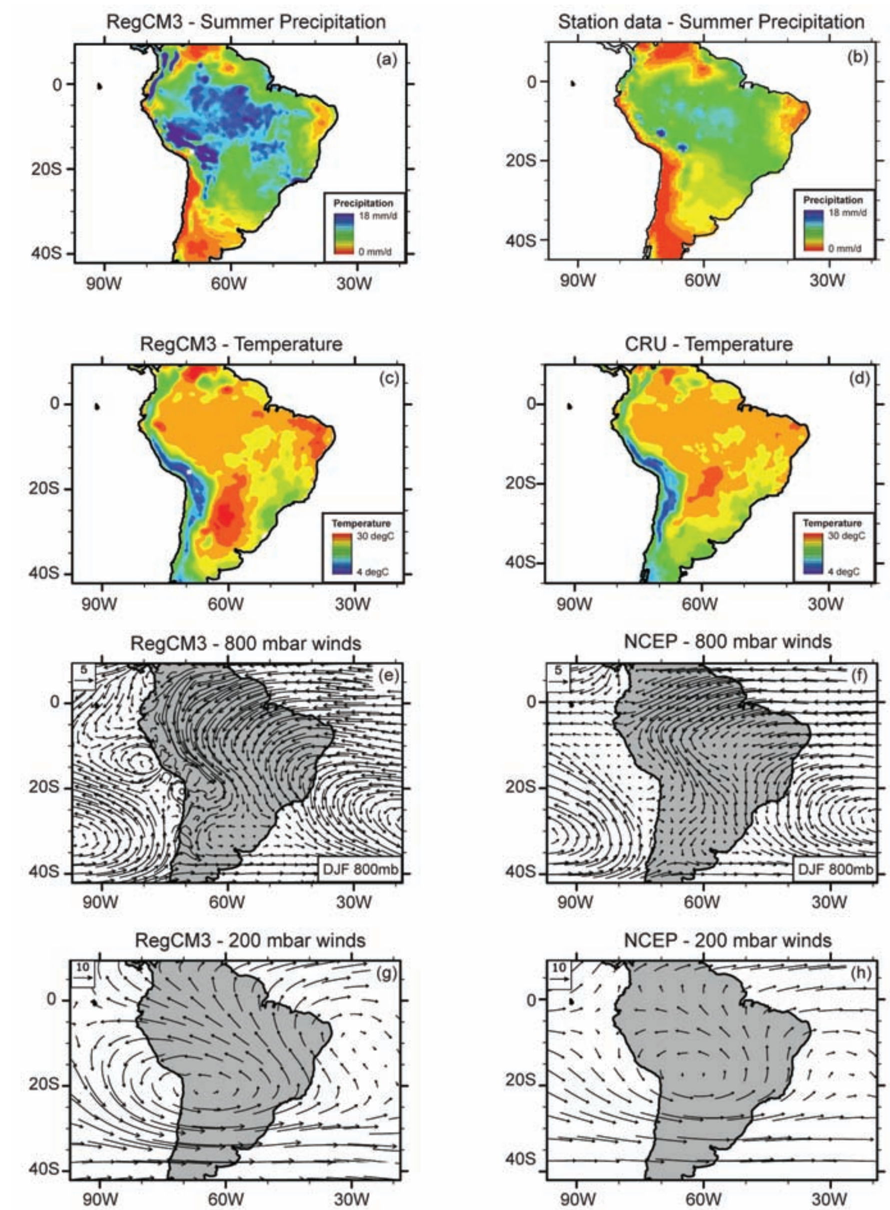

Figure 3.2: Comparison of modeled data versus observations for precipitation, temperature, and winds. All plots show summer conditions (December, January, February). (a) RegCM3 modeled modern summer precipitation in South America. (b) Observed summer precipitation, based on precipitation time series from the Global Historical Climatology Network (GHCN) database. Interpolated monthly precipitation data are from climate stations that recorded more than 10 years of precipitation for each month to ensure the relevance of the data. (c) RegCM3 modeled summer temperature. (d) Same as c, but interpolated from CRU data. (e) RegCM3 modeled winds at 800 mbar sigma level. (f) Same as e, but interpolated from NCEP reanalysis data. (g) RegCM3 modeled winds at 200 mbar sigma levels. (h) Same as g, but interpolated from NCEP reanalysis data. Small discrepancies between the climatologic fields from modeled data and reanalysis data are based on the different horizontal resolution of the datasets. Note that the RegCM3 model simulated climate parameters with a horizontal resolution of 60 km, the CRU data are based on a 0.5 x 0.5° grid, while the NCEP data are from a global grid with spatial resolution of 2.5 x 2.5°.

3.5 Results

3.5.1 Precipitation and low-level circulation for simulations with modern Andes

Precipitation in South America is highly seasonal with $\sim$50$-$80% of precipitation falling in austral summer. Summer precipitation in South America is focused in the Amazon Basin, along the eastern flanks of the northern and central Andes, and the SACZ (Fig. 3.3a). Precipitation maxima are generally $\sim$15 mm day^{-1} for all three regions. Most of the precipitation is convective in origin, but the climatological conditions that promote convection differ between regions.

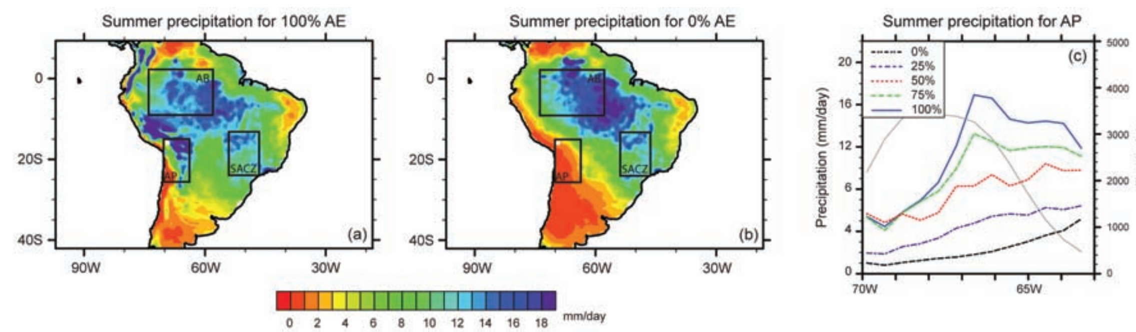

Figure 3.3: Simulated precipitation in South America during the summer (averaged over December, January, February). (a) Total precipitation for simulations with modern Andes. Boxes represent the Amazon Basin (AB), the Andean plateau (AP), and the South Atlantic Convergence Zone (SACZ), respectively. (b) Same as a, but for simulations with no Andes. (c) Total precipitation over the Andean plateau region (15-26°S) for different Andean heights (in percent from modern elevation). Solid gray line represents modern topography

In the Amazon Basin, precipitation is nearly uniform throughout the year. Convection over the Amazon Basin is triggered by convergence of moisture-laden northeasterly trade winds across the basin with the North Atlantic Ocean as the primary moisture source (Fig. 3.4a). Transport of moist, warm air by zonal winds and strong evapotranspiration (not shown) due to rainforest vegetation and high soil moisture provide additional conditions that favor vigorous convection over the Amazon Basin. Convection in the lower and middle troposphere is indicated by the development of thick clouds to ~400 mbar (not shown). In the extratropics, simulated precipitation is highly seasonal. The model captures the summer precipitation maxima over east-central South America associated with the SACZ (Fig. 3.3a). This precipitation is predominantly convective, as indicated by the presence of high clouds (Fig. 3.5a). The formation of convective precipitation in this region is related largely to the seasonal strengthening of the South Atlantic High, which directs low-level flow from the tropics to the subtropics (Fig. 3.4a). The convergence of this warm moist air from the Amazon Basin provides the moisture and energy for deep convection and precipitation. A significant seasonal precipitation cycle exists in the Andean plateau region with strong summer precipitation (Fig. 3.3a) and very dry conditions during the winter. Seasonality in Andean precipitation is related to the seasonal insolation cycle over South America and the associated migration of the inter-tropical convergence zone. As indicated by a strong southward component of wind directions, moisture is supplied by transport of water vapor from the Amazon Basin up the eastern slopes of the Andes (Fig. 3.4a). Through orographic lifting, the Andes trigger condensation, latent heat release, and strong convective updrafts during the summer. The formation of high clouds that extend into the lower stratosphere up to 150 mbar is symptomatic of these convective updrafts (Fig. 3.5a). Deep convection provides 65% of the simulated precipitation. A smaller portion of the precipitation results from the passage and orographic lifting of frontal systems, i.e., large- scale precipitation. Orographic and convective lifting along the eastern side of the Andes is evident by the strong negative vertical velocity (omega) (Fig. 3.6a), indicating upward airflow.

Summertime, low-level flow over the Amazon Basin, the SACZ, and Andes is dominated by northerly winds. Along the eastern flanks of the Andes, this low-level flow organizes into a fast-flowing low-level jet (LLJ). A cross section of meridional

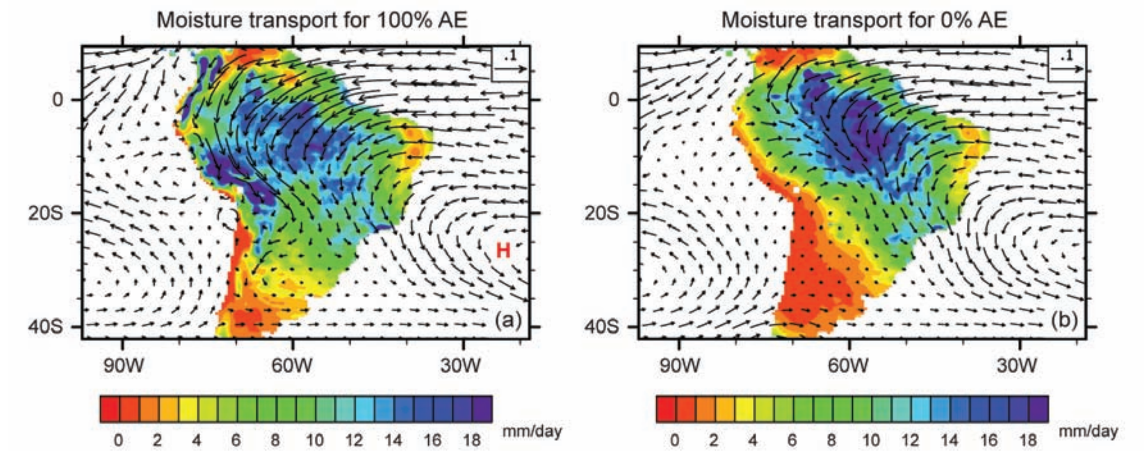

Figure 3.4: Low- level (800 mbar) moisture transport/winds in South America. (a) Moisture transport during the summer for simulations with modern Andes. H represents the South Atlantic High. (b) Same as a, but for simulation with no Andes.

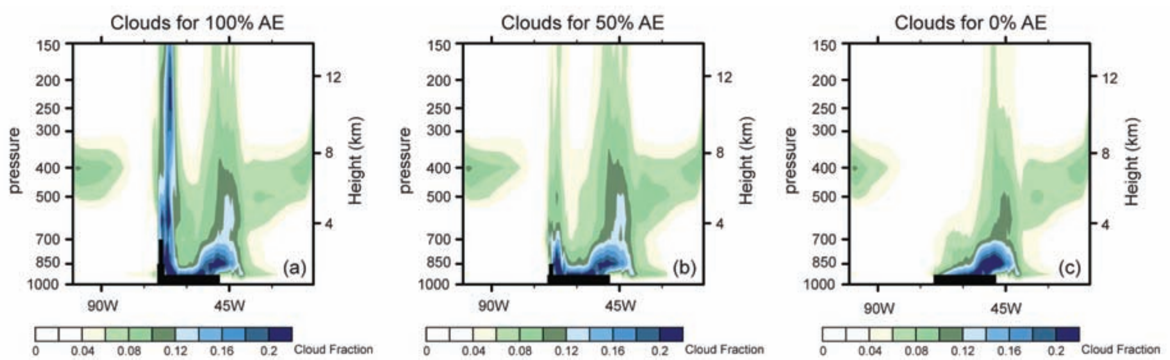

Figure 3.5: Simulated clouds over South America between 15 and 26°S latitude during summer. (a) Height/Pressure-longitude profile for clouds over the Andean plateau region and the SACZ for simulations with modern Andes. (b) Same as a, but for simulations with 50% Andean heights. (c) Same as a, but for simulations with no Andes

wind at 15-26°S, depicted in Fig. 3.7a, illustrates the well-develop jet, which has maximum northerly velocities of over 8 m s^{-1} and monthly average peak velocities up to ∼11 m s^{-1}. The LLJ is also a region of high specific humidity (Fig. 3.7b)and high relative humidity (Fig. 3.7c). In fact, it is this large southward transport of water vapor that defines the LLJs role in South American climate. The southward-transported vapor provides the latent heat and moisture source for precipitation along the Andean flanks. In support of this view, strong convection, cloud formation (Fig. 3.5a) and upward motion (Fig. 3.6a) correspond with regions of maximum latent heating and near-surface convergence (Fig. 3.8a) along the eastern margin of the Andes. In contrast, the subtropical Pacific on the western side of the Andes does not contribute substantial amounts of moisture or latent heat, because the low-level flow is blocked by the steep Andean topography and large-scale subsidence (Figs. 3.6a and 3.7a).

In sum, our model results indicate that the role of the Andes in precipitation processes is not only due to orographic lifting. Rather, the Andes influence precipitation through dynamical processes involving the development of the LLJ, moisture transport, and the development of deep convection.

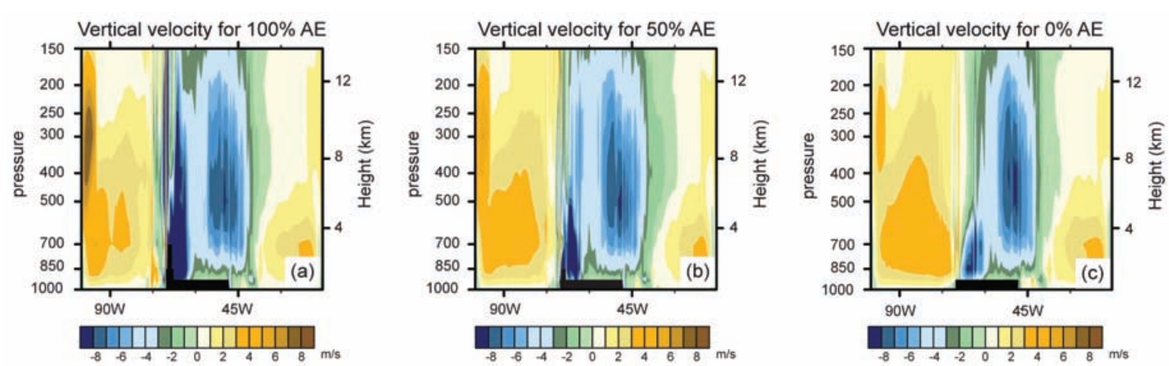

Figure 3.6: Simulated vertical velocity (omega) across South America between 15 and 26°S latitude during summer. Height/pressure-longitude profile with negative values indicating a strong upward air component. (a) Simulations with modern Andes. (b)Simulations with 50% Andean heights. (c) Simulations with no Andes.

3.5.2 Effects of uplifting topography on precipitation and low-level circulation

In the previous section, we describe on the basis of climatological relationships that the modern Andes play an important role in modulating low-level circulation, moisture transport and precipitation. To explicitly demonstrate the interplay between the Andes, convection, and precipitation, and to improve our understanding of how and when Andean topography influences local and regional processes, we explore changes in South American climatology over a range of prescribed Andean elevations.

The Andes have a substantial impact on precipitation across much of western South America. When the Andes are absent, precipitation along the eastern flanks of the central Andes is extremely low with $\sim$2$-$4 mm day^{-1} (Fig. 3.3b). With increasing Andean plateau height, precipitation increases continuously to $\sim$15 mm day^{-1} for the modern Andes (Fig. 3.3c). The reduction in Andean precipitation is related to a decrease in moisture transport and suppression of convection.

Moisture transport along the central Andes is strongly affected by the removal of topography. Without an orographic barrier, the LLJ and its transport of relatively warm, moist air disappears (Figs. 3.7g and 3.7h) and latent heat along the flanks of the Andes is low ($<$100 W m^{-2}; Fig. 3.8b). With a deficit in moisture and latent heat, convective processes are suppressed, evident by a reduction in high clouds over the central Andes (compare Figs. 3.5a and 3.5c). In the absence of the Andes, prevailing winds over the plateau region are sourced from the Pacific Ocean (Fig. 3.4b). The southwesterly flow is characterized by low water vapor content ($<$6 g kg^{-1}) and low relative humidity ($<$0.5) (Figs. 3.7g-i) due to low surface temperatures associated with the Humboldt Current along the west coast of South America and subtropical atmospheric subsidence (e.g., Rutllant and Ulriksen, 1979). Moreover, without a barrier, the lifting mechanism disappears and vertical velocities in the lower atmosphere are strongly reduced (Fig. 3.6c).

Initial uplift of the Andes to less than 50% of modern elevations leads to an increase in precipitation, specific humidity and relative humidity over the plateau area and along the eastern Andean flanks (Figs. 3.3c, 3.9a, and 3.9b). An increase in water vapor content over these regions during initial uplift of the Andes is re-

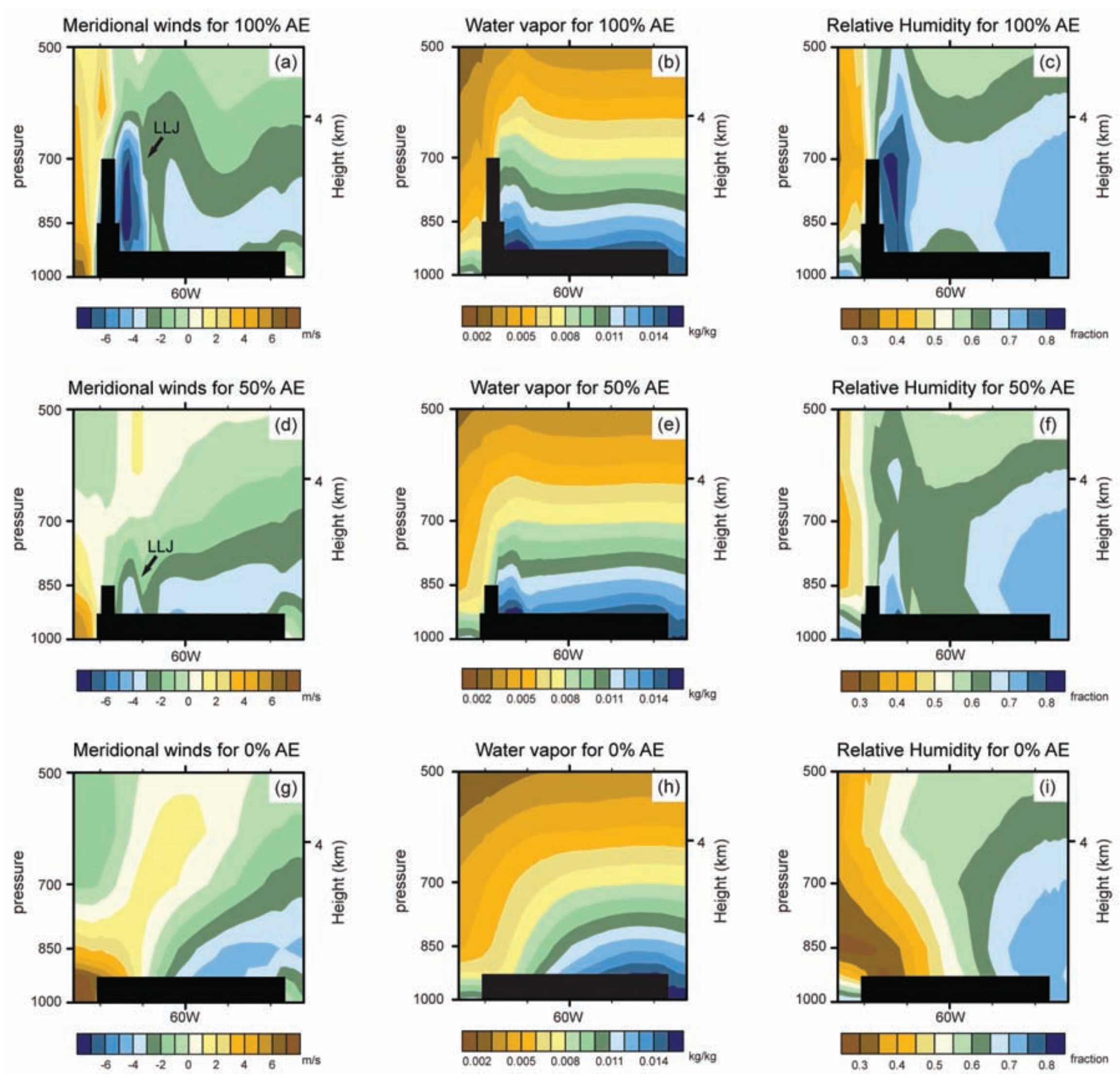

Figure 3.7: Simulated meridional winds, water vapor and relative humidity across South America between 15 and 26°S latitude during summer. (a) Simulation with modern Andes indicate the formation of a low-level jet (LLJ) with a strong northerly component along the eastern flanks of the Andes, (b) bringing high water vapor content (c) and results in high relative humidity. (d), (e) and (f) show meridional wind, water vapor and relative humidity for simulation with 50% Andean heights. (g), (h), and (f) same as d, e, f, but for simulation with no Andes.

lated to a strengthening of the Chaco Low over central South America that redirects the moisture flux from lower to higher latitudes (not shown). The increased moisture transport increases surface latent heating from ~60 W m^{-2} to >140 W m^{-2} (Fig. 3.9c). With increasing moisture and latent heat release, clouds start to form along the eastern flanks of the Andes (Fig. 3.5b) causing the reflection of incoming solar radiation to space. The reduction in surface heating results in a decrease in sensible heating from ~120 W m^{-2} to less than ~60 W m^{-2} (Fig. 3.9d).

When the Andes reach 50% of their modern elevation, the LLJ is initiated (Fig. 3.7d). Atmospheric dynamics similar to modern are established and amplify as the Andes rise to their modern elevation. At 50% of their modern elevation, the Andes block the dry westerly flow and drastically change zonal and meridional moisture transport. The deflection of easterly winds originating over the Amazon Basin results in the establishment of strong northerly airflow along the eastern flanks of the Andes that transport moisture from the tropics to the central Andes, increasing the surface water vapor and the relative humidity (Fig. 3.7d-f).

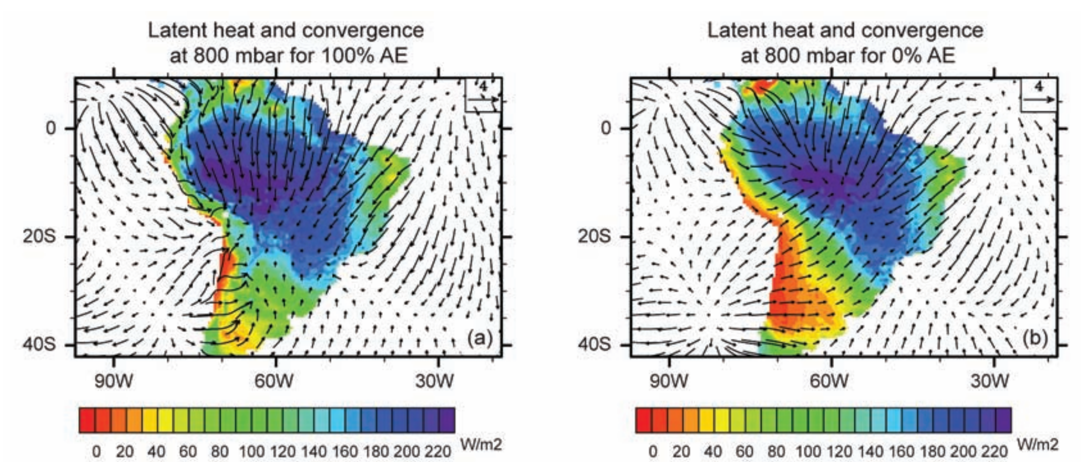

Figure 3.8: Simulated surface latent heat (shown in colors) and convergence at 800 mbar (arrows) during summer. (a) Simulations with modern Andes. (b) Simulations with no Andes.

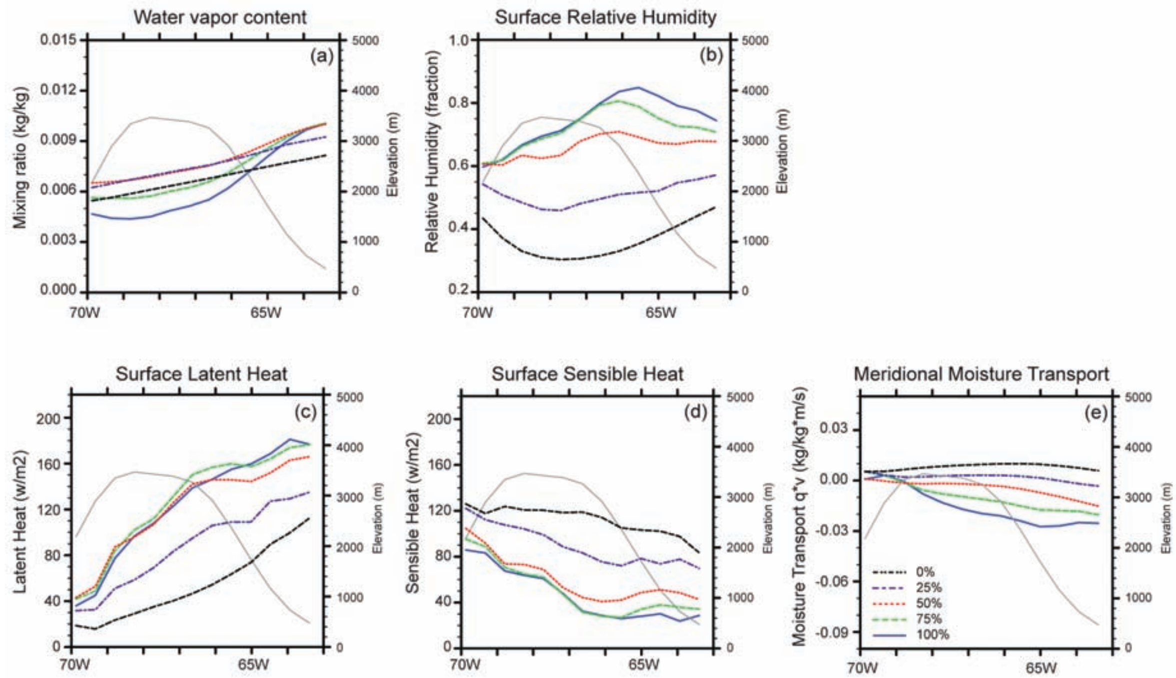

Figure 3.9: Moisture and heat over the Andean plateau region (1526°S) for different Andes heights (in percent from modern elevation) during summer. Solid gray line represents modern topography. (a) Water vapor content at 800 mbar. (b) Surface relative humidity. (c) Surface latent heat. (d) Surface sensible heat. (e) Meridional moisture transport (q x v) at 800 mbar. Positive values show moisture transported from the south, negative values indicate northerlies.

Further uplift of the Andes to modern elevations causes a strengthening of the LLJ (compare Figs. 3.7a and 3.7d) and increases the meridional moisture transport to modern values of $\sim$25 g kg^{-1} m s^{-1} at atmospheric pressures of 800 mbar (Fig. 3.9e). The significant increase in moisture flux due to the LLJ along the eastern flanks of the Andes correlates with a substantial increase in relative humidity (Figures 3.7c and 3.9b) and a significant increase in precipitation (Fig. 3.3c). Due to rainout along the Andean flanks and enhanced subsidence on parts of the plateau, water vapor amounts on the plateau decrease (Fig. 3.9a). Because most of the moisture is transported to the central Andes at high atmospheric levels, surface latent heat and sensible heat remain almost constant during the final stage of Andean uplift (Figures 3.9c and 3.9d). Changes in Andean topography also modify precipitation and moisture transport across the Amazon Basin. In the absence of the Andes, precipitation in the eastern and central part of the basin is ~3−4 mm day^{-1} higher than under modern conditions (Fig. 3.10a). The higher precipitation magnitudes are the result of enhanced low-level convergence over the Amazon Basin due to a reversal of wind direction over the western part of the basin (Fig. 3.4b). Low-level convergence of westerlies and easterlies focuses moisture convergence (Fig. 3.8b) and deep convection over large parts of the basin. With increasing Andean elevations, the eastern part of the Amazon Basin experiences a significant increase in zonal moisture flux that transports water vapor to the west (Fig. 3.10b) and causes a decrease in precipitation of up to 25% (Fig. 3.10a). The western part of the Amazon Basin is characterized by a strong increase in north-south directed transport of moisture from 25 to 90 g kg^{-1} m s^{-1} (Fig. 3.10c) and a change from predominant westerlies to easterlies between three quarters and modern Andean elevations. The significant increase in meridional moisture transport provides the source for increasing moisture flux into the Andean plateau region, resulting in higher precipitation along the eastern flanks of the Andes.

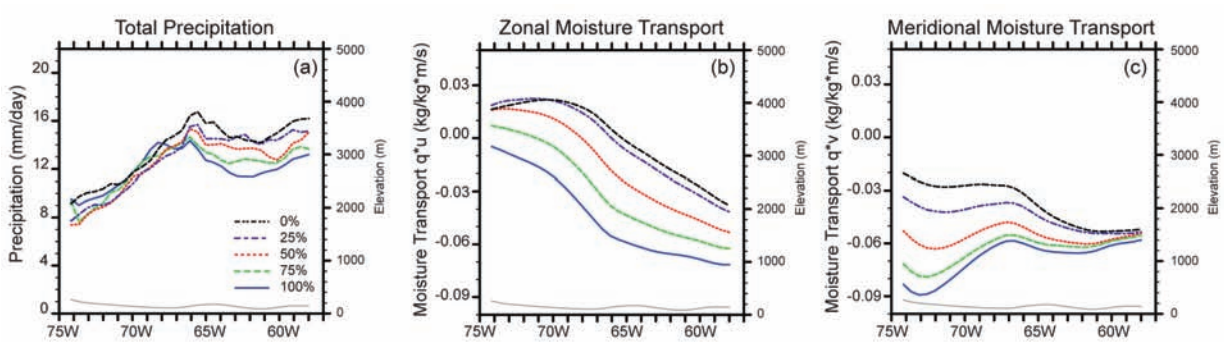

Figure 3.10: Simulated moisture over the Amazon Basin (3°N to 9°S) for different plateau heights (in percent from modern elevation) during summer. Solid gray line represents modern topography. (a) Total precipitation. (b) Zonal moisture transport (q x u) at 800 mbar. Positive values indicate moisture transported from the west, negative values indicate moisture transport from the east. (c) Meridional moisture transport (q x v) at 800 mbar. Positive values show moisture transported from the south, negative values indicate northerlies.

The SACZ is largely unaffected by changes in Andean topography. Precipitation across the SACZ stays almost the same; differences between modern and no-Andes simulations are smaller than 1 mm day^{-1}. Prevailing wind directions, water vapor content, and moisture transport across the SACZ are also unchanged (not shown). The absence of any significant changes is confirmation that this region is largely controlled by the influence of the South Atlantic High, which is not substantially affected by changes in Andean elevations.

Our results emphasize the influence of the Andes and their uplift on moisture transport. A direct relationship is observed between the strength of the LLJ, precipitation, and moisture flux in the Amazon Basin and along the Andes. Moisture transport via the LLJ is the dominant factor in triggering modern precipitation along the Andes. Sensible heat is not the primary cause for modern convection over the Andean plateau area.

3.5.3 Large-scale upper-level circulation

Previous studies have suggested that climate over the Andean plateau is closely related to the upper-level circulation, because mid- and upper-tropospheric winds influence low-level circulations (e.g., Garreaud, 1999; Garreaud et al., 2003; Lenters and Cook, 1999). Figure 3.11a emphasizes the strong correlation between 200-mbar zonal winds and modern precipitation. Although our modeled maximum zonal flow exceeds observational magnitudes (Garreaud et al., 2003), the relationship with upper-level easterlies favoring high modern precipitation over the Andean plateau region, while westerly flow causes dry conditions, is evident (Fig. 3.11a). Previous studies have shown that easterly flow in the upper troposphere over the central Andes leads to stronger than average upslope flow over the eastern slopes and easterly low-level winds, increasing the moisture transport from the continental lowlands that feeds the convection over the Andean plateau region (Garreaud, 1999). Our simulations reveal that the connection between upper- level flow and precipitation breaks down when the Andes are absent. In the absence of the Andes, the direction and magnitude of upper-level flow changes very little, while precipitation over the Andean plateau area decreases significantly (compare Figures 3.11a and 3.11b). The dynamical link between the upper-level zonal wind and precipitation is weak, because low-level winds are predominantly from the west.

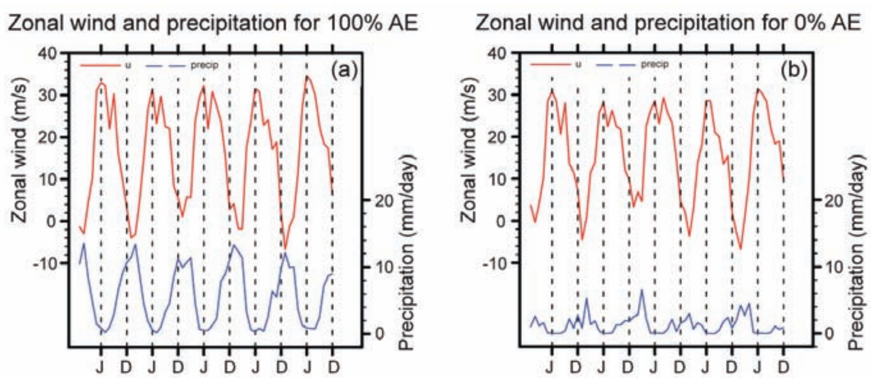

Figure 3.11: Inter-annual variations (J = June, D = December) in simulated upper-level (200 mbar) circulation (red line) and precipitation (blue line) across the Andean plateau area (15°-26°S/71° -62°W). (a) Total precipitation and zonal wind for simulations with modern Andes. (b) Same as a, but for simulations with no Andes. Note that the easterlies exceed observational magnitudes, but the correlation between zonal winds and precipitation can be still observed for modern simulations

Different factors have been proposed to influence the upper-air circulation, including the strength and the position of the Bolivian High (e.g., Garreaud et al., 2003; Lenters and Cook, 1997). The Bolivian High is the characteristic feature in the modern upper-level circulation of South America (Fig. 3.12) (e.g., Lenters and Cook, 1997; Virji, 1981). Although the center of the anticyclone is located close to the Andean plateau (Figs. 3.1a and 3.12a), previous studies have shown that direct mechanical effects of Andean topography on the Bolivian High are insignificant (e.g., Silva-Dias et al., 1983; Lenters and Cook, 1997; Schwerdtfeger, 1961). Our simulations are consistent with these findings and indicate that the Bolivian High also forms in simulations with no Andes (Fig. 3.12b). The Bolivian High weakens and shifts eastward when the Andes are absent. This shift is related to a shift in the low-level convergence associated with the maximum latent heat release in the southern part of the Amazon Basin for the no Andes case (Fig. 3.8) and implies that the Bolivian High develops as a direct response to low- to mid-tropospheric heating. This is in good agreement with previous studies that have shown that Amazonian heating is the dominant driving force in generating the upper-level high pressure system over South America, while the dynamic effect of the Andes is relatively unimportant (e.g., Silva-Dias et al., 1983; Lenters and Cook, 1997; Schwerdtfeger, 1961).

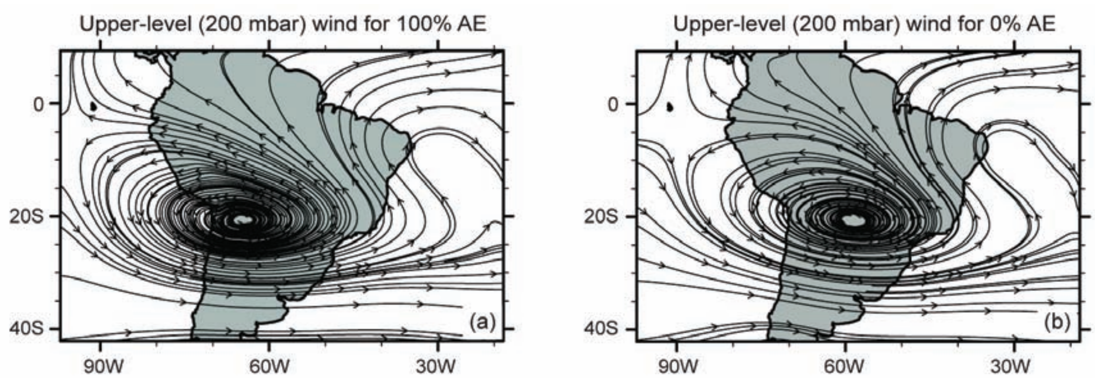

Figure 3.12: Simulated upper-level (200 mbar) winds during summer. (a) Winds for simulations with modern Andes. (b) Winds for simulations with no Andes

3.6 Discussion

3.6.1 Interaction between the Andes and regional climate dynamics

Our results indicate that the Andes play an important role in modulating regional atmospheric conditions. Previous studies have demonstrated that low-level northerly flow develops due to diabatic heating over the Amazon Basin and the presence of a subtropical high (e.g., Figueroa et al., 1995; Rodwell and Hoskins, 2001). Our results support this conclusion; northerly low-level flow over central South America and the South Atlantic High are well developed in our no-Andes experiment. However, in our simulations the establishment of the LLJ, which is a dominant factor in modern South American climatology, is directly related to the elevation of Andean topography. The LLJ represents the geostrophic response to the trade winds converging with the front of the northern eastern Andes. The deflection of easterly trade winds and the initiation of the LLJ occur once Andean elevations are 50% of their modern heights. With further uplift of the Andes, the LLJ strengthens, as indicated by an increase in southward velocities by nearly 100% on the eastern flank of the Andes. Previous studies have indicated that the LLJ is mainly related to mechanical forcing by the Andes (e.g., Campetella and Vera, 2002; Figueroa et al., 1995). Our results certainly support the role of mechanical forcing in the development of the LLJ, but also suggest that moist physics may be playing an important role in amplifying the LLJ. Our results support the idea that the uplift of the Andes enhances low and mid-tropospheric latent heating, increasing convergence at low levels and divergence at upper tropospheric levels along the Andes (Fig. 3.8). In turn, the enhanced low-level (zonal) flow perpendicular to the Andes (Fig. 2.13) drives a stronger LLJ, and further moisture transport. However, a better understanding of the horizontal and vertical structure of the LLJ and its relationship to convection is critical to quantify the individual mechanisms responsible for the intensification of the LLJ. For example, a strengthening of the modern LLJ has been associated with amplification of the Chaco Low in northern Argentina (e.g., Salio et al., 2002). Yet, in our studies, the Chaco Low is most intense when the Andes are low due to high sensible heating and reduced cloud cover (not shown), whereas the LLJ forms at higher Andean elevation.

The LLJ is the key feature providing moisture and energy for convection and pre-

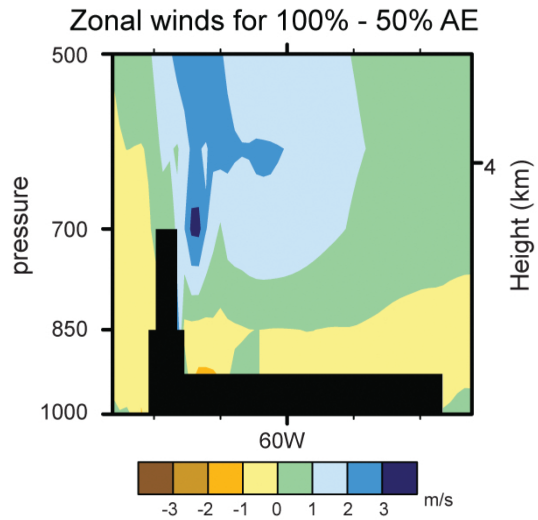

Figure 3.13: Difference in zonal wind between simulations with modern Andes and 50% Andean heights. Enhanced low- level zonal flow perpendicular to the Andes in the modern case intensifies the LLJ and increases the moisture transport.

cipitation along the Andes. Therefore, the influence of the Andes on regional climate is not purely mechanical through orographic lifting, but mainly due to modifications of dynamical processes. Through their impact on low-level circulation, the Andes not only influence the climate in immediate vicinity of the mountain range, but also have a direct impact on the climatology of remote areas such as the Amazon Basin. In the absence of the Andes, westerly winds can penetrate into parts of the Amazon Basin resulting in an enhanced convergence of low-level flow, strengthening convection and precipitation over the basin. If the Andes are present, the LLJ draws in moisture from the Amazon region and modifies the moisture flux within the basin.

Overall the formation of the Andes is a key aspect for driving the mechanisms that control the regional wind pattern and precipitation over South America.

3.6.2 Moisture transport from the tropics to higher latitudes

The transport of water vapor from the Amazon Basin to the central Andes is critically important to Andean precipitation. Previous studies have suggested that the Amazon Basin is an open system and that outflow of atmospheric moisture from the basin may contribute an important input to the hydrological cycle in the surrounding regions (e.g., Eltahir and Bras, 1994). However, evidence for potential effects on moisture supply and precipitation in surrounding regions was missing. Moreover, a few studies have suggested that moisture variability over the Andean plateau region cannot be accounted for by moisture fluctuations over the eastern lowlands (e.g., Garreaud et al., 2003; Garreaud, 2000). Our results indicate that precipitation in the central Andes region is directly related to the moisture content of the Amazon Basin. The LLJ is the dominant feature transporting moisture from the tropics to higher latitudes. The moisture transported by the LLJ provides the latent heat required to drive convective updrafts and enhances convection and precipitation along the eastern flank of the Andes. The LLJ draws in water vapor from the Amazon region and modifies the moisture flux within the basin. The strong moisture flux out of the Amazon Basin is balanced by stronger moisture influx from the Atlantic Ocean and slightly reduced convection and precipitation due to less pronounced convergence of low-level winds over the basin. Therefore, the surface water vapor content over the Amazon Basin remains constant and changes in surface latent heat over the region are small (not shown) for different Andean heights.

Uplift of the Andes and associated changes in the moisture transport across the Amazon Basin and along the eastern flanks of the Andes have a very small influence on the convection and precipitation across the SACZ. These results are in contrast to previous studies that have suggested that the generation of the SACZ is the result from the combined action of an Amazonian latent heat source and the steep Andean topography (Figueroa et al., 1995; Nogues-Paegle et al., 1998). An observed dipole structure between the SACZ and the LLJ with a weak SACZ associated with stronger LLJ and vice versa has been associated with intra-seasonal convective anomalies (e.g., Garreaud and Aceituno, 2001; de Goncalves et al., 2006; Lenters and Cook, 1999; Nogues-Paegle and Mo, 1997). However, on the longer timescales investigated here, we do not find a direct dynamical effect of the Andes on convective activity across the SACZ or a correlation between the strength of the LLJ and the SACZ. Our results lead us to conclude that convection and precipitation across the SACZ is mainly related to the latent heat over the Amazon Basin and the strength of the South Atlantic High that govern the low-level flux between the Amazon Basin and the SACZ.

3.6.3 Implications for paleoclimate

Our results have implications for the paleoclimatic evolution of South America, and show that modern climate is not representative of past climates when the Andes were lower. In general, our experiments predict that uplift of the Andes results in (1) a significant increase in precipitation along the eastern flanks of the Andes, (2) more arid conditions along the western flanks, and (3) no significant precipitation change over the Amazon Basin. These changes begin and intensify when the Andes reach approximately one-half of its modern elevation.

Our results are consistent with observations inferred from geological observations (Strecker et al. (2007) and references therein). For example, several studies have proposed a climate shift from arid to humid conditions along the eastern flanks of the Andes in Bolivia and Argentina during the Late Miocene (between 10 and

7 Ma) based on changes in stratigraphic units, plant fossils and faunal assemblages (e.g., Kleinert and Strecker, 2001; Starck and Anzotegui, 2001; Uba et al., 2005, 2006). Along the western flanks, a change from semiarid to hyperarid conditions has been proposed for the middle Miocene (e.g., Alpers and Brimhall, 1988; Rech et al., 2006). In the Atacama Desert, changes in soil composition between 19 and 13 Ma (Rech et al., 2006) as well as the termination of supergene alteration and copper-sulfide enrichment between 14 and 8.7 Ma (Alpers and Brimhall, 1988) and a strong reduction in sediment transfer from the Andes to the western lowlands between 10 and 6 Ma (Hoke et al., 2004) have been interpreted to reflect a significant shift towards more arid conditions along the western flanks of the Andes. In addition, a decrease in modeled net precipitation (difference between total precipitation and evapotranspiration) across the southern part of the Andean plateau is consistent with observations that commonly link the onset of aridification over the plateau area with the onset of internal drainage and the deposition of salt-bearing units between 24 and 15 Ma (Alonso et al., 1991; Vandervoort et al., 1995).

Although our model results are in good agreement with observations from the Andean flanks and the Amazon Basin, a mismatch between model and observations exists over the northern part of the Andean plateau. Despite an increase in evapotranspiration with increasing Andean heights, our simulations suggest an increase in net precipitation over parts of the Andean plateau. The mismatch may be due to the specific domain used for plateau interpretations, and/or prescription of constant boundary conditions such as vegetation and sea-surface temperature. For example, modeled changes in climate are interpreted for the entire Andean plateau area between 15 and 26°S, while proxy data are often based on interpretations of local observations. In addition, changes in vegetation across the Andes may influence the moisture availability over the plateau area. Prescribing dense vegetation at low Andean elevations in place of the modern desert biome could facilitate moisture retention in the topsoil on the mountain slopes, potentially contributing to greater local evapotranspiration and higher precipitation in the no Andes case.

Overall, our findings show how the tectonic evolution of the Andes has influenced South American climate. This knowledge may help constrain the surface uplift history of the Andes by constraining minimum Andean elevations during the Cenozoic. The onset of hyperaridity during the middle Miocene in the Atacama Desert has been related to surface uplift and the creation of a rain shadow along the western flanks of the Andes. Our results suggest that at least half the modern Andean elevation is necessary to block zonal flow and establish easterlies that bring moisture from the Amazon Basin to the central Andes. These findings are in very good agreement with estimated minimum Andean paleoelevations of >2 km prior to 12-15 Ma for the central Andes (e.g., Alpers and Brimhall, 1988; Rech et al., 2006), but suggests an earlier uplift history than that based on stable isotope paleoaltimetry (e.g., Garzione et al., 2006; Ghosh et al., 2006). However, changes in amount and source of rainfall reported here could have a substantial influence on the δ^{18}O composition of rainwater on the Andean plateau, significantly complicating paleoaltimetry estimates (Ehlers and Poulsen, 2009).

3.6.4 Caveats

The objective of this study is to understand how the Andes influence regional climate over South America and to analyze climate sensitivity to progressive Andean uplift. The model setup is designed to provide the most straightforward assessment of how climate responses to mechanical uplift of the Andes. We emphasize two important caveats to this work, one related to the modeling methodology and the other related to the paleoclimate implications. First, results presented in this study are from experiments with modern global reanalysis data as atmospheric lateral boundary conditions. The advantage of this method is that boundary conditions are based on assimilated observed data and do not include biases from global models. We have previously run experiments with the regional model nested within a global atmospheric climate model (Genesis.2.3.). The global model was run for different Andean elevations and then predicted atmospheric variables were used as boundary conditions to RegCM3. In this case, the atmospheric boundary conditions included the effects of changing Andean elevations. In general, both methods show a similar sensitivity of regional climate to different Andean elevations, indicating that the boundary conditions at the model domain are not significantly affecting our results.

Second, our experiments are clearly idealized and are not meant to be simulations of specific Cenozoic timeslices. The uplift of the Andes was not uniform, but likely varied along the range (Allmendinger et al., 1997; Barnes et al., 2008; McQuarrie et al., 2008). Moreover, during the Cenozoic uplift of the Andes, additional tectonic and climatic factors were evolving that may have influenced regional and global climate including minor continental drift of South America, the glaciation of Antarctica, changes in large-scale ocean circulation and SST, the decline of atmospheric pCO_2, and evolution of land-surface characteristics. The influences of modern SSTs and landsurface characteristics on South American precipitation have previously been investigated (Cook and Vizy, 2008; Enfield, 1996; Lenters and Cook, 1995; Seth and Rojas, 2003). These studies have shown that despite an influence of annual variations in SSTs and precipitation magnitude over the eastern parts of South America (e.g. northeast Brazil), changes in the SSTs do not have a significant effect on precipitation on the interior and western part of the Amazon Basin (e.g., Enfield, 1996; Lenters and Cook, 1995; Seth and Rojas, 2003). Precipitation over the Andean plateau has been reported to be influenced by El Niño/ La Niña conditions with a tendency towards below average summer precipitation during El Niño events (e.g., Aceituno, 1988; Vuille, 1999).

Changes in the modern distribution of Amazon rainforest can have a large influence on precipitation in the basin (Cook and Vizy, 2008) and past changes may have influenced the Amazon hydrological cycle. With vegetation and soil moisture as important factors driving convection over the Amazon Basin more studies are necessary to evaluate the effect of changing Amazon rainforest on precipitation in the basin itself and its influence on moisture transport towards the Andean plateau region. However, although the Amazon Basin is a dynamic environment, it has been proposed that the Amazon rainforest existed throughout the Cenozoic (e.g., Colinvaux and Oliveira, 2001; Hoorn, 2006; van der Hammen and Hooghiemstra, 2000). Marine incursions from the north have been reported to reach the western Amazon Basin during the Miocene, but the spatial and temporal extent of these incursion is still a matter of debate (Hoorn et al., 1996; Rasanen et al., 1995). The replacement of rainforest land cover by a water body could result in an increase in moisture availability and transport, and requires future investigation.

3.7 Conclusions

We used a high-resolution (∼60 km) limited-domain climate model with a reasonable representation of Andean topography to investigate the effect of the Andes on South American climate. The Andes have a direct mechanical influence on the climatology of South America by forcing orographic precipitation along the eastern flanks of the Andes, and blocking westerly flow from the Pacific. Importantly, the Andes Mountains are critical to the development of the LLJ that draws in and transports moisture from the Amazon Basin to the Andean region. When the Andes are absent the LLJ is absent; southward moisture transport is low; convection is suppressed; and precipitation decreases dramatically along the eastern flanks of the Andes. The Andes also influence convection over the Amazon basin. The absence of the Andes reduces moisture export from the Amazon, and leads to enhanced low-level convergence and increased convection and precipitation in parts of the Amazon Basin.

Our model results indicate that atmospheric flow and processes similar to modern initiated once Andean elevations reached approximately 50% their modern heights. At around 2000 m elevation the Andes start to block zonal flow, resulting in a reversal of dominant wind direction and a change in water vapor source over the western part of the continent. The LLJ starts to form and intensifies with further Andean uplift due to enhanced latent heat release, increasing low-level convergence and stronger low-level (zonal) flow perpendicular to the Andes. Local processes (local latent heating) drive precipitation for Andean elevation lower than half the modern, while regional-scale processes (transport of moist warm air from the Amazon) initiate precipitation when the Andes are higher than 50% their modern elevation.

3.8 Acknowledgments

Support for this research was provided by grants to C. Poulsen and T. Ehlers from the University of Michigans Graham Environmental Sustainability Institute and from the US National Science Foundation (EAR Award 0738822). We thank two anonymous reviewers for constructive comments on the manuscript.

Bibliography

Aceituno, P. On the Functioning of the Southern Oscillation in the South American Sector. Part I: Surface Climate. *Monthly Weather Review*, 116:505 – 524, 1988.

Allmendinger, R. W., Jordan, T. E., Kay, S. M. and Isacks, B. L. The evolution of the Altiplano-Puna Plateau of the Central Andes. *Annual Review of Earth and Planetary Sciences*, 25:139–174, 1997.

Alonso, R., Jordan, T. E., Tabbutt, K. T. and BVandervoort, D. S. Giant evaporite belts of the Neogene central Andes. *Geology*, 19:401–404, 1991.

Alpers, C. N. and Brimhall, G. H. Middle Miocene climate change in the Atacama Desert, northern Chile: Evidence from supergene mineralization at La Escondida. *Geological Society of America Bulletin*, 100:1640 – 1656, 1988.

Barnes, J. B., Ehlers, T. A., McQuarrie, N., O'Sullivan, P. B. and Tawackoli, S. Thermochronometer record of central Andean plateau growth, Bolivia (19.5S). *Tectonics*, 27(TC3003):doi:10.1029/2007TC002174, 2008.

Berbery, E. H. and Collini, E. A. Springtime precipitation and water vapor flux over southeastern South America. *Monthly Weather Review*, 128:1328 – 1346, 2000.

Broccoli, A. and Manabe, S. The effects of orography on midlatitude Northern Hemisphere dry climates. *Journal of Climate*, 5:1181 – 1201, 1992.

Campetella, C. M. and Vera, C. S. The influence of the Andes mountains on the South American low-level flow. *Geoophysical Research Letters*, 29(17)(1826):doi:10.1029/2002GL015451, 2002.

Chou, S. C., Tanajura, C. A. S., Xue, Y. and Nobre, C. A. Validation of the coupled Eta/SSiB model over South America. *Journal of Geophysical Research*, 107(D20)(8088):doi:10.1029/2000JD000270, 2002.

Colinvaux, P. and Oliveira, P. Amazon plant diversity and climate through the Cenozoic. *Palaeogeography, Palaeoclimatology, Palaeoecology*, 166:51–63, 2001.

Cook, K. H. and Vizy, E. K. Effects of Twenty-First-Century climate change on the Amazon Rain Forest. *Journal of Climate*, 21:542 – 560, 2008.

de Goncalves, L., Shuttleworth, W., Nijssen, B., Burke, E., Marengo, J., Chou, S., Houser, P. and Toll, D. Evaluation of model-derived and remotely sensed precipitation products for continental South America. *Journal of Geophysical Research*, 111(D16113):doi:10.1029/2005JD006276, 2006.

DeMaria, M. Linear response of a stratified tropical atmosphere to convective forcing. *Journal of Atmospheric Sciences*, 42(18):1944–1959, 1985.

DeSales, F. and Xue, Y. Investigation of seasonal prediction of the South American regional climate using the nested model system. *Journal of Geophysical Research*, 111(D20107):doi:10.1029/2005JD006989, 2006.

Dickinson, R. E., Henderson-Sellers, A. and Kennedy, P. Biosphere-Atmosphere Transfer Scheme (BATS) version 1E as coupled to the NCAR Community Climate Model. *NCAR technical report TN-397+STR*, page 72 pp, 1993.

Ehlers, T. and Poulsen, C. J. Influence of Andean uplift on climate and paleoaltimetry estimates. *Earth and Planetary Science Letter*, 281:238–248, 2009.

Eltahir, E. A. and Bras, R. L. Precipitation recycling in the Amazon basin. *Quaternary Journal. Royal Meteorological Society*, 120:861 – 880, 1994.

Emanuel, K. A. A scheme for representing cumulus convection in large-scale models. *Journal of Atmospheric Sciences*, 48(21):2313–2335, 1991.

Enfield, D. B. Relationship of inter-American rainfall to tropical Atlantic and Pacific SST variability. *Geophysical Research Letters*, 23(23):3305–3308, 1996.

Figueroa, S. N., Satyamurty, P. and Da Silva-Dias, P. L. Simulations of the summer circulation over the South American region with an Eta Coordinate Model. *Journal of Atmospheric Sciences*, 52(10):1573–1584, 1995.

Gandu, A. W. and Geisler, J. E. A Primitive Equations Model Study of the Effect of Topography on the Summer Circulation over Tropical South America. *Journal of Atmospheric Sciences*, 48(16):1822–1836, 1991.

Garreaud, R. Multiscale analysis of the summertime precipitation over the central Andes. *Monthly Weather Review*, 127:901 – 921, 1999.

Garreaud, R., Vuille, M. and Clement, A. C. The climate of the Altiplano; observed current conditions and mechanisms of past changes. *Palaeogeography, Palaeoclimatology, Palaeoecology*, 194:5–22, 2003.

Garreaud, R. D. Intraseasonal variability of moisture and rainfall over the South American Altiplano. *Monthly Weather Review*, 128:3337 – 3346, 2000.

Garreaud, R. D. and Aceituno, P. Interannual rainfall variability over the South American Altiplano. *Journal of Climate*, 14:2779–2789, 2001.

Garzione, C. N., Molnar, P., Libarkin, J. and MacFadden, B. Rapid late Miocene rise of the Bolivian Altiplano: Evidence for removal of mantle lithosphere. *Earth and Planetary Science Letters*, 241:543–556, 2006.

Ghosh, P., Garzione, C. and Eiler, J. Rapid uplift of the Altiplano revealed through 13C-18O bonds in paleosol carbonates. *Science*, 311:511 – 515, 2006.

Giorgi, F. and Marinucci, M. R. An investigation of the sensitivity of simulated precipitation to model resolution and its implication for climate studies. *Monthly Weather Review*, 124:148 – 166, 1996.

Giorgi, F., Marinucci, M. R. and Bates, G. T. Development of a second-generation regional climate model (RegCM2). Part I: boundary-layer and radiative transfer processes. *Monthly Weather Review*, 121:2794 – 2813, 1993a.

Giorgi, F., Marinucci, M. R., Bates, G. T. and De Canio, G. Development of a second-generation regional climate model (RegCM2). Part II: convective processes and assimilation of lateral boundary conditions. *Monthly Weather Review*, 121:2814–2832, 1993b.

Grell, G. Prognostic evaluation of assumptions used by cumulus parametrizations. *Monthly Weather Review*, 121:764 – 787, 1993.

Grell, G., Dudhia, J. and Stauffer, D. R. Description of the fifth generation PennState/NCAR Mesoscale Model (MM5). *NCAR technical report TN-398+STR*, page 121 pp., 1994.

Hoke, G. D., Isacks, B. L., Jordan, T. E. and Yu, J. S. Groundwater-sapping origin for the giant quebradas of northern Chile. *Geology*, 32(7):605–608, 2004.

Hoorn, C. The birth of a mighty Amazon. *Scientific American*, 294(5):52–59, 2006.

Hoorn, C., Paxton, C. G. M., Crampton, W. G. R., Burgess, P., Marshall, L. G., Lundberg, J. G., Rasanen, M. E. and Linna, A. M. Miocene deposits in the Amazonian foreland basin. *Science*, 273(5271):122–125, 1996.

Horel, J. D., Hahmann, A. N. and Geisler, J. E. An investigation of the annual cycle of convective activity over the tropical Americas. *Journal of Climate*, 2:1388 – 1403, 1989.

Isacks, B. L. Uplift of the Central Andean Plateau and bending of the Bolivian Orocline. *Journal of Geophysical Research*, 93(4):3211–3231, 1988.

Kleeman, R. A Modeling Study of the Effect of the Andes on the Summertime Circulation of Tropical South America. *Journal of Atmospheric Sciences*, 46(21):3344–3362, 1989.

Kleinert, K. and Strecker, M. R. Climate change in response to orographic barrier uplift; Paleosol and stable isotope evidence from the late Neogene Santa Maria Basin, northwestern Argentina. *Geological Society of America Bulletin*, 113(6):728–742, 2001.

Kutzbach, J. E., Guetter, P. J., Ruddiman, W. F. and Prell, W. L. Sensitivity of climate to late Cenozoic uplift in southern Asia and the American West; numerical experiments. *Journal of Geophysical Research*, 94(D15):18,393–18,407, 1989.

Lenters, J. D. and Cook, K. H. Simulation and diagnosis of the regional summertime precipitation climatology of South America. *Journal of Climate*, 8(12):2988–3005, 1995.

Lenters, J. D. and Cook, K. H. On the origin of the Bolivian high and related circulation features of the South American climate. *Journal of the Atmospheric Sciences*, 54(5):656–677, 1997.

Lenters, J. D. and Cook, K. H. Summertime precipitation variability over South America: role of the large-scale circulation. *Monthly Weather Review*, 127(3):409–431, 1999.

McQuarrie, N., Ehlers, T. A., Barnes, J. B. and Meade, B. J. Temporal variation in climate and tectonic coupling in the central Andes. *Geology*, 36(12):999–1002, 2008.

NOAA/NESDIS/NCDC. Global - The Global Historical Climatology Network Precipitation (GHCN). *URL:http://gov.noaa.nosa:Global-GHCN-Precipitation*, 2003.

Nogues-Paegle, J. and Mo, K. C. Alternating wet and dry conditioons over South America during summer. *Monthly Weather Review*, 125:279 – 291, 1997.

Nogues-Paegle, J., Mo, K. C. and Paegle, J. Predictability of the NCEP-NCAR reanalysis model during austral summer. *Monthly Weather Review*, 126:3135–3152, 1998.

Pal, J. S., Giorgi, F., Bi, X. and etal. Regional climate modeling for the developing world - The ICPT RegCM and RegCNET. *Bulletin of the American Meteorological Society*, 88(9):1395 – 1409, 2007.

Rasanen, M. E., Linna, A. M., R, S. J. C. and R, N. F. Late Miocene tidal deposits in the Amazonian foreland basin. *Science*, 269:386 – 390, 1995.

Rech, J. A., Currie, B. S., Michalski, G. and Cowan, A. M. Neogene climate change and uplift in the Atacama Desert, Chile. *Geology*, 34(9):761–764, 2006.

Reynolds, R. W., Rayner, N. A., Smith, T. M., Stokes, D. C. and Wang, W. An improved in situ and satellite SST analysis for climate. *Journal of Climate*, 15:1609–1625, 2002.

Rodwell, M. and Hoskins, B. Subtropical Anticyclones and Summer Monsoons. *Journal of Climate*, 14:3192 – 3211, 2001.

Rojas, M. and Seth, A. Simulation and sensitivity in a nested modeling system for South America. Part II: GCM boundary forcing. *Journal of Climate*, 16:2454–2471, 2003.

Rutllant, J. and Ulriksen, P. Boundary-layer dynamics of the extremely arid northern part of Chile. *Boundary Layer Meteorology*, 17:41–55, 1979.

Salio, P., Nicolini, M. and Saulo, C. Chaco low-level jet events characterization during the austral summer season. *Journal of Geophysical Research*, 107(D24):doi:10.1029/2001JD001315, 2002.

Schwerdtfeger, W. Stroemungs- und Temperaturfeld der freien Atmosphere ueber den Anden. *Meteorologische Rundschau*, 14:1–6, 1961.

Seth, A. and Giorgi, F. The effects of domain choice on summer precipitation simulation and sensitivity in a regional climate model. *Journal of Climate*, 11:2698 – 2712, 1998.

Seth, A., Rauscher, S. A., Camargo, S. J., Qian, J.-H. and Pal, J. S. RegCM3 regional climatologies for South America using reanalysis and ECHAM global model driving fields. *Climate Dynamics*, 28:461–480, 2006.

Seth, A. and Rojas, M. Simulation and sensitivity in a nested modeling system for South America. Part I: Reanalysis boundary forcing. *Journal of Climate*, 16(15):2437 – 2453, 2003.

Silva-Dias, P. L., Schubert, W. H. and DeMaria, M. Large-scale response of the tropical atmosphere to transient convection. *Journal of Atmospheric Sciences*, 40:2689–2707, 1983.

Starck, D. and Anzotegui, L. The late-miocene climate change - persistence of a climate signal through the orogenic stratigraphic record in nortwestern Argentina. *Journal of South American Earth Sciences*, 14:763–774, 2001.

Strecker, M. R., Alonso, R. N., Bookhagen, B., Carrapa, B., Hilley, G. E., Sobel, E. R. and Trauth, M. H. Tectonics and climate of the southern Central Andes. *Annual Review of Earth and Planetary Sciences*, 35:747–787, 2007.

Uba, C. E., Heubeck, C. and Hulka, C. Facies analysis and basin architecture of the Neogene Subandean synorogenic wedge, southern Bolivia. *Sedimentary Geology*, 180(3-4):91–123, 2005.

Uba, C. E., Heubeck, C. and Hulka, C. Evolution of the late Cenozoic Chaco foreland basin, southern Bolivia. *Basin Research*, 18(2):145–170, 2006.

USGS. GTOPO30. *URL:http://eros.usgs.gov/*, 1996.

van der Hammen, T. and Hooghiemstra, H. Neogene and Quaternary history of vegetation, climate, and plant diversity in Amazonia. *Quaternary Science Reviews*, 19:725–742, 2000.

Vandervoort, D. S., Jordan, T. E., Zeitler, P. K. and Alonso, R. N. Chronology of internal drainage development and uplift, southern Puna Plateau, Argentine Central Andes. *Geology*, 23(2):145–148, 1995.

Vera, C., Baez, J., Douglas, M., Emmanuel, C., Marengo, J., Meitin, J., Nicolini, M., Nogues-Paegle, J., Paegle, J., Penalba, O., Salio, P., Saulo, C., Silva-Dias, P. L. and Zipser, E. The South American low-level jet experiment. *Bulletin of the American Meteorological Society*, 87(1):63 – 77, 2006.

Virji, H. A preliminary study of summertime tropospheric circulation patterns over South America estimated from cloud winds. *Monthly Weather Review*, 109:599–610, 1981.

Vuille, M. Atmospheric circulation over the Bolivian Altiplano during dry and wet periods and extreme phases of the Southern Oscillation. *International Journal of Climatology*, 19:1579–1600, 1999.

Wang, H. and Fu, R. Cross-equatorial flow and seasonal cycle of precipitation over South America. *Journal of Climate*, 15:1591 – 1608, 2002.